Dissertation

Outlining active bed materials for dual fluidised bed biomass gasification
-
In-bed catalysts and oxygen/carbonate looping behaviour

ausgeführt zum Zwecke der Erlangung des
akademischen Grades eines Doktors der technischen Wissenschaften
unter Leitung von

Univ. Prof. Dipl.-Ing. Dr. Hermann Hofbauer
Dipl.-Ing. Dr. Christoph Pfeifer

am

Institut für Verfahrenstechnik, Umwelttechnik und Technische Biowissenschaften der
Technischen Universität Wien

eingereicht an der Technischen Universität Wien
Fakultät für Maschinenwesen und Betriebswissenschaften

von
Dipl.-Ing. Stefan Koppatz
Jadengasse 4/19
1150 Wien

Wien, Juni 2012

....
Stefan Koppatz

ABSTRACT

The dual fluidised bed system is a reliable concept for steam gasification of woody biomass into a valuable product gas. The nitrogen free product gas can be used for a wide range of applications. In addition to conventional generation of heat and power, the product gas can be used as feed for synthesis processes into liquid fuels, synthetic natural gas, methanol or other chemicals. The purity, which concerns the solid and gaseous pollutants, is an essential requirement for the application. In particular, the condensable hydrocarbons (tar) are an obstacle for the operation of gasifiers. Their condensation can cause clogging or blockages in downstream process units.

The application of a active bed material in the fluidised bed process is a favourable option for the gasification process, as the active material is employed directly in the gasification reactor. Generally, the active material promotes the decomposition of tar and other gas–gas reactions (e.g. the CO-shift). This primary measure for in-situ hot gas cleaning allows a compact gasifier design, which is essential for its industrial application. This thesis aims at the experimental investigation of different bed materials to show their activity in the context of a dual fluidised bed system. The materials considered are limestone, natural olivine, Fe-olivine (a synthetic material), and silica sand, which is taken as the reference case, as this material is catalytically inactive. The main part of the experimental work was carried out at a $100\,kW$ dual fluidised bed pilot plant for steam gasification of biomass. Furthermore, a dual circulating fluidised bed reactor system is used for the experiments to expose the solid materials to surrogate gas mixtures.

The performance of the pilot plant is shown by means of general aspects such as its temperature profile, pressure profile, and gas residence times. The activity is elucidated on the basis of product gas composition, tar content and composition, water conversion, and the extent of the CO-shift. In particular, the oxygen transfer from the combustion reactor to the gasification reactor and its general impact, which is developed by the cyclic oxidation and reduction of iron, are illustrated. The transfer behaviour and the impacts on gas production and tar decomposition is shown for olivine and Fe-olivine.

As a result, limestone is found as the material which best promotes tar decomposition, water conversion, and CO-shift. However, a drawback for its application is its rather low attrition resistance. The capability of Fe-olivine for tar decomposition is well developed, and is found to be higher than that of natural olivine. However, it was found that the water conversion is low for Fe-olivine, as the H_2 is selectively oxidised by the oxygen input. Furthermore, the importance of intense gas–solid contact and gas residence time in the bubbling bed of the gasification reactor is shown. Unlike the solid-free freeboard zone, the bubbling bed is considered to be the active zone for effective heterogenous catalysis. Based on experimental findings and considerations on the evolution and character of the tar, a scheme is proposed which shows the possible interactions of the tar compounds in the gasification reactor.

Finally, the activity of limestone for carbonate looping in the dual fluidised bed system is illustrated. This characteristic is used for the combination of biomass gasification

with sorption enhanced reforming. By means of the sorption enhanced reforming, CO_2 is selectively removed from the reaction atmosphere in the gasification reactor. This process yields a product gas which is poor in CO_2 and rich in H_2.

This work underlines the potential of active bed materials in dual fluidised bed systems. This covers the capability of the material for an effective conversion process (i.e., high tar reduction, high water conversion), and the possibility for different operation modes such as sorption enhanced reforming.

KURZFASSUNG

Das Zweibett-Wirbelschichtsystem zur Dampfvergasung holzartiger Biomasse stellt ein zuverlässiges Verfahren zur Herstellung eines heizwertreichen Produktgases dar. Das Reaktorsystem basiert auf der hydraulischen Verschaltung zweier als Vergasungs- und Verbrennungsreaktor bezeichneten Wirbelschichtreaktoren. Die Kopplung der Wirbelschichtreaktoren erlaubt eine kontinuierliche Zirkulation des Wirbelschichtinventars zwischen den Reaktoren. Das im Verfahren erzeugte Produktgas ist frei von Stickstoff und enthält zu einem Großteil die Synthesegaskomponenten CO und H_2. Neben der konventionellen Strom- und Wärmeerzeugung eignet sich das Produktgas als Einsatzstoff zur Synthese von flüssigen Treibstoffen, synthetischem Erdgas oder Methanol. Voraussetzung für eine uneingeschränkte Nutzung des Produktgases ist die Qualität, die wesentlich durch feste und gasförmige Verunreinigungen bestimmt wird. Insbesondere stellen die allgemein als Teer bezeichneten kondensierbaren Kohlenwasserstoffverbindungen eine wesentliche Einschränkung des Anlagenbetriebs dar. Das Kondensieren der Teere verursacht Ablagerungen und Verunreinigungen in den Anlagenteilen (z. B. Wärmetauscher). Die Zersetzung der Teere kann mittels katalytisch aktiver Bettmaterialien erfolgen. Durch die direkte Anwendung im Vergasungsreaktor werden Verfahrensschritte zur Entfernung der Teere vereinfacht bzw. gegebenenfalls erübrigt. Diese als primäre Maßnahme bezeichnete in-situ Heißgasreinigung erlaubt eine Kompaktierung des Gesamtprozesses. Allgemein unterstützt das katalytisch aktive Material die Zersetzung der Kohlenwasserstoffe, aber auch den Reaktionsfortschritt weiterer Reaktionen (z. B. CO-Shift).

Neben den katalytischen Eigenschaften können aktive Bettmaterialien Transportvorgänge übernehmen. Im Zweibett-Wirbelschichtsystems können die Spezies CO_2 bzw. O_2 mit Hilfe des Bettmaterials transportiert werden. Der O_2-Transport vom Verbrennungsreaktor in den Vergasungsreaktor wird durch zyklische Oxidation und Reduktion des Fe-Olivins erwirkt. Der selektive CO_2-Transport vom Vergasungsreaktor in den Verbrennungsreaktor erfolgt durch zyklisches Karbonatisieren und Kalzinieren des CaO-haltigen Bettmaterials Kalkstein. Die als Sorption-Enhanced-Reforming (SER) bezeichnete Prozessoption ermöglich die Erzeugung eines H_2-reichen Produktgases.

Die vorliegende Arbeit widmet sich dem Themenschwerpunkt der aktiven Bettmaterialien im Zweibett-Wirbelschichtsystem. Dabei wurden experimentelle Untersuchungen mit den Bettmaterialien Quarzsand, Olivin, Fe-Olivin und Kaltstein durchgeführt. Schwerpunkt der Untersuchungen sind die Auswirkungen auf die allgemeine Gasproduktion, das Vermögen zur Reduktion der Teere sowie die Darstellung des selektiven Transports von O_2 bzw. CO_2.

Der Hauptteil der experimentellen Untersuchungen wurde an einer 100 kW Zweibett-Wirbelschicht Pilotanlage zur Dampfvergasung von Biomasse durchgeführt, mit der sich reale Prozessbedingungen vergleichbar zur industriellen Anwendung realisieren lassen. Darüber hinaus wurde ein weiterer Versuchsstand verwendet, dessen Reaktorsystem auf der Verschaltung von zwei zirkulierenden Wirbelschichtreaktoren basiert.

Der 120 kW Versuchsstand ist für den Betrieb mit gasförmigen Brennstoffen konzipiert und erlaubt eine gezielte Dosierung von Gasmischungen. In der Arbeit wird eine Gegenüberstellung der Materialien (Quarzsand, Olivin, Fe-Olivin, Kalkstein) gezeigt, wobei die katalytische Aktivität anhand charakteristischer Größen, wie z. B. der Gaszusammensetzung, Gasausbeute, Teergehalt und Teerzusammensetzung, Wasserumsatz oder der Abweichung vom CO-Shift Gleichgewicht, verdeutlicht wird. Die Untersuchungen zeigen weiterhin die Auswirkungen des O_2-Transports auf die Stoffströme, die allgemeine Gaszusammensetzung und den Teergehalt. Der CO_2-Transport wird anhand experimenteller Untersuchungen an der 100 kW Pilotanlage wie auch an einer industriellen Anlage gezeigt. Eine abschließende experimentelle Studie untersucht den Einfluß von Bettmaterialinventaren (Olivin) mit unterschiedlicher mittlerer Korngröße auf die Gasproduktion und den Teergehalt.

Im Ergebnis ist festzustellen, dass das CaO-basierte Bettmaterial Kalkstein die höchste katalytische Aktivität hinsichtlich des Wasserumsatzes, der Teerzersetzung und des Reaktionsfortschritts zum CO-Shift Gleichgewicht aufweist. Jedoch ist die geringe Materialhärte und damit verbundene erhöhte Abriebsneigung in der Wirbelschicht als Nachteil zu nennen. Die Aktivität des Fe-Olivins zur Teerreduktion kann anhand der Untersuchungen als gut eingestuft werden und liegt höher als die des Olivins. Quarzsand wird als Referenzmaterial herangezogen, da dieses Bettmaterial als katalytisch inaktiv anzusehen ist. Der selektive Sauerstofftransport ist bei Olivin nur sehr gering erkennbar und hat folglich kaum wahrnehmbare Auswirkungen auf die Stoff- und Energieflüsse und Teerzersetzung. Für Fe-Olivin zeigt sich ein ausgeprägter Sauerstofftransport der sich deutlich auf die Stoff- und Energieflüsse auswirkt. Der selektive O_2-Transport zeigt sich durch die partielle Oxidation der Gaskomponenten CO und H_2 im Vergasungsreaktor. Verbunden damit ist ein geringer Wasserumsatz. Die Auswirkung des Sauerstoffeintrags auf die Teerumsetzung wird als sehr gering festgestellt. Die Untersuchungen mit den Bettmaterialinventaren (Olivin) unterschiedlicher mittlerer Korngröße zeigen die Bedeutung eines intensiven Gas-Feststoff-Kontaktes in der Wirbelschicht. Deutlich zu erkennen ist der geringere Teergehalt bei der Anwendung des Bettmaterialinventars mit geringerer Korngröße. Dies wird auf die höhere Turbulenz und somit den intensiveren Gas-Feststoff-Kontakt in der Wirbelschicht zurückgeführt.

Die Arbeit verdeutlicht das Potenzial aktiver Bettmaterialien im Zweibett - Wirbelschichtsystem. Dies schließt die katalytische Aktivität wie auch die Eigenschaft zum Transport von CO_2 oder O_2 ein.

LIST OF PUBLICATIONS

This thesis is based on the work published in the following articles:

I.   Koppatz, S., Pfeifer, C., Kreuzeder, A., Soukup, G., Hofbauer, H., "Application of CaO-based bed material for dual fluidized bed steam biomass gasification", in: *Proceedings of the 20th International Conference on Fluidized Bed Combustion Conference, Xi'an, China*, **2009**, Vol. II, pp. 712–718.

II.   Koppatz, S., Pröll, T., Pfeifer, C., Hofbauer, H., "Investigation of reforming activity and oxygen transfer of olivine in a dual circulating fluidised bed system with regard to biomass gasification", in: *Proceedings of the Fluidization XIII Conference, Gyeong-ju, Korea*, May 16–21, **2010**, pp. 901–908.

III.   Koppatz, S., Pfeifer, C., Pröll, T., Hofbauer, H., "Experimental Study on Reforming Activity and Oxygen Transfer of Fe-Olivine in a Dual Circulating Fluidized Bed System", in: *Pugsley, T. et al. (Eds.), Proceedings of the 10th International Conference on Circulating Fluidized Bed Technology (CFB10), Sunriver, Oregon, USA*, May 1–5, **2011**, pp. 449–456

IV.   Koppatz, S., Pfeifer, C., Rauch, R., Hofbauer, H., Marquard-Moellenstedt, T., Specht, M., "H_2 rich product gas by steam gasification of biomass with in situ CO_2 absorption in a dual fluidized bed system of 8 MW fuel input", *Fuel Processing Technology*, 90 (7–8), pp. 914–921, **2009**.

V.   Koppatz, S., Pfeifer, C., Hofbauer, H., "Comparison of the performance behaviour of silica sand and olivine in a dual fluidised bed reactor system for steam gasification of biomass at pilot plant scale", *Chemical Engineering Journal*, 175, pp. 468–483, **2011**.

VI.   Koppatz, S., Schmid, J. C., Pfeifer, C., Hofbauer, H., "The effect of bed particle inventories with different particle sizes in a dual fluidised bed pilot plant for biomass steam gasification", *accepted for publication in Ind. Eng. Chem. Res.*, **2012**.

VII.   Pfeifer, C., Koppatz, S., Hofbauer, H., "Catalysts for dual fluidised bed biomass gasification—an experimental study at the pilot plant scale", *Biomass Conversion and Biorefinery*, Springer-Verlag, Berlin, **2011**, 1, pp. 63–74.

VIII.	Koppatz, S., Pfeifer, C., Hofbauer, H., "Application of Fe-olivine as catalytic active bed material in biomass gasification", in: *Proceedings of the International Conference on Polygeneration Strategies (ICPS10)*, 7–9 September, **2010**, Leipzig, Germany.
IX.	Wolfesberger, U., Koppatz, S., Pfeifer, C., Hofbauer, H., "Effect of iron supported olivine on the distribution of tar compounds derived by steam gasification of biomass", in: *Proceedings of the International Conference on Polygeneration Strategies (ICPS11)*, 30 August–1 September, **2011**, Vienna, Austria.

Contribution by the author:

I., IV.	Responsible for data evaluation, writing and partially responsible for experimental work
II., III., V., VI., VIII.	Responsible for data evaluation, experimental work and writing
VII.	Partially responsible for experimental work, data evaluation and writing
IX.	Responsible for experimental work, data evaluation and partially responsible for writing

RELATED PUBLICATIONS NOT INCLUDED IN THIS THESIS

The following papers have also been published during the course of the work but are not included in this thesis since their content either is outside the scope of the present work or partly overlaps with the papers included in the thesis.

- Schmid, J.C., Wolfesberger, U., Koppatz, S., Pfeifer, C., Hofbauer, H., "Variation of Feedstock in a Dual Fluidized Bed Steam Gasifier - Influence on Product Gas, Tar Content and Composition", *Environmental Progress & Sustainable Energy*, John Wiley & Sons, 31, pp. 205–215, **2012**.

- Wilk, V., Kern, S., Kitzler, H., Koppatz, S., Schmid, J.C., Hofbauer, H., "Gasification of plastic residues in a dual fluidized bed gasifier- Characteristics and performance compared to biomass", in: *Proceedings of the International Conference on Polygeneration Strategies (ICPS11)*, 30 August - 1 September, **2011**, Vienna, Austria.

- Wilk, V., Kitzler, H., Koppatz, S., Hofbauer, H., 2011, "Gasification of waste wood and bark in a dual fluidized bed steam gasifier", *Biomass Conversion and Biorefinery*, **2011**, 1., pp. 91–97.

- Pfeifer C., Koppatz S., Hofbauer H., "Steam gasification of various feedstocks at a dual fluidised bed gasifier: Impacts of operation conditions and bed materials", *Biomass Conversion and Biorefinery*, **2011**, 1., pp. 39-53.

- Wilk, V., Kitzler, H., Koppatz, S., Pfeifer, C., Hofbauer, H., 2010, "Gasification of residues and waste wood in a dual fluidised bed steam gasifier", in: *Proceedings of the International Conference on Polygeneration Strategies (ICPS10)*, 7 - 9 September **2010**, Leipzig, Germany.

- Varga, C., Koppatz, S., Pfeifer, C., Nacken, M., Di Marcello, M., Gallucci, K., Rapagna, S., Heidenreich, S., Foscolo, P. U., Hofbauer, H., 2010, "Integration of a catalytic filter candle into the Guessing gasifier for hot gas cleaning of biomass derived syngas", in: *Proceedings of the International Conference on Polygeneration Strategies (ICPS10)*, 7 - 9 September **2010**, Leipzig, Germany.

- Varga, C., Koppatz, S., Pfeifer, C., Hofbauer, H., "Hot Gas Cleaning of Biomass Derived Syngas by Catalytic Filter Candles", in: *Proceedings of the 18th European Biomass Conference and Exhibiton*, 3 - 7 May **2010**, Lyon, France.

- Koppatz, S., Pfeifer, C., Hofbauer, H., "Primary tar reduction by Fe-olivine as catalytically active bed material in a dual fluidised bed system for steam gasification of biomass", in: *Proceedings of the 18th European Biomass Conference and Exhibiton*, 3 - 7 May **2010**, Lyon, France.

- Brellochs, J., Marquard-Möllenstedt, T., Zuberbühler, U., Specht, M., Koppatz, S., Pfeifer, C., Hofbauer, H., "Stoichiometry adjustment of biomass steam gasification in DFB process by in situ CO_2 absorption", in: *Proceedings of the 1st International Conference on Polygeneration Strategies (ICPS09)*, September 1st-4th, **2009**, Vienna, Austria.

- Koppatz, S., Pfeifer, C., Hofbauer, H., "Primary Tar Reduction in a Dual Fluidised Bed Gasification System by means of Fe-supported Olivine", in: *Proceedings of the 17th European Biomass Conference & Exhibition*, 29 June - 03 July **2009**, Hamburg, Germany,

- Marquard-Moellenstedt, T., Specht, M., Zuberbuehler, U., Koppatz, S., Pfeifer, C., Rauch, R., Soukup, G., Hofbauer, H., Koch, M., "Transfer of Absorption Enhanced Reforming Process (AER) from Pilot Scale to an 8 MW Gasification Plant in Guessing, Austria", in: *Proceedings of the 16th European Biomass Conference & Exhibition*, 2-6 June **2008**, Valencia, Spain.

Danksagung

Contents

XI

1 Introduction

1.1 Economy, Energy and Environment

World energy consumption and demand is constantly growing. In particular, developing countries, with their emerging markets, have high rates of growth which is attended by their rising economies. The economic power, growth and prosperity of a national economy as well as its increase in population or a high degree of urbanisation is unquestionably linked to the consumption and demand for energy. So far, the uncoupling of economic growth and energy consumption has not been achieved. The world primary energy demand by region since 1980 with an estimate until 2030 for the reference scenario reported in the World Energy Outlook (WEO, 2008) by the International Energy Agency (IEA) in 2008 is illustrated in Figure 1.1, [1].
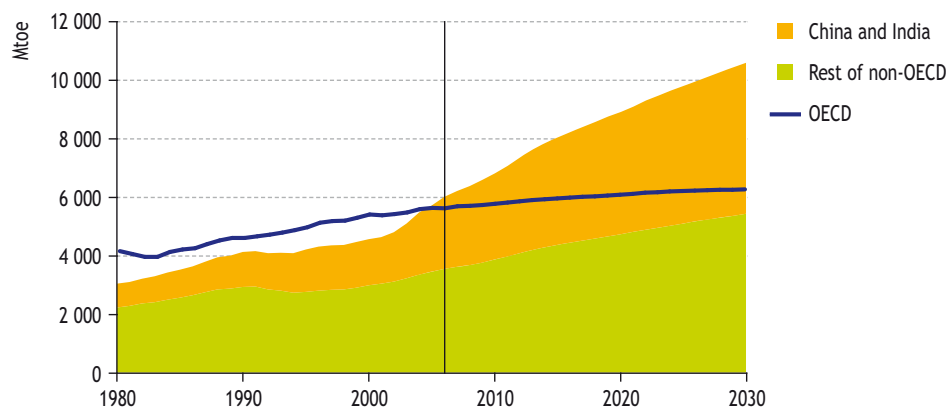
Figure 1.1: Primary energy demand by world region (Mtoe: million tons of oil equivalent), reported in the World Energy Outlook by the International Energy Agency (IEA) in 2008, [1]

In 2005 the energy demand in non-OECD countries exceeded that in OECD countries, with a continuously increasing tendency. 87 % of the increase in demand between 2006 and 2030 is attributed to non-OECD countries, whereas this growth is mainly driven by China and India. The share of primary energy demand is expected to rise from 51 % to 62 % between 2006 to 2030 for non-OECD countries, [1]. Figure 1.2 shows world primary energy demand by fuel since 1980 combined with an estimate for 2030 for the reference scenario. According to this scenario, fossil fuels will dominate the primary energy mix with oil in first place followed by coal and gas. The average annual rate of

growth (between 2006 and 2030) for biomass and waste is stated to be at 1.4 % by the WEO, 2008; [1].
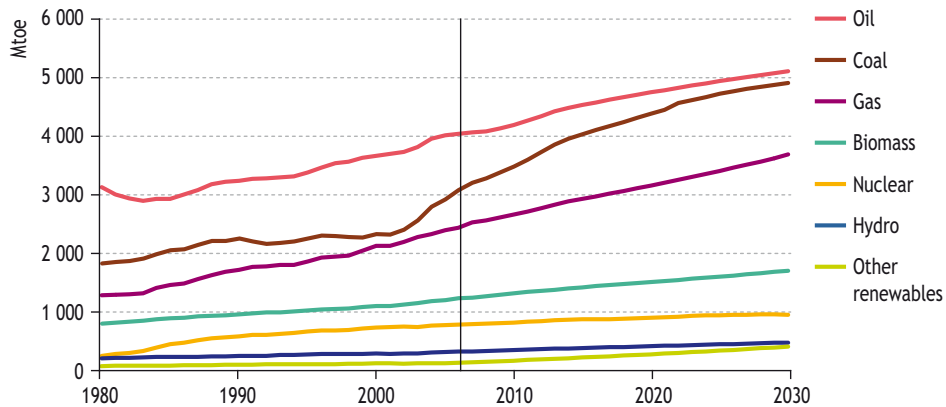
Figure 1.2: World primary energy demand by fuel (Mtoe: million tons of oil equivalent), reported in the World Energy Outlook by the International Energy Agency (IEA) in 2008, [1]

The consumption of energy, however, is closely related to environmental concerns, which mainly address:

- global warming due to the release of greenhouse gas emissions,
- destruction of landscape or habitat, and
- acid rain.

In particular, global warming and the climate change due to anthropogenic reasons has been raised to a global interest. In a sense, there is a triangle of inter-related concerns, which is described in the literature [2] as the trilemma of:

- energy demand,
- economic development, and
- environment.

Besides, the latter concerns of energy supply and consumption can be stretched to further issues, which are related to national interests:

- global competition of economic areas,
- rising intensity in electricity,
- increasing dependence on energy imports,
- progressive energy prices, or
- security of energy supply.

1.2 Renewables – Biomass

Circumstances of energy policy have experienced significant changes in the past decades at the international, european, and national levels. The deregulation of the electricity market and generally the liberalisation of the energy market have changed the market environment of the energy economy and developed new structures or policies, e.g.:

- the directive (2009/28/EC) of the European Parliament and of the Council, which regulates the national shares of renewable energy use within the European Union, [3];

- the Austrian Green Electricity Act, which regulates subsidy conditions for renewable energy sources, [4] or the

- the German Renewable Energy Act, which regulates the share of renewable energy and feed in tariff, [5].

Furthermore, climate change caused by greenhouse gas emissions has led to a strong need for actions for climate protection. The European Union has made the decision to reduce greenhouse gas emissions by 20 % by 2020, [6]. An indispensable part for the future energy supply will be consequently its integration with renewable energy sources. Despite their volatility and availability in supply (e.g., wind energy, solar energy), renewables can offer local solutions for the energy supply by a mutual combination or complementation (e.g., energy storage).
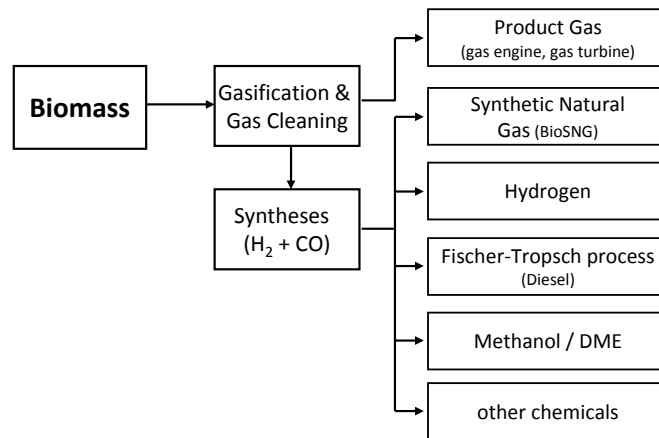
Figure 1.3: Concept of polygeneration, possible products and generation of secondary energy carriers

Clearly, biomass can contribute to covering the demand for heat and power. In contrast to other renewables (e.g., wind, solar or geothermal energy), biogenous feedstock is the only carbon sources. The scope of possible end products or secondary energy carriers is referred to as *polygeneration*, see Figure 1.3.

1.3 Principal processes and technologies of autothermal gasification

Thermo-chemical conversion aims at the conversion of the chemical energy of feedstock into a usable form of energy (e.g., heat, gas). This conversion commonly consists of a process at high temperature which decomposes the carbonaceous material in the absence or in the presence of a reaction agent. Appropriate processes are listed in Table 1.1. The listing demonstrates the product flexibility, dependent on the process, which covers the conventional generation of heat and power as well as the generation of secondary energy carriers or products.

Table 1.1: Thermo-chemical conversion processes

Process	Reaction agent	Temperature	Pressure	Conversion products
Combustion	air, O_2	800–1100 °C	atmospheric	heat
Pyrolysis	none	400–600 °C	atmospheric	pyrolysis oil, char and gases
Gasification	air, O_2, H_2O, CO_2	600–1200 °C	atmospheric/ pressurised	product gas[1], syngas
Liquefaction	H_2	250–350 °C	pressurised	liquid products

[1] occasionally the term *producer gas* is used in literature

With regard to this thesis, the subsequent content is limited to the subject of gasification. The process of the decomposition of feedstock into a valuable product gas at high temperatures requires a certain quantity of energy (heat), which is supplied by partial oxidation (release of heat) of a fuel. Thus, a certain quantity of fuel is used to realise the process. Several concepts of gasifiers have been developed in the past. The principal types of gasifiers are sketched in Figure 1.4.

The types of gasifiers can be distinguished by their hydrodynamics, auxiliary materials, gasification agents, and basically different methods of bringing into contact the solid fuel with the gasification agent. The benefits of gasification over conventional combustion are principally its greater potential efficiency and product flexibility. Mainly, the higher exergetic efficiency of the gasification process (from solid fuel to the product gas) compared to the exergetic content of steam from steam generation (via combustion) in combination with the efficiency of a gas engine is favourable, [7]. Further aspects are:

- easy handling of gasesous fuel,

- lower volume flow for gas treatment and

- diverse range of products.

Bubbling fluidised bed

product gas

feedstock

gasification
agent/oxidant

Circulating fluidised bed

product gas

feedstock

gasification
agent/oxidant

Entrained flow

feedstock

gasification
agent/oxidant

product gas

Counter current moving bed

feedstock

product gas

drying
pyrolysis
reduction
oxidation

gasification
agent/oxidant

Co current moving bed

feedstock

gasification
agent/oxidant

drying
pyrolysis
oxidation
reduction

product gas

Figure 1.4: Overview of principal types of autothermal gasifiers

1.4 The DUAL FLUID bed technology for allothermal gasification

The different types of gasifiers as illustrated in Figure 1.4 are technologies which are appropriate for operation with the gasification agents air or O_2. The heat demand of gasification is directly supplied by the heat release from partial oxidation of the fuel. Air or oxygen based gasification processes (autothermal, exothermic processes) are usually operated at a λ[1] of $0.2 \ldots 0.3$. However, gasification using air generates a product gas, which is highly diluted by N_2 at the expense of its heating value (4–6 MJ/Nm^3). Gasification with oxygen yields a similar product gas, but significant energy penalties for the oxygen supply have to be taken into consideration. Steam gasification yields a nitrogen-free product gas with a lower heating value of about 12–15 MJ/Nm^3. The conversion with steam is an allothermal (endothermic) process, which requires an input of energy (heat) from an external source, since an oxidant for partial oxidation and heat supply is not present. A solid carrier (bed material) for transport of heat is the basic

---

[1]another term often used in literature is: ER, equivalence ratio

character of the DUAL FLUID[2] technology to supply endothermic processes from an external source.

The term DUAL FLUID has arisen at Vienna University and is used as a collective term for various processes which include a combination of fluidised beds. Some essential aspects are given in the following to detail this concept, adapted form [8].

The liquid-like characteristics of a fluidised bed may be utilised for the combination of fluidised bed reactors. For this reason, a connection of two fluidised beds allows the communication of the solid matter. The basic principle of the DUAL FLUID technology is sketched in Figure 1.5.
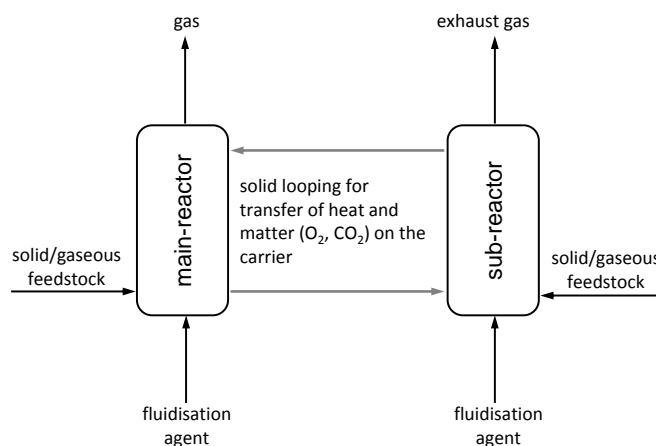
Figure 1.5: Basic principle of the DUAL FLUID concept

This principle is also the basic configuration of all DUAL FLUID bed reactor systems. In the fluidised beds, different thermo-chemical processes take place, which are mainly:

- gas–gas reactions, or

- solid–gas reactions.

The common objective of the processes in the fluidised bed is the conversion of matter at high temperatures. The circulating solid serves primarily as a carrier. But there are also further features which are utilised, which can be:

- catalytic properties for effective conversion or,

- carrier properties for transport of certain species (O_2, CO_2) for looping processes and applications.

The direct or indirect (i.e., catalytic, transport of matter) impact on the process is clearly dependent on the nature of the solid particles. Various kinds of solids are employed,

---

[2]A collective term for various conversion processes using a combination of fluidised beds for the transfer of heat and matter with circulating solids, at the Vienna University of Technology; a former term, which has been used in the literature is FICFB.

which can be generally grouped into natural or synthetic materials. However, some prequisites for any suitability for the fluidised bed have to be fulfilled. The DUAL FLUID systems are divided into a main-reactor, which involves the ultimate process like cracking, gasification, combustion or reforming and the sub-reactor, which involves processes like solid heat up, uptake, or the release of species from the carrier, or the regeneration of the solids. Furthermore, the reactors might be distinguished by their thermal behaviour, which is either endothermic (heat consuming) or exothermic, for providing the overall process with heat. The technology is applied to various thermochemical processes and operation modes. A selection is listed in Table 1.2.

The DUAL FLUID technology can be applied to steam biomass gasification as indicated in Table 1.2. Commonly, this configuration is is referred to as a **dual fluidised bed** (DFB) system for steam gasification[3]. The DFB system is further detailed in Section 2.4. In the recent past this technology has become prevalent for steam gasification. Research institutes and groups working on dual fluidised bed systems (combined systems) for biomass gasification are briefly listed in Table 1.3. Technological challenges, which are in the current focus of research and development or will arise in near future, are:

- process-internal reduction of impurities (tars),

- fuel flexibity (waste, residues),

- reduction of impurities caused by problematic feedstock (sulphur, nitrogen, chlorine),

- solid depositions or agglomerations caused by certain ash species,

- improved solid conversion.

---

[3]further terms used in the literature are: twin-bed gasifier/gasification, two-stage gasification

Table 1.2: Overview of types and applications of DUAL FLUID systems[1]

Application	Main-reactor/process	Sub-reactor/process	State of the art
fluid catalytic cracking (FCC)	cracker/catalytic cracking of long chain oily feed	regenerator/regeneration of catalyst through combustion of char, heat up	industrial plants at large scale are established
dual fluidised bed steam gasification	gasifier/steam gasification, catalytically supported	combustor/combustion for solid heat up and/or regeneration of the catalyst	industrial plants >8 MW established
carbonate looping supported gasification, sorption enhanced reforming (SER)	gasifier/steam gasification and CO_2 uptake by carbonation of calcite	combustor/combustion for solid heat up and release of CO_2 by calcination of carbonate	pilot plant >100 kW and test runs at 8 MW industrial scale plant
chemical looping combustion (CLC) for gaseous fuels	fuel reactor / oxygen combustion of a gaseous fuel only in contact with the oxygen delivering bed material	air reactor/oxygen uptake on the oxygen-carrier (bed material), high temperatures in a combustion atmosphere; regeneration of bed material from possible depositions	pilot plant 120 kW, proven feasibility
chemical looping reforming (CLR) for gaseous fuels	fuel reactor/high temperature, solid catalysed reforming, e.g. CH_4 into synthesis gas, reduction of the oxygen carrier	air reactor/combustion for solid heat up and/or regeneration of the reforming catalyst	pilot plant >100 kW
CLC and CLR for solid fuels	fuel reactor/devolatilizing, gasification and full or partial endoxidation of volatiles from the solid fuel by oxygen delivering bed material	air reactor/oxidation and regeneration of bed material as oxygen carrier	concept study

1) adapted from [8]

Table 1.3: Institutes and working groups with research on dual fluidised bed systems for biomass gasification

Institution	Scale of exerimental device	Ref.
Chalmers University, Sweden	demo scale, 2–4 MW	[9]
University of Canterbury, New Zealand	pilot plant, 100 kW	[10]
Mid Sweden University, Härnösand, Sweden	pilot plant, 150 kW	[11]
Dalian University of Technology, Department of Chemical Engineering, Dalian, China	lab-scale	[12]
National Institute of Advanced Industrial Science and Technology, Japan	lab-scale	[13]
Institute of Process Engineering, Chinese Academy of Sciences, Beijing, China	lab-scale	[14]
Energy research Centre of the Netherlands (ECN)	pilot plant, 800 kW (Milena gasifier)	[15]
Vienna University of Technology	pilot plant, 100 kW (DFB gasifier)	

1.5 Gas cleaning strategies and methods

This thesis addresses the gas cleaning of biomass-derived product gas with regard to reduction and removal of condenable hydrocarbons (tar). However, commonly gas cleaning also include the removal of undesired species which contains sulphur, nitrogen or chlorine. These gaseous impurities may occur as H_2S, NH_3 or HCL and are hinderance for the application, such as synthesis processes. The removal of the tar may be classified into:

- physical methods (e.g, scrubber at CHP Güssing, Austria, [16]; OLGA process, [17]),

- non-catalytic methods (thermal cracking at high residence times and temperature $> 900\,°C$ [18]) or

- catalytic methods.

The catalytic approach to gas cleaning is frequently discussed in the literature [19–26] and is also referred to as catalytic hot gas cleaning. Catalytic hot gas cleaning focusses on two different strategies. The processing of the measures differs in their location whether the cleaning is applied directly in the gasifier or is carried out in a separate process unit downstream from the gasifier. Thus, it is referred to as primary and secondary measure for tar reduction, respectively. The principles are sketched in Figure 1.6.
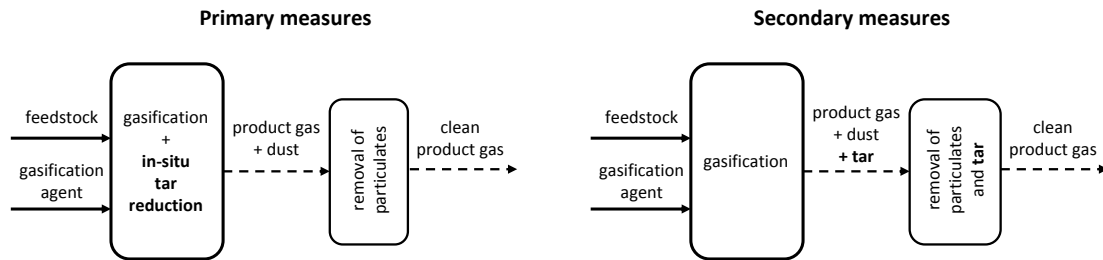
Figure 1.6: Principle of primary and secondary measures for tar reduction; impurities caused by sulphur, chlorine and nitrogen are not considered

Primary measures are directly applied in the gasification reactor during the process of gasification by:

- combination of the fluidised bed processing with catalytic material as the bed material (in-bed catalyst) [21, 27–30] or

- the combination of the gasification reactor with catalytic filter candles (which also effects and retention of particulates) [31–34],

- tar reducing operation mode (e.g. temperature, steam-to-fuel ratio)

On the other hand, secondary measures treat the product gas downstream of the gasifier. The removal of tar is carried out in a separate unit, [19,35]. Hot gas cleaning by primary measures is preferred, as:

- process simplification,

- product gas is available at high temperatures (e.g., for fuel cells),

- clogging (of heat exchangers) is avoided during cooling of tar free product gas.

1.6 Objective, relevance, and scope of this work

The dual fluidised bed system for steam gasification of biomass is an attractive technology for the conversion of solid feedstock into a valuable product gas. This technology has been successfully proven at the pilot plant and industrial scales. The subject of the recent development and research might be summarised as follow:

- *fuel-oriented*: fuel flexibility, which involves the gasification of different kinds of biomasses (straw, bark), waste wood, residues or co-gasification of coal and biomass

- *process-oriented*: application/investigation of reactive/catalytic solid materials, and

- *reactor-concept oriented*: different configuration/combinations of fluidisation regimes in the DFB system, integration of efficient gas-solid separation systems

The list of related publications[4] contains some experimental studies at the DFB pilot plant, which are matched to the subject of fuel oriented investigations. A major concern in the operation of the gasifier is the purity of the product gas. This addresses solid impurities and gaseous impurities, such as the application (e.g., gas engine, synthesis processes) require a certain gas purity. Condensable hydrocarbons (tars) are one to the main hindrances for the operation of biomass gasifiers and the establishment of biomass gasification technology. The condensation of tar at already high temperatures causes clogging or blockage in the downstream process units.

The content of the thesis is part of a process oriented development. Basically, in terms of this topic, the thesis addresses the question of the effect of different bed materials. The key subjects are:

- the investigation and evaluation of the effect of different in-bed catalysts on performance, which is defined by exhaust gas composition, extent of CO-shift, water conversion, and tar decomposition (Paper I to III, V and VII to IX),

- elucidation of the effect of selective CO_2 and O_2 transport in the DFB system, which is caused by carrier materials (e.g., CaO or Fe), (Paper IV, III and VIII) and

- aspects of fluidised bed operation, intensity of the gas–solid contact (Paper VI),

In particular, the water conversion, the extent/promotion of CO-shift, and the decomposition of tar in the presence of different materials is the focus of this thesis. Basically, the water conversion, the tar content and composition and specific yields are specified for different bed materials and process operation. The tar content and composition is presented as well as a simple estimate of the maturation of tar in the gasification reactor. The effect of solid inventories with different particle sizes on the behaviour of the fluidised bed and the decomposition of tar is studied and presented in Paper VI. The

---

[4]which are not included in the content of the thesis, see page VII

investigation of the catalytic activity and oxygen transport behaviour of natural olivine and the synthetic material Fe-olivine is presented in Paper II and Paper III. The effect of different bed material (olivine, Fe-olivine, limestone) on the steam biomass gasification (product gas and decomposition of tar) at the pilot plant is presented in Papers I and VII to IX. In particular, Paper V shows the effect on the product gas and decomposition of tar of the use of olivine in comparison to the inert bed material silica sand. The experimental work for the thesis was carried in different facilities:

- The 100 kW pilot plant at the Vienna University of Technology was used for the experimental studies which are presented in the Papers I, V to IX. This system is related to industrial application and is therefore close to the conditions of industrial operation. Due to the high potential in up-scale of the DFB technology, the results of the experimental work are basically transferable to industrial scale applications. The pilot plant is detailed in the thesis and in the papers.

- The experimental work for Papers II and III was carried out in the 120 kW dual circulating fluidised bed (DCFB) pilot rig at the Vienna University of Technology and is described in the thesis and in the papers. Specific data for the DCFB pilot rig can be found elsewhere: [36,37]. This facility was used to investigate the oxygen transfer and reforming acitvity as well as their interactions. The DCFB pilot rig was operated with a surrogate gas mixture.

- Paper IV is an execption, as its experimental work was carried out at the industrial combined heat and power plant (CHP) Güssing. The CHP Güssing is described in Paper IV.

2 Fundamentals

2.1 Gasification of biomass

2.1.1 Characterisation of wood

This section aims at generally characterising woody biomass. Wood pellets that are applied in the experiments at the $100\,kW$ pilot plant are specified in Paper V or VI. In terms of molecular structure, dry wood is essentially composed (95%–98wt%) of the biopolymers cellulose, hemicellulose, and lignin. Minor constituents of wood (2%–5wt%) are fats, resins and ash. The constituents with their mass fractions and functions are listed in Table 2.1.

Table 2.1: Constituents and structure of woody (dry) biomass

Component	Mass fraction[1] in wt%		Function	Structural/chemical composition
	softwood	hardwood		
cellulose	40–50	40–50	wood builder	repeated glucose molecules of $C_6H_{10}O_5$
hemicellulose	25–30	25–35	wood builder	polysaccharide
liginin	25–35	20–25	binding material, mechanical support	3-dimensional phenylpropan-polymer $C_{10}H_{12}O_4$

[1] mass fractions are adapted from: [38–41]

The chemical stuctures of cellulose, hemicellulose and lignin are shown in Figures 2.1 to 2.3.
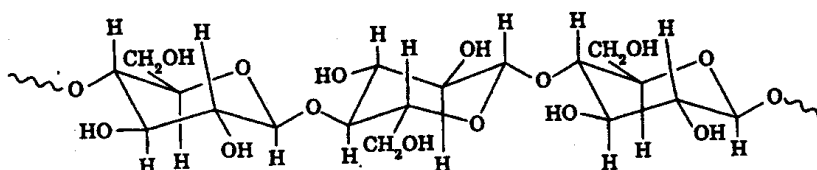
Figure 2.1: Chemical structure of cellulose, [42]

14

Cellulose is basically composed of glucose molecules, which are branchlessly connected to a linear chain (polysaccharide). In contrast, hemicellulose is composed of a polysaccharide related to cellulose. It is branched, which results in a more complex structure.
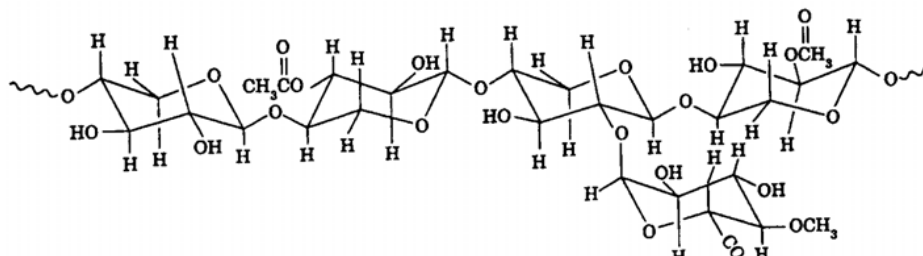
Figure 2.2: Chemical structure of hemicellulose, [42]
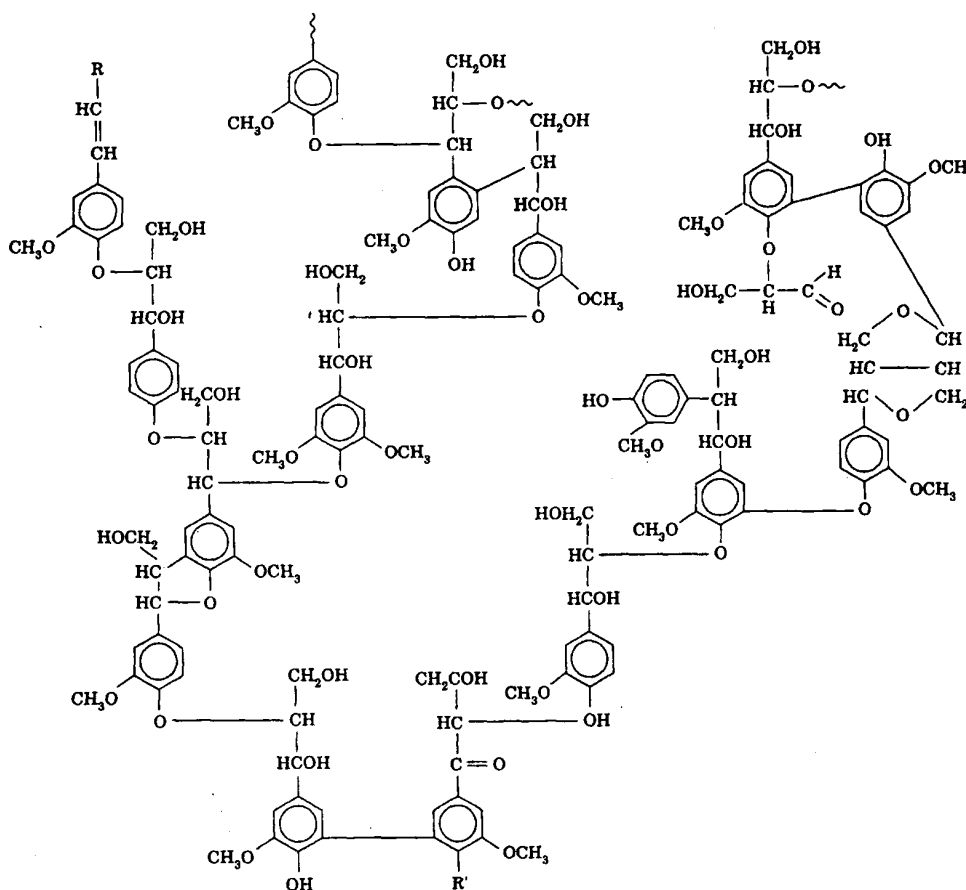
Figure 2.3: Chemical structure of lignin, [42]

15

Lignin is a three dimensional high molecular weight polymer built upon phenylpropane-monomer units. The structure of lignin contains:

- a hydroxide (-OH),

- an alkyl (-C_nH_{2n+1}), e.g., methyl - CH_3 or

- a methoxy group (-OCH_3)

connected to a phenyl group (C_6H_5). Lignin is relatively stable in terms of mechanical stability compared to cellulose and hemicellulose due its cross-linked structure. However, the exact structure of lignin is not known as lignin is altered by its extraction. Generally, more lignin is found in softwood than in hardwood, [41]. Beside these two categories, the relative content of the constituents varies in the different parts of the tree.

The overall thermal behaviour of the biomass is the sum of the properties of the organic constituents, [43]. The main components show different thermal behaviour regarding their degradation/decomposition, which can be explained by their chemical structure, [44]. The qualitative progress of degradation (adapted from [43, 45–49] derived by TGA/DTGA measurements) of the main components of woody biomass over temperature is shown in Figure 2.4.
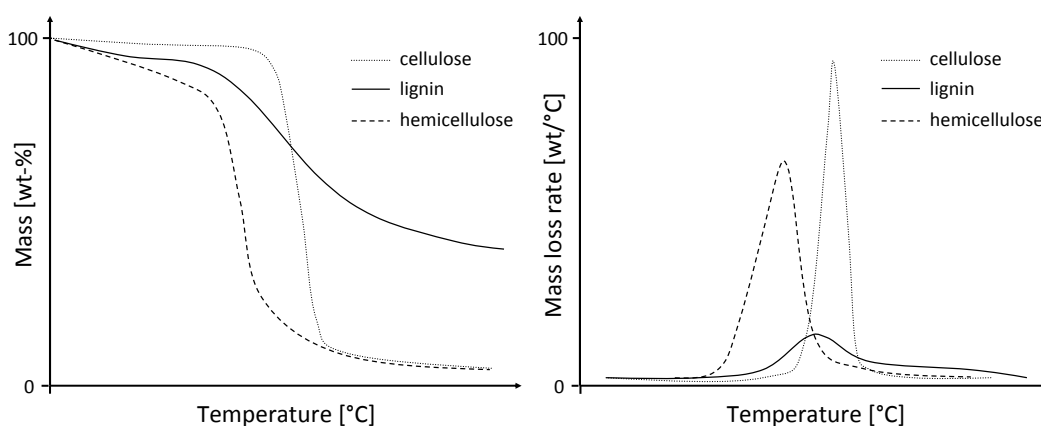
Figure 2.4: Qualitative progress of temperature dependent decomposition of lignin, cellulose and hemicellulose, adapted from [43, 45–49] by TGA/DTGA measurement

The mass loss of cellulose takes places in a relatively narrow temperature range due to its relative simple structure. The decomposition of hemicellulose starts at lower temperatures than cellulose. On the other hand, lignin decomposes more slowly, over a wider range of temperatures. According to [48], the decomposition of hemicellulose and cellulose takes place in the temperature range of 200°C–380°C and 250°C–380°C. While the lignin decomposition seems to appear from 180°C up to 600°C.

In addition to its structural and molecular characterisation, biomass can be characterised by proximate and ultimate analysis. The proximate analysis reveals its fuel moisture,

ash content, and its content in volatiles and fixed carbon. The elementary composition is determined by ultimate analysis. Typical ranges for the elementary composition of woody biomass (e.g., spruce, beech or willow) is shown in Table 2.2.

Table 2.2: Elementary composition of woody biomass, typical ranges (in wt$\%_{db}$) according to [38]

C	H	O	N	S	Cl	ash
47–50	5–7	40–45	0.10–0.60	0.01–0.05	<0.01	<1.5

Furthermore, the share of volatiles is also an important criterion for characterising the feedstock. For ligno-cellulose material, the fraction of volatiles is relatively high with a typical range of 74% to 83wt%, [38]. Besides, the quantitiy of elements might be specified at a molar basis, which is essential if reactions are to be discussed.

Simplified, the woody biomass (50wt$\%_{daf}$ carbon, 6wt$\%_{daf}$ hydrogen and 44wt$\%_{daf}$ oxygen) is specified by the molar content[1] (mol/kg$_{daf}$) of:

- $41.7\,\mathrm{mol_C/kg_{daf}}$,

- $60\,\mathrm{mol_H/kg_{daf}}$ and

- $27.5\,\mathrm{mol_O/kg_{daf}}$.

---

[1]in literature the molar composition is also given by the molar ratios H/C and O/C, which is $CH_{1.44}O_{0.66}$ for the present case

2.1.2 Process of conversion during gasification

The overall process may be distinguished into the phases of: heating up and drying of the fuel particle, pyrolytic decomposition, oxidation and reduction. However, the oxidation and reduction is only applicable to the authothermal process (e.g., air, O_2 as gasification agent). A model concept of the process of the conversion is sketched in Figure 2.5. Heating up and drying of the fuel particle takes place up to temperatures of $150\,°C$.
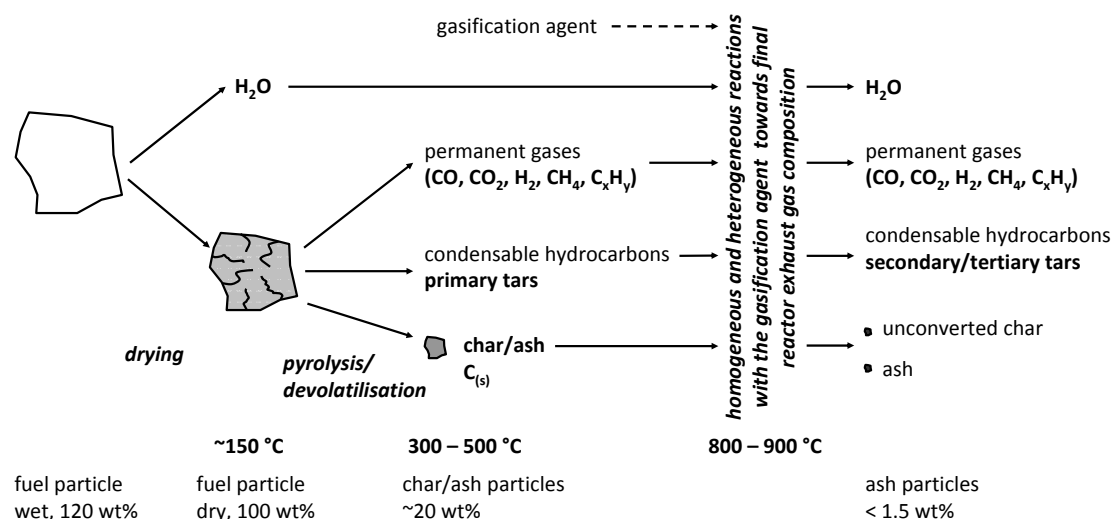
Figure 2.5: Schematic progress of the fuel particle conversion

The chemical structure is unaltered during this phase. Only the particle structure is changed by macroscopic and microscopic fissures. During the pyrolytic process ($150°C$–$500°C$) the structure (cellulose, hemicellulose and lignin) is decomposed and the volatiles (CO, CO_2, H_2, CH_4, H_2O, hydrocarbons) are released. The overall complex of volatiles contains a certain fraction of gaseous hydrocarbons, which are referred to as primary tars. The solid fraction which remains after the release of the volatiles is referred to as residual char or pyrolytic char. The overall process is endothermic. The heat balance of the process is principally influenced by the fuel water content.

During the conversion process of gasification the feedstock comes into contact with the oxygen-containing gasification agent. The gasification agent effects:

- the conversion (heterogeneneous reactions) of the residual char, which remains after the pyrolytic decomposition/devolatilisation,

- the conversion/reforming (homogeneous reactions) of gas species, which are released during pyrolytic decomposition/devolatilisation).

18

Beside the favoured gaseous combustable product (H_2, CO, CH_4, C_2-C_5), certain impurities are formed during the conversion process:

- inorganic gaseous species (NH_3, H_2S, HCl) attributed to the input in N, S and Cl,

- organic gaseous/condensable hydrocarbons[2] and

- solid impurities/particulates caused by unreacted charbon and the ash, which is mainly composed of Ca, Na, Si, and K.

2.1.3 Reactions, thermodynamics and reaction equilibria

Basically, the heterogeneous reactions involve the reaction of solid carbon with the present gaseous species (gasification agent), see Eqs. 2.1 to 2.5.

$$C + O_2 \quad \longrightarrow \quad CO_2 \qquad \Delta H^0_{R,850} = -394.9\,\text{kJ/mol} \qquad (2.1)$$

$$C + {}^1\!/2O_2 \quad \longrightarrow \quad CO \qquad \Delta H^0_{R,850} = -112.7\,\text{kJ/mol} \qquad (2.2)$$

$$C + H_2O \quad \longrightarrow \quad CO + H_2 \qquad \Delta H^0_{R,850} = +135.7\,\text{kJ/mol} \qquad (2.3)$$

$$C + CO_2 \quad \longrightarrow \quad 2CO \qquad \Delta H^0_{R,850} = +169.4\,\text{kJ/mol} \qquad (2.4)$$

$$C + 2H_2 \quad \longrightarrow \quad CH_4 \qquad \Delta H^0_{R,850} = -89.8\,\text{kJ/mol} \qquad (2.5)$$

A reversible chemical reaction can be generally expressed according to Eq. 2.6.

$$|\nu_A|\,\text{A} + |\nu_B|\,\text{B} \rightleftharpoons |\nu_C|\,\text{C} + |\nu_D|\,\text{D} \qquad (2.6)$$
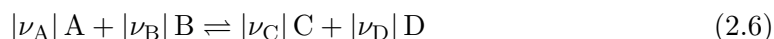
The reaction is characterised by forward and reverse reactions. Forward and reverse reactions may occur simultaneously. In case of chemical equilibrium, the forward and reverse reactions have the same reaction rate (kinetic). Practically, in macroscopic terms, the conversion does not proceed anymore in equilibrium. Thus, the share of the involved species remain at the same quantities. The relation of the quantitative amount of reagents to products in equilibrium is defined as the equilibrium constant (K_p), Eq. 2.7.

$$K_p = \prod_i (p_i^*)^{\nu_i} = \frac{(p_C)^{\nu_C} \cdot (p_D)^{\nu_D}}{(p_A)^{\nu_A} \cdot (p_B)^{\nu_B}} \qquad (2.7)$$

The stoichiometric coefficients (ν_i) are signed: reagents are negative, products are positive. For homogeneous reactions (gas–gas reactions) the amount of a species is equivalent to the partial pressure (p_i) of the species. In case of solid species (heterogeneous reactions) p_i=1 by default. The position of equilibrium describes the direction (e.g., towards the products) of the reaction progress. In the case of a position of equilibrium at the side of the reactants, the reaction may occur towards the products. The reaction equilibra versus temperature (at 1 bar) for the heterogeneous reactions Eqs. 2.1 to 2.5 are shown in Figure 2.6. HSC Chemistry [50] was applied to calculate K_p.

---

[2]the character and nature of the condensable hydrocarbons is further detailed in Section 2.2
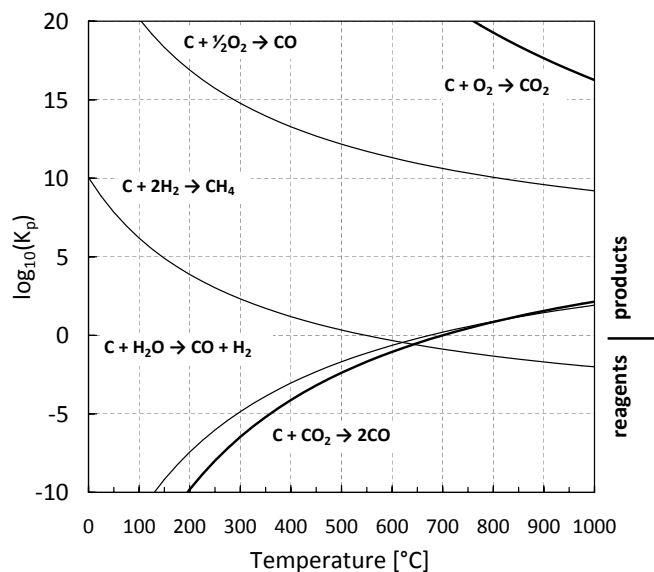
Figure 2.6: Heterogeneous reaction equilbria versus temperature, at 1 bar

In particular, the position of equilibrium of the oxdiation reactions Eqs. 2.1 and 2.2 is predominately at the product side. A equilibrium constant K_p of 1 is the limiting case as this state is not necessarily achieved in an actual reaction progress.

Futhermore, the reaction kinetics essentially determine the extent of the reaction as this is a parameter which is limited by the residence time. The kinetic reaction rates for the char gasification are considerably lower than that of pyrolysis and devolatilisation, respectively, [51].

Table 2.3: Relative rates of reaction during the gasification process at 800 °C and 1 atm, adapted from [51]

Reaction	Eq.	Relative rate
pyrolysis	-	10^6
carbon oxidation,	2.1	10^5
heterogeneous water gas reaction	2.3	3
Boudouard reaction	2.4	1
hydrogasification	2.5	10^{-3}

Hence, the overall progress is determined by the kinetics of the heterogeneous reactions Eqs. 2.3 to 2.5. Table 2.3 shows the kinetic rates (summarised by [51]) of the pyrolysis and the heterogeneous char gasification relative to the Boudouard reaction (Eq. 2.4). Thus, it appears that the extent of the heterogeneous water gas reaction (Eq. 2.3) may be higher than the Boudouard reaction (Eq. 2.4). The kinetics of the hydrogasification (Eq. 2.5) are apparently very slow, so that this reaction may be almost neglected. Moreover,

at appropriate gasification temperatures of 800°C–900°C, the position of equilibrium for the hydrogasification is at the side of the reagents.

Important homogeneous reactions are listed as follows in Eqs. 2.8 to 2.12. The list also includes the oxidation of the gas species H_2 and CO.

$$CO + \text{\textonehalf} O_2 \quad \longrightarrow \quad CO_2 \qquad \Delta H^0_{R,850} = -282.1\,\text{kJ/mol} \qquad (2.8)$$

$$H_2 + \text{\textonehalf} O_2 \quad \longrightarrow \quad H_2O \qquad \Delta H^0_{R,850} = -248.5\,\text{kJ/mol} \qquad (2.9)$$

$$CO + H_2O \quad \longleftrightarrow \quad CO_2 + H_2 \qquad \Delta H^0_{R,850} = -33.6\,\text{kJ/mol} \qquad (2.10)$$

$$CH_4 + H_2O \quad \longleftrightarrow \quad CO + 3H_2 \qquad \Delta H^0_{R,850} = +225.5\,\text{kJ/mol} \qquad (2.11)$$

$$CH_4 + CO_2 \quad \longleftrightarrow \quad 2CO + 2H_2 \qquad \Delta H^0_{R,850} = +259.1\,\text{kJ/mol} \qquad (2.12)$$

Further reactions, which involve the decomposition of tar (e.g., via steam and dry reforming) are shown in Section 2.2.2. The reaction equilibria versus temperature (at 1 bar) for the homogeneous reactions (Eqs. 2.8 to 2.12) are shown in Figure 2.7. The equilibrium contant K_p was calculated with HSC Chemistry, [50].
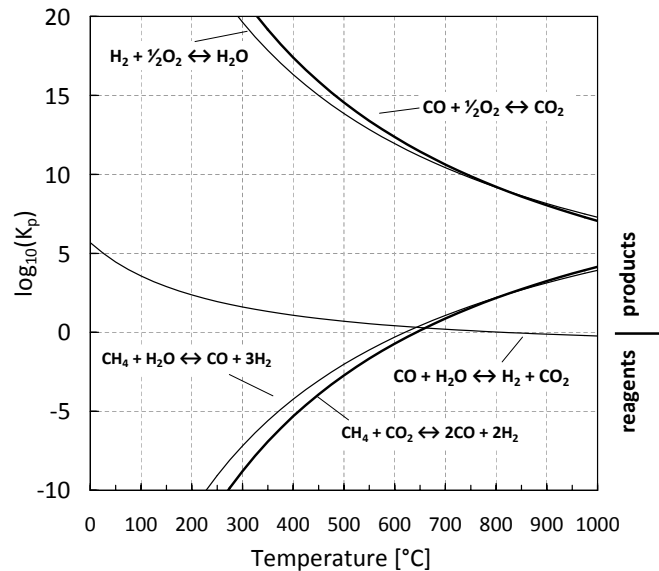
Figure 2.7: Homogeneous reaction equilbria versus temperature, at 1 bar

At temperatures above $800\,°\text{C}$, which is a typical process temperature for gasification, the position of the reaction equilibria are strongly at the product side (CO, H_2, H_2O) except for the water–gas shift reaction (Eq. 2.10). Between 800°C–900°C the equilibrium constant (K_p) is close to 1 for the water–gas shift reaction (Eq. 2.10). Thus, almost similar quantities of reagents and products are present.

Apart from the thermodynamic equilibria of individual reactions, the thermodynamic gas-phase equilibrium for the $C_xH_yO_z$ and H_2O (see also Eq. 2.14) might be considered. The software HSC Chemistry [50] was used to calculate the thermodynamic equilibria. The gas phase equilibrium calculation considers the thermodynamical gas species stability:

- CO, CO_2, H_2, CH_4, H_2O are gas species, which are fully or partially stable (thermodynamical) at temperatures of 500°C–1000°C,

- light hydrocarbons (e.g., C_2H_4, C_2H_6 or C_3H_8) and condensable hydrocarbons (tar, e.g., naphthalene) are omitted as these components are not stable at temperatures above 500 °C.

Figures 2.8(a–f) present the gas phase equilibrium composition for the system $C_xH_yO_z$[3] versus temperature at 1 bar for different steam-to-fuel ratios. The definiton for $\varphi_{SF,wt}$ is given in Eq. 2.16 in Section 2.1.4. It appears that the equilibrium gas composition is clearly influenced by the steam-to-fuel ratio. In case of $\varphi_{SF,wt}$=0.2, H_2O is almost consumed at temperatures above 800 °C. Thus, in this case the present $C_xH_yO_z$ system is almost in stoichiometric conditions. Further details on the stoichiometric case of steam gasification are presented in Section 2.1.4 and in Paper V. The equilibrium composition for the steam-to-fuel ratios ≥ 0.4 as shown in Figures 2.8 b–f is characterised by an increasing fraction of H_2O in the gas composition as H_2O is not consumed completely. The steam-to-fuel ratio of 0.8 is close to the steam-to-fuel ratio usually applied in the experiments of this work, see Papers V and VI. Table 2.4 shows the molar fraction of the involved gas species for a steam-to-fuel ratio of 0.8 at 850 °C (see also Figure 2.8 d).

Table 2.4: Volume fraction (vol%) of involved gas species at thermodynamic equilibrium for steam-to-fuel ratio of 0.8 at 850 °C

Reference	Unit	H_2	H_2O	CO	CO_2	CH_4
wet	vol%	47.1	16.8	27.3	8.7	0.0
dry	vol%$_{db}$	56.6	–	32.8	10.5	0.0

Further comparable thermodynamic studies and calculations of equilibrium gas composition are published by Trommer [52], Prins [53], Damiani and Trucco [54], Salaices [55], and Detournay et al. [56].

---

[3]parameterised by wood pellets used in this study; $x = 42, y = 60, z = 27$, see also Paper V or VI

The thermodynamic analysis of the product gas also involves an assessment of the deviation of the actual gas phase (product gas) composition from that of the thermodynamic equilibrium state. Thus, the logarithmic deviation of the actual product gas composition according to the CO-shift equilibrium is calculated according to Eq. 2.13. The actually measured gas phase partial pressure of the species i is expressed as p_i and ν_i is the stoichiometric factor (ν_{CO_2} and ν_{H_2}=1, ν_{CO} and ν_{H_2O}=-1) of the species i.

$$p\delta_{eq,CO-shift}\left(p_i,T\right) = log_{10}\left[\frac{\prod\limits_i p_i^{\nu_i}}{K_{p,CO-shift}\left(T\right)}\right] \qquad (2.13)$$

In the case where $p\delta_{eq,CO-shift} < 0$, the actual ratio of the (CO-shift involved) species is below equilibrium constant ($K_{p,CO-shift}$). Thus, a continuing progress of the reaction towards the product side is possible. By contrast, values of $p\delta_{eq,CO-shift} > 0$ indicate that the actual ratio of the species is above the equilibrium constant.

(a) $\varphi_{SF,wt}=0.2$

(b) $\varphi_{SF,wt}=0.4$

(c) $\varphi_{SF,wt}=0.6$

(d) $\varphi_{SF,wt}=0.8$

(e) $\varphi_{SF,wt}=1.0$
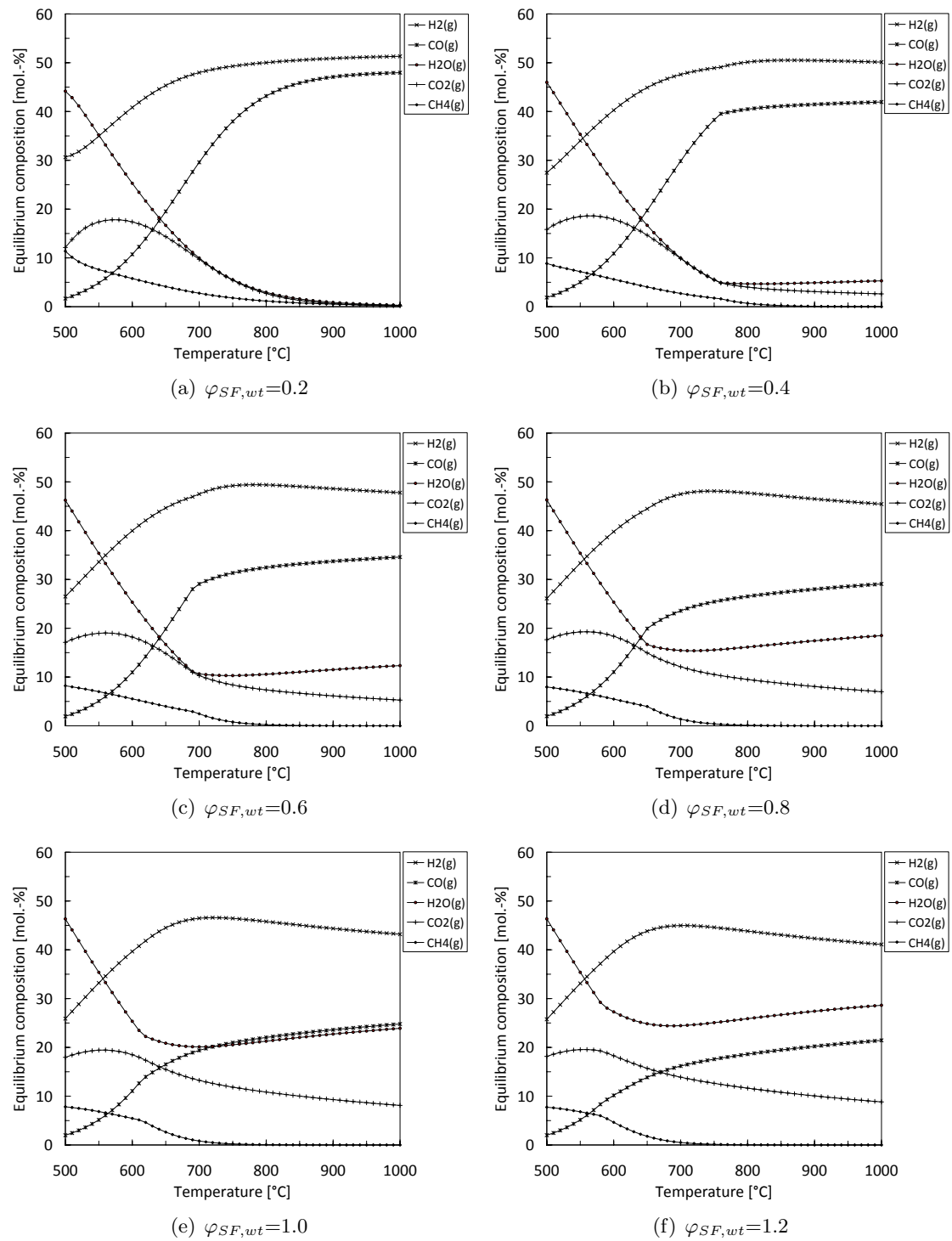
(f) $\varphi_{SF,wt}=1.2$

Figure 2.8: Thermodynamic equilibrium for the system $C_xH_yO_z$ (x=42, y=60, z=27; wood pellets used in this study) versus temperature for different steam-to-fuel ratios at 1 bar

2.1.4 Global mass and species balance considerations

Figure 2.9 presents the essential material flows for the gasification reactor, in which steam is used as the gasification agent. The species and mass balance consideration in this section refer to this scheme. Gasification aims at the decomposition of the initial

Figure 2.9: Global mass and species balance for the gasification reactor

high molecular structure of the organic matter. In terms of the production of syngas, the gaseous species CO and H_2 are the favoured products, which present the final state of decomposition. The idealised overall reaction for gasification of biomass can be expressed as shown in Eq. 2.14.

$$C_xH_yO_z + (x-z)H_2O \rightarrow xCO + (\frac{y}{2}+x-z)H_2 \quad (x \geq z) \quad \Delta H^0_{R,850} > 0\,\text{kJ/mol} \quad (2.14)$$
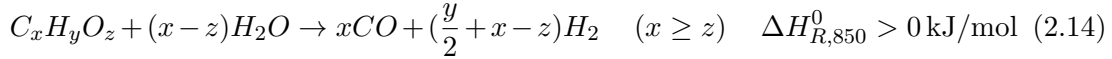
The stoichiometric H_2O demand (Φ_{H_2O}) related to the system $C_xH_yO_x$ is defined by Eq. 2.15. This theoretical steam demand equals the amount of water per fuel unit (dry and ash free) required for full conversion.

$$\Phi_{H_2O} = x - z \quad (2.15)$$

The global mass balance, which involves the feedstock and the gasification agent (H_2O), is characterised by the steam-to-fuel ratio, which relates the total steam input to the fuel input (dry and ash free), Eq. 2.16. To compare different feedstocks, the total steam input can be related to the carbon input on the weight and molar bases, respectively, Eq. 2.17 and Eq. 2.18.

$$\varphi_{SF,wt} = \frac{\dot{m}_{H_2O} + \mu_{H_2O} \cdot \dot{m}_{fuel}}{(1 - \mu_{H_2O} - \mu_{ash}) \cdot \dot{m}_{fuel}} \quad (2.16)$$

$$\varphi_{SC,wt} = \frac{\dot{m}_{H_2O} + \mu_{H_2O} \cdot \dot{m}_{fuel}}{\mu_C \cdot \dot{m}_{fuel}} \quad (2.17)$$

$$\varphi_{SC,mol} = \frac{2}{3} \cdot \frac{\dot{m}_{H_2O} + \mu_{H_2O} \cdot \dot{m}_{fuel}}{\mu_C \cdot \dot{m}_{fuel}} \quad (2.18)$$

In terms of the stoichiometry of the system $C_xH_yO_z$ and $(x-z)\,H_2O$, the stoichiometric H_2O ratio (λ_{H_2O}) is defined by Eq. 2.19, wherein $\dot{m}_{H_2O,act.}$ is the actual feed of water into the gasifier and $\dot{m}_{H_2O,stoich.}$ is the stoichimetric feed of the water. Some calculations with regard to this value are given in Paper V.

$$\lambda_{H_2O} = \frac{\dot{m}_{H_2O,act.}}{\dot{m}_{H_2O,stoich.}} \quad (2.19)$$

The gasification agent (H_2O) is consumed within the process due to gas–gas or gas–solid reactions, which involve H_2O as reactant. Principally, the high share of hydrogen originating from H_2O as the elemental fraction of hydrogen (in wt%) in woody biomass is low (see Table 2.2). The highest fraction of water is converted by the water–gas shift reaction, Eq. 2.10. As hydrogen is a favoured gas species in the product gas, obtaining a high rate of water conversion is the aim. To assess and compare the water conversion in the gasifier, the quantity of water which is converted ($\dot{m}_{H_2O,conv.}$) in the gasifier might be related to various bases:

- related to the total input of water, which is referred to as the absolute water conversion, $X_{H_2O,abs}$; see Eq. 2.20,

$$X_{H_2O,abs} = \frac{\dot{m}_{H_2O,conv.}}{\dot{m}_{steam} + \mu_{H_2O} \cdot \dot{m}_{fuel}} = \frac{X_{H_2O,rel}}{\varphi_{SF,wt}} \qquad (2.20)$$

- related to the fuel input (dry and ash free), which is referred to as the relative water conversion, $X_{H_2O,rel}$; see Eq. 2.21 and

$$X_{H_2O,rel} = \frac{\dot{m}_{H_2O,conv.}}{(1 - \mu_{H_2O} - \mu_{ash}) \cdot \dot{m}_{fuel}} = X_{H_2O,abs} \cdot \varphi_{SF,wt} \qquad (2.21)$$

2.2 Tar
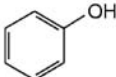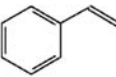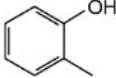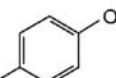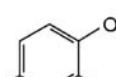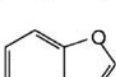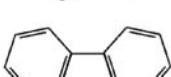
2.2.1 Definition, properties and classification

The term *tar* is often used in the literature. However, there is no common agreement on the definition of tar. In general, the term tar describes a mixture of condensable organic hydrocarbons with a molar mass higher than benzene ($78.1 \, \mathrm{g/mol}$). According to the tar guideline [57], tar is:

Generic (unspecific) term for entity of all organic compounds present in the producer gas excluding gaseous hydrocarbons (C1 through C6). Benzene is not included in tar.
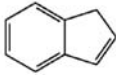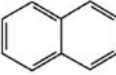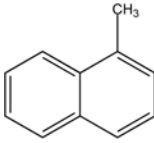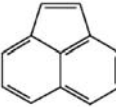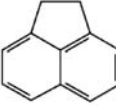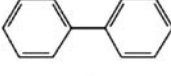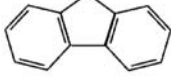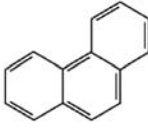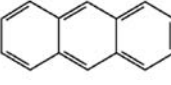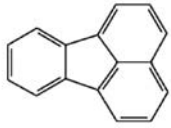
The main property of tar is the high boiling point of its constituents (e.g., naphthalene $218 \, °\mathrm{C}$), which is increasing with molecular mass. The condensation of tar causes clogging or blockages in downstream process units (e.g., heat exchanger) of the gasifier. Typical representatives of tar and their properties are listed in Tables 2.5 and 2.6, (data from [58]).

Table 2.5: Typical representatives of tar from biomass gasification, data from [58]

Species	Structure	Chemical formula	Molar mass [g/mol]	Melting point [°C]	Boiling point [°C]
Phenol		C_6H_6O	94.11	43	182
Styrene		C_8H_8	104.15	-30.63	145.2
2-Methylphenol		C_7H_8O	108.18	31	191
4-Methylphenol		C_7H_8O	108.18	35	202
2,4-Dimethylphenol		$C_8H_{10}O$	122.17	26	211.5
Benzofuran		C_8H_6O	118.14	-	173-174
Dibenzofuran		$C_{12}H_8O$	168.19	86-87	287

continuation next page

Table 2.6: Typical representatives of tar from biomass gasification, data from [58]

Species	Structure	Empirical formula	Molar mass [g/mol]	Melting point [°C]	Boiling point [°C]
1H-indene		C_9H_8	116.16	-1.8	182.6
Napthalene		$C_{10}H_8$	128.17	80.2	218
1-Methylnaphthalene		$C_{11}H_{10}$	142.20	-30.5	245
Acenaphtylen		$C_{12}H_8$	152.20	92	265
Acenaphten		$C_{12}H_{10}$	154.21	96.2	279
Biphenyl		$C_{12}H_{10}$	154.21	70.72	255
Fluorene		$C_{13}H_{10}$	166.22	115	298
Phenanthrene		$C_{14}H_{10}$	178.23	101	340
Anthracene		$C_{14}H_{10}$	178.23	218	340
Fluoranthene		$C_{16}H_{10}$	202.26	110	384
Pyrene		$C_{16}H_{10}$	202.26	150	393

Condensation of tar depends on the tar dewpoint temperature. At the dewpoint temperature, the actual partial pressure of the tar or a certain component equals its saturation pressure. Thus, a further property for characterising a tar mixture of specific components is the saturation vapour pressure and the saturation concentration. Depending on the process temperature reached in the downstream process unit, the dewpoint temperature is undercut or not. Figures 2.10 and 2.11 show the saturation vapour pressure and the saturation concentration versus temperature for selected tar components, see also Tables 2.5 and 2.6. The data for the saturation vapour pressure are taken from the Landolt-Börnstein Database [59] and the saturation concentration was calculated using the ideal gas law. It is apparent that the saturation vapour pressure decreases with increasing
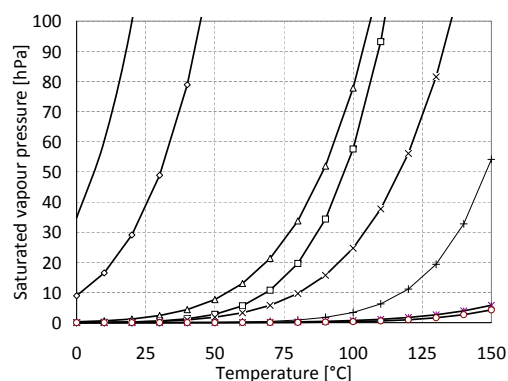
Figure 2.10: Saturation vapour pressure versus temperature for different tar species, at 1 bar
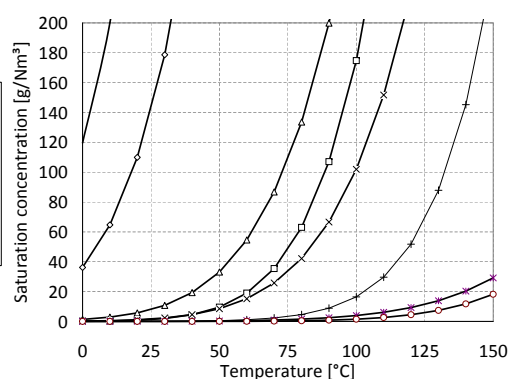
Figure 2.11: Saturation concentration versus temperature for different tar species, at 1 bar

molecular size of a species. The dewpoint (lower limit) is dominated by the fraction of higher molecular tars (aromatics).

In order to categorise the overall mixture of tar which arises within the process, different aspects (oriented to the process or the character of the tar) may be used for an appropriate classification. In the literature the process temperature and the tar substance groups have gained general acceptance:

- **Temperature based classification** into primary (400°C–700°C), secondary (700°C–850°C) and tertiary (850°C–1000°C) tars according to their temperature of formation or the process temperature. This classification was set up by Milne et al. [60] and is based on the work by Evans and Milne [61–63]. The primary tars are characterised by oxygenated compounds and the secondary tars by phenols, olefines and monoaromatic hydrocarbons. The tertiary tars are characterised by polyaromatic hydrocarbons. This class may be further subdivided into: alkyl tertiary products (e.g., methyl derivates of aromatics) and condensed tertiary products (polyaromatic hydrocarbons), which show polynuclear chains (e.g., of benzene or naphthalene) without substituents. Figure 2.12 shows the fractional distribution of the tar classes as a function of the temperature, Evans and Milne [63].
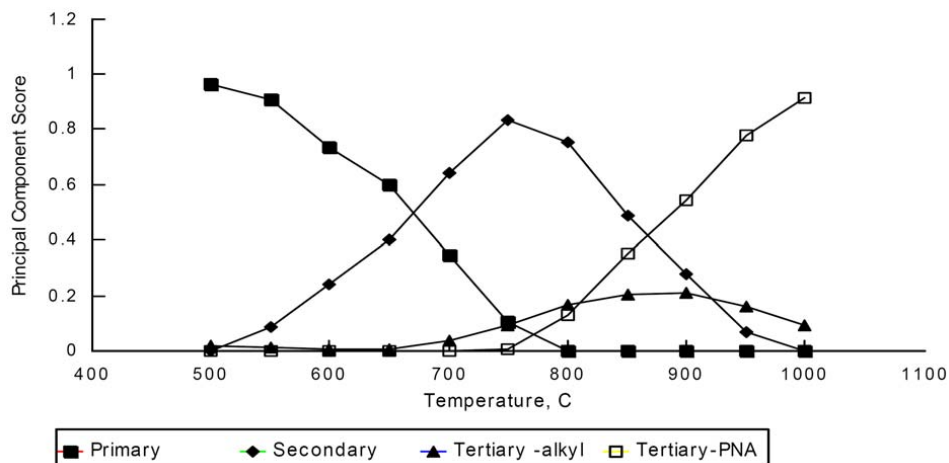
Figure 2.12: Fractional distribution of tar classes as a function of temperature (at 300 ms gas-phase residence time), Evans and Milne [63] (PNA = polynuclear aromatic hydrocarbons, other term for PAH)

- **Tar substance group/class[4] based classification** into:
  - five substance classes as proposed by the Energy Research Centre of the Netherlands (ECN) [64, 65]: *CLASS I: GC-undetectable (heaviest) tars; CLASS II: heterocyclic aromatics; CLASS III: aromatics (1-ring) compounds; CLASS IV: light PAH compounds (2–3 ring) and CLASS V: heavy PAH compounds (4–7 ring).*
  - six substance groups as proposed by Corella et al. [66]: *benzene, 1-ring compounds, naphthalene, 2-ring compounds, 3- and 4-ring compounds and phenolic compounds.*
  - eight substance classes as proposed by Wolfesberger et al. [67]: *phenols, furans, aromatic compounds, aromatic nitrogen compounds, naphthalenes, polyaromatic hydrocarbons (without naphthalenes), guaiacols*
  - eight compound class as proposed by Morf [51]: *acids, sugars, ketones, phenols/cresols, guaiacols, furans, BTX, PAH*

Besides the latter classification, other categories have been reported in the literature, but have no significance, e.g.:

- classification according to the type of gasifier (counter-current, co-current, fluidised bed)

- characterisation according to Perez et al. [68] or Corella et al. [69] of the tar into the groups *easy to destroy* and *hard to destroy*

---

[4]group and classe are used as similar terms

At present, the classifications of Milne and of ECN are the most used in the literature. Some of the components classified by Milne et al. [60] appear together in the second and primary or tertiary group. Thus, the groups are partially overlapping without fixed boundaries in their temperature based development, see also Figure 2.12. The ECN classification is more detailed with regard to the polyaromatic compounds, which are generally classified as tertiary tars according to Milne. The ECN classification aims at differentiating by physical tar properties (water solubility and condensation). In contrast to the ECN, Milne et al. uses the approach of describing the temperature evolutionary development, which is established by taking the pyrolysis as the initial point. Morf et al. [70] suggest a breakdown of the Milne categories based on chemical structure, which is comparable to ECN. The tar measurement method applied in this work is detailed in Section 3.3. The methods yield a gravimetric tar fraction (referred to as gravimetric tar) and a GCMS detectable tar fraction (referred to as GCMS tar). Based on the measurement method, the tar is specified as gravimetric tar or GCMS tar, see Section 3.3 or Paper V. The gravimetric tar corresponds to the CLASS I (GC-undetectable) of ECN. The GCMS tar can be divided into the ECN classification of CLASS II to V. A detail listing of the GCMS components and their classification according to ECN as well as Milne can be found in Paper V.

2.2.2 Formation, conversion and decomposition

The terms *primary*, *secondary* and *tertiary* tar have become prevalent in the literature. A favourable aspect of these terms is that they describe the evolution and reaction progress over temperature, which have undergone the process (impact of temperature) starting from the initial point of pyrolysis. Thus, by means of these categories, the formation of the tars might be pictured. On the other hand, the term *secondary (tar) reactions*, which is frequently used in the literature, does not solely refer to the reactions which yield secondary tars. The secondary tar reactions involve reactions progressing from the initially produced primary tars to their conversion into secondary and/or tertiary tars. Fundamental work on the evolution and maturation of pyrolysis products (secondary tar reactions) was published by Elliott [71], Evans and Milne [61, 62], Egsgaard and Larsen [72], and Morf [51].
The findings of Evans and Milne [61] of the pyrolysis pathway over temperature are pictured in Figure 2.13. A similar pathway is given by Elliott [71].
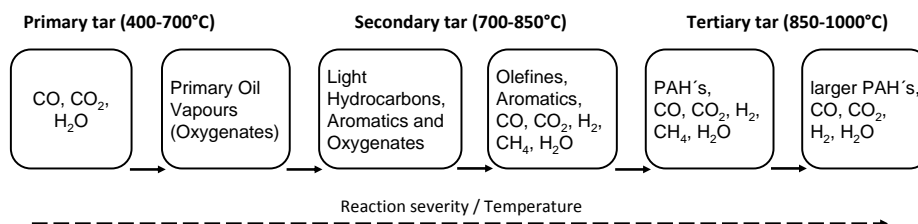
Figure 2.13: Pyrolysis pathway according to Evans and Milne [61]

Primary tars are the first products, which are produced during the initial progress of pyrolysis. The macro-molecular structure of the fuel particle is decomposed under the release of volatiles including condensable gases. In particular the decomposition of the polymer lignin yields the tar compounds phenol, cresol, and guaiacol, [73].

The combination of increasing temperature and the presence of further reactants (H_2O, CO_2) promotes the reaction towards secondary tar products, which are alkylated aromatics with one or two benzene rings. The principal mechanisms for the conversion of primary into secondary tar are dehydration or decarboxylation, [74, 75]. Typical representatives are: toluene, xylene, indene, styrene, and 1/2-methylnaphthalene.

The formation of tertiary tars (PAH) mainly occurs at temperatures above 850 °C. Alkyl groups or hetercylic aromatic compounds are decreasingly existent but the spectrum is characterised by stable PAH with more than one benzene ring. Typical representatives are: benzene, naphthalene, phenantren, anthracene, pyrene, and larger PAH. Larger PAH (with increasing molecular mass, e.g., coronene) are products of PAH growth reactions by combining small aromatic compounds or unsaturated hydrocarbons through condensation, dimerisation, or polymerisation, [21, 65].

The feedstock structure (lignin, cellulose, hemicellulose) seems to have an impact on the character of the primary tar products, as these compounds will have a molecular structure with similar functional groups as the precursor monomer, Evans and Milne [61]. The molecular structure of lignin involves a hydroxide (-OH), alkyl ($-C_nH_{2n+1}$), or methoxy group ($-OCH_3$) connected to a phenyl group (C_6H_5), see Figure 2.3. Thus, this lignin structure is apparently a precursor for the formation of phenol as primary tar.

In particular, the tertiary tars (large PAH) or the Class 1 and Class 5 tars according to ECN, are very stable and hard to convert. Several authors have reported that temperatures of 1100°C–1300°C are required in combination with appropriate residence times to effect the thermal decomposition of these hydrocarbons, [51, 60, 65, 73, 76]

Decomposition of tar is a complex process, which may involve several reactions and subprocesses. Principally, the decomposition of a tar species can occur through steam and dry reforming towards the final stable products CO and H_2. The global reaction for steam reforming and dry reforming, which are considered to be catalysed by solids, are given in Eq. 2.22 and 2.23.

$$C_xH_y + xH_2O \quad \xrightarrow{cat.} \quad xCO + (x + \frac{y}{2})H_2 \qquad \Delta H^0_{R,850} > 0\,\mathrm{kJ/mol} \qquad (2.22)$$

$$C_xH_y + xCO_2 \quad \xrightarrow{cat.} \quad 2xCO + \frac{y}{2}H_2 \qquad \Delta H^0_{R,850} > 0\,\mathrm{kJ/mol} \qquad (2.23)$$
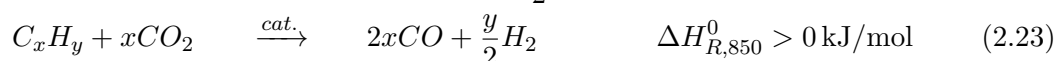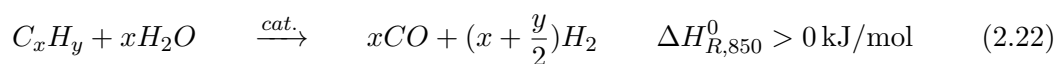
In detail, the process of reforming occurs via several intermediate steps and intermediate products. Further possible reactions, which may occur [77, 78] are listed below, Eq. 2.24 to 2.27. Toluene (C_7H_8) is taken as a sample to elucidate hydro-cracking, steam-dealkylation and hydro-dealkylation. The initial tar is generalised by the formula: C_xH_y and C_mH_n refer to the tar with lower molecular weight.

thermal cracking: $\qquad aC_xH_y \qquad \xrightarrow{cat.} \qquad bC_mH_n + cH_2 \qquad$ (2.24)

hydro-cracking: $\qquad C_7H_8 + 10H_2 \qquad \xrightarrow{cat.} \qquad 7CH_4 \qquad$ (2.25)

steam dealkylation: $\qquad C_7H_8 + H_2O \qquad \xrightarrow{cat.} \qquad C_6H_6 + 2H_2 + CO \qquad$ (2.26)

hydro-dealkylation: $\qquad C_7H_8 + H_2 \qquad \xrightarrow{cat.} \qquad C_6H_6 + CH_4 \qquad$ (2.27)

At reasonable gasification temperatures ($> 800\,°C$), the latter reactions are considered as irreversible as higher hydrocarbons are involved, [77]. The thermodynamic reaction equilibria of steam and dry reforming for the model compounds naphthalene ($C_{10}H_8$) and anthracene ($C_{14}H_{10}$) are shown in Figure 2.14. Thus, it appears that at high temperatures the equilibria are strongly at the side of CO and H_2.
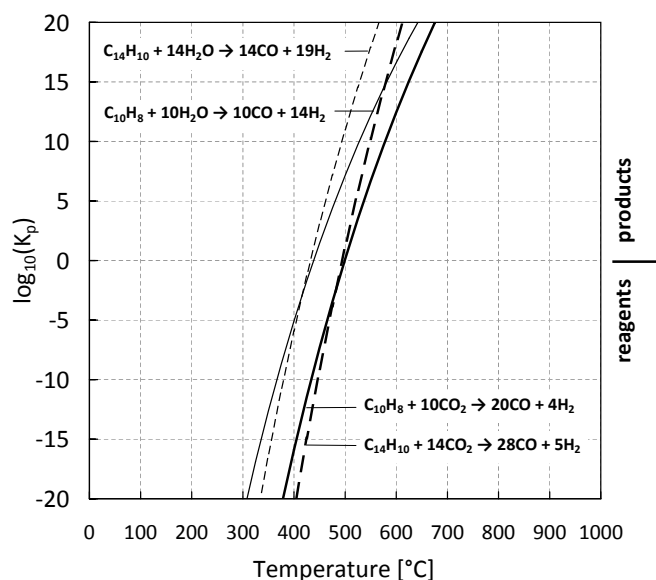
Figure 2.14: Reaction equilbria of steam and dry reforming of naphthalene and anthracene versus temperature, at 1 bar

The occuring reactions during tar decomposition may be categorised into [51]:

- homogenous gas-phase reactions (e.g., thermal cracking, partial oxidation, re-polymerisation) and

- heterogenous (catalysed) reactions, which may occur on the particle surfaces.

Generally, the heterogenous reactions are considered to be catalysed by solids. However, also the homogenous gas-phase reaction can occur at appropriate surfaces.

2.3 Fundamentals of fluidised bed technology

This section highlights the essential fundamentals of fluidisation technology. The subject is only touched on, to emphasise the basics. As fluidisation is an extensive subject, which is well described in the scientific literature, the author refers to the relevant published literature given by Yang [79], Kunii and Levenspiel [80], Fan and Zhu [81] and Grace et al. [82,83].

When a gaseous fluid is contacted by an upward flow with a fixed bed of particles, different hydrodynamic conditions will arise depending on the volume of the flow and the superficial velocity of the fluid. The different patterns of hydrodynamic gas–solid regimes are sketched in Figure 2.15, [84].
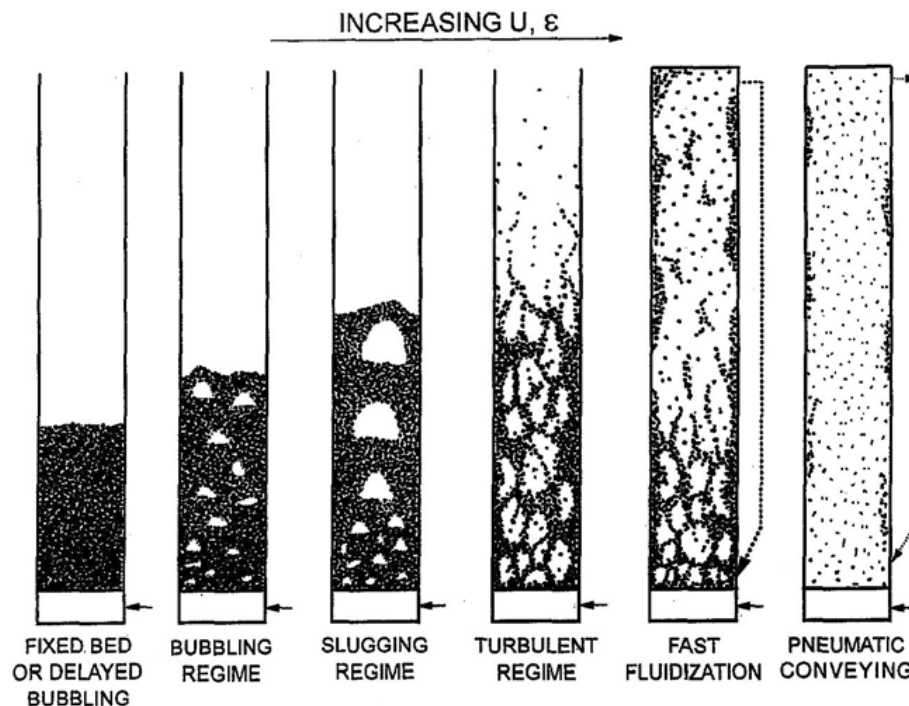
Figure 2.15: Scheme of gas–solid flow patterns in fluidised beds (adapted from [84])

The solid particle inventory will remain in a fixed position (fixed bed) at low gas velocities. At a sufficient gas velocity, which is the minimum fluidisation velocity (U_{mf}), the bed of particles starts to be fluidised. At the minimum fluidisation velocity, the frictional force between the particle and the upward flowing fluid counterbalance the weight of the particle.

An expansion of the fluidised bed is caused by a further increase of the gas velocity. In most cases, dependent on the particle properties (particle density and particle size), a bubbling fluidisation regime is developed at a gas velocity slightly above the miniumum fluidisation velocity, which is referred to as the bubbling fluidised bed. The bubbling

regime changes to a slugging regime if the bubble size becomes comparable with the column diameter. However, this characteristic is only valid for sufficient bed height and specific particle properties such as particle density and particle size and is typically observed in small installations or at small column diameters. A further increase of the gas velocity enhances the hold-up of the particles and causes a considerably higher turbulency of the particles in the column. At a significant gas velocity (U_{se}) and above, fast fluidisation occurs, which causes a progressive entrainment of particles. At that point a constant solid particle inventory is maintained through continuous recycling of separated particles from the gas stream to the bed. Finally, at even higher gas velocities, pneumatic conveying arises, where no axial variation of particle concentration occurs except in the bottom (acceleration) zone, [82].

The gas–solid flow patterns (Figure 2.15) exhibit different characteristics of distribution of the particle inventory over the height of the column. The void fraction of the bed (voidage or fraction void) ε_f, which emerges between the particles, relates the volume of the fluid to the total volume of the fluid–solid suspension. By contrast, the fraction of solids in the fluid–solid suspension is (Eq. 2.28):

$$\varepsilon_s = 1 - \varepsilon_f \tag{2.28}$$

Typical distributions of solids over the height characterised by the fraction of solids are shown in Figure 2.16.
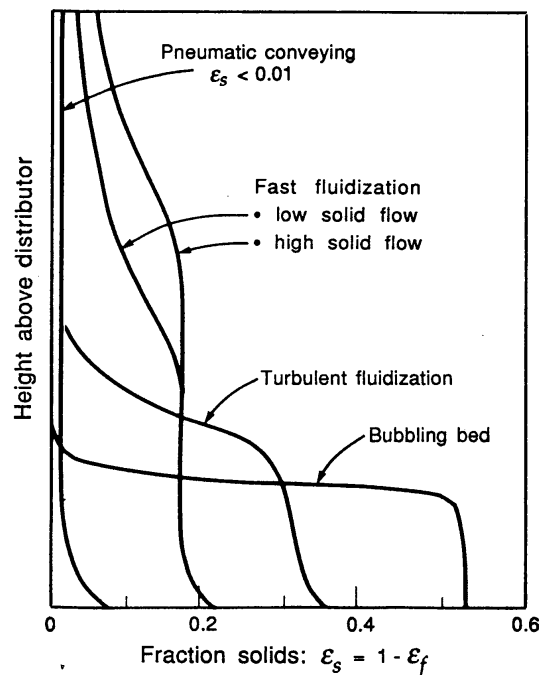
Figure 2.16: Profiles of the solids fraction (ε_s) over height for different regimes of fluidisation (adapted from [80])

It appears that each fluidisation regime offers a different profile, which is identified by a zone of intense or lean solid fractions. Typically, bubbling bed reactors have a bottom zone rich in solids followed by a freeboard zone, which is almost free of particles except the very fine particle fraction. But in the turbulent bed or fast fluidised bed regimes, the solids are more spread over the height.

The onset of the particle fluidisation and the boundaries of the transition regimes are very much dependent on the particle characteristics:

- the particle density ρ_p,

- the particle diameter d_p,

- particle shape, and

- particle distribution.

Dependening on the particle characteristics, Geldart [85], has classified the particles into four different groups, which distinguish their fluidisation behaviour, see Figure 2.17.
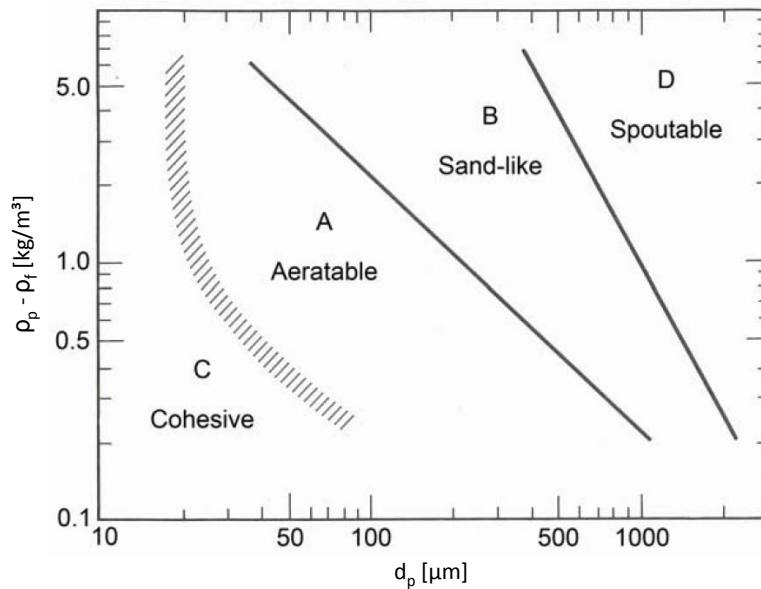
Figure 2.17: Geldart particle classification for air at ambient conditions (adapted from [80])

The fluidisation properties of the groups are described in brief by Kunii and Levenspiel [80] as follows (sorted from smallest to largest):

- *Group C*: cohesive or very fine powders, which are extremely difficult to fluidise owing to great interparticle forces. Face powder, flour, and starch are typical examples of group C particles.

- *Group A*: aeratable materials, or materials with a small mean particle size and/or low density. These particles fluidise easily with smooth fuidisation at low gas velocities and controlled bubbling at higher gas velocities.

- *Group B*: Group B: sand-like particles with increased particle size and particle density ($40 < d_p < 500\ \mu$mand $1.4 < \rho_p < 4.0$ kg/m^3, respectively). These particles fuidise well and show intense bubbling action with bubbles that grow large.

- *Group D*: spoutable or large and/or dense particles. Deep beds of these particles are hard to fluidise. Severe channeling and spouting behavior is observed when the gas distribution is very uneven. Drying grains, coffee beans, gasifying coal, and some roasting metal ores are examples of group D particles.

However, the classification of Geldart [85] is based on an experimental study at ambient conditions with air as fluidisation agent. As this classification does not account for behaviour apart from ambient condition, several authors have revised and modified the Geldart diagramme with respect to conditions of elevated pressure and temperature. For more details, the author refers to the studies by Yang [86] or Yates [87].

In the following, a set of equations is provided to describe some basic characteristics of fluidised beds. Independently of the gas velocity, the pressure drop is almost constant over the fluidised bed (or bed length L). The pressure drop is determined by the gravitational force of the solids inventory, see Eq. 2.29

$$\Delta p \approx \frac{m \cdot g}{A} \approx (\rho_p - \rho_g)(1 - \epsilon)\, g \cdot L \tag{2.29}$$

The minimum fluidisation velocity (U_{mf}) can be derived from the correlation for the Archimedes number (Ar) given in Eq. 2.30. Ar is given by Eq. 2.31

$$Ar = c_1 \cdot Re_{mf} + c_2 \cdot Re_{mf}^2 \tag{2.30}$$

$$Ar = \frac{\rho_g \cdot d_p^3 \cdot (\rho_p - \rho_g) \cdot g}{\mu^2} \tag{2.31}$$

Finally, the Reynolds number at the minimum fluidisation velocity is derived by an empirical formula, Eq. 2.32. The approximation is fitted with the values proposed by Grace [88]. Wen and Yu [89] have proposed this correlation. The Reynolds number is given in Eq. 2.33.

$$Re_{mf} = \sqrt{27.2^2 + 0.0408 \cdot Ar} - 27.2 \tag{2.32}$$

$$Re = \frac{\rho_g \cdot d_p \cdot U}{\mu} \tag{2.33}$$

At the terminal velocity (U_t), the single particle starts to be entrained and can be derived from balancing the particle weight, buoyancy and friction force, see Eq. 2.34

$$U_t = \sqrt{\frac{4}{3} \cdot \frac{\rho_p - \rho_g}{\rho_g} \cdot \frac{d_p \cdot g}{C_w}} \tag{2.34}$$

C_w is the drag coefficient of the single particle and depends very much on the Reynolds number. C_w is calculated in:

- the laminar (Stokes) region ($Re < 0.2$) from

$$C_w = \frac{24}{Re} \tag{2.35}$$

- the turbulent (Newton) region ($Re > 1000$) from

$$C_w = 0.43 \tag{2.36}$$

- and in the transition region ($0.2 < Re < 1000$) an implicit formulation is used:

$$C_w = \frac{24}{Re} + \frac{4}{\sqrt{Re}} + 0.4 \tag{2.37}$$

Grace has proposed in [84] a regime map for gas upflow through solid particles to illustrate the typical operation regions of bubbling, turbulent and fast fluidisation. This basic regime map is based on empirical data and combines experimental findings from various authors, [84]. The logarithmic plot displays the dimensionless superficial gas velocity (U^* on y-axis, Eq. 2.38) plotted against the dimensionless particle diameter (d_p^* on x-axis, Eq. 2.39). U is the superficial gas velocity of the upward gas flow in Eq. 2.38.

$$U^* = U \left(\frac{\rho_g}{\nu g \left(\rho_p - \rho_g \right)} \right)^{\frac{1}{3}} = \frac{Re}{Ar^{\frac{1}{3}}} \tag{2.38}$$

$$d_p^* = d_p \left(\frac{g \left(\rho_p - \rho_g \right)}{\nu^2 \rho_g} \right)^{\frac{1}{3}} = Ar^{\frac{1}{3}} \tag{2.39}$$

A general regime map extended from that of Grace [84] is shown in Figure 2.18. This plot combines basic data following Grace [90–92]. The range of U_{mf} covers various experimentally determined equations for U_{mf} as given in literature, [84]. The data for the range of U_t are derived from Haider and Levenspiel [93], which covers various particle sphericity 0.8 to 1.0. Paper VI presents the mapping of the fluidisation regime in the gasification reactor and combustion reactor derived from experimental data at the DFB pilot plant.
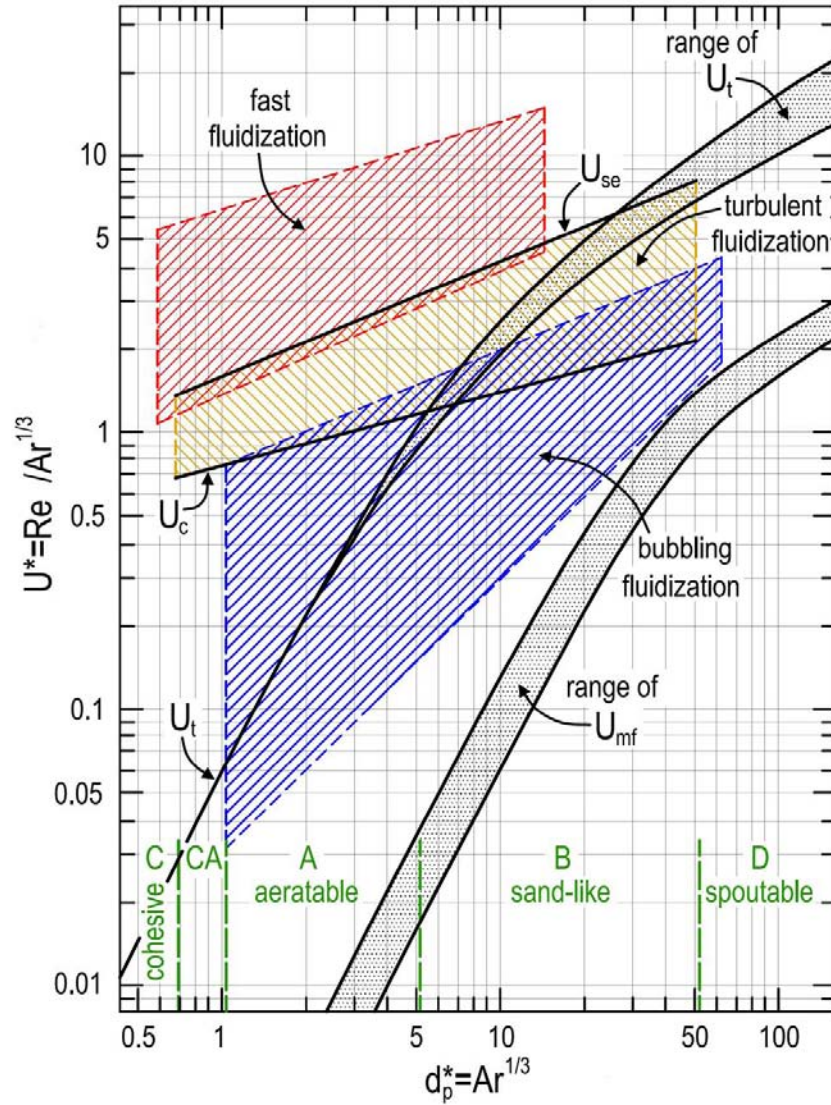
Figure 2.18: Regime map for gas upflow through solid particles with typical boundaries, fluidisation regimes and Geldarts particle classification; adapted from Grace [84,90], Haider and Levenspiel [93] and Abba et al. [94]

2.4 Dual fluidised bed system for steam gasification

The dual fluidised bed (DFB) system enables a heat supply for endothermic steam gasification by transport of a solid heat carrier between the combustion and gasification reactor. The principle of the DFB system is depicted in Figure 2.19
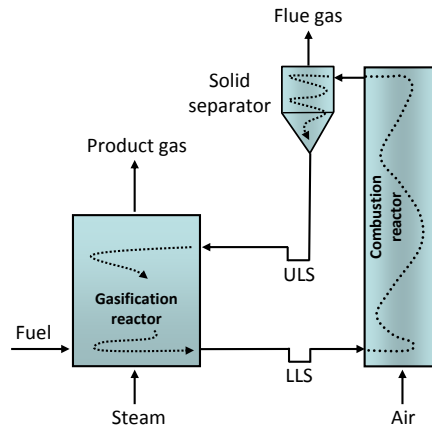
Figure 2.19: Concept of the dual fluidised bed reactor system (ULS: upper loop seal; LLS: lower loop seal)

The process contains two fluidised bed reactors whose connections enable an interchange of solid matter. Steam gasification takes place in the gasification reactor at temperatures between 850°Cand 900°C. The gasification part is continuously fed with the feedstock, steam and hot bed material coming from the combustion reactor[5]. Along with the bed material from the gasifier, char is transported to the riser.

The combustion of the residual fuel particles serves to heat up the bed material for subsequent energy supply of the gasifier. The gasification reactor is designed as a bubbling fluidised bed fluidised with steam for gasification and reforming reactions. The air blown combustion reactor is operated in a fast fluidised regime to enable the solid transport. The reactors are connected using steam fluidised loop seals, which effectively prevent gas leakage between the fluidised beds and allow high solid throughput.

A cyclone is used to separate the entrained particles from the fast fluidised combustion reactor. The temperature difference between the combustion and the gasification reactor is determined by the energy demand for gasification as well as the bed material circulation rate. The system is inherently auto-stabilising since a decrease of the gasification temperature leads to higher amounts of residual char, which results in more fuel for combustion. This, in turn, transports more energy into the gasification zone and thereby stabilises the temperature. In practical operation, the gasification temperature can be influenced and controlled by the addition of fuel (e.g. recycled product gas) to the combustion reactor. The pressure in both reactors, gasification and combustion, is close to atmospheric conditions.

---

[5]the term *riser* is used in parallel with combustion reactor

Further, the DFB system features the following aspects:

- excellent gas-solid contact and heat transfer,

- high potential for scale-up,

- generation of nitrogen free product gas,

- separate optimisation of both reactors,

- solid circulation between the reactors influences the particle residence times,

- in-bed catalysts or additives are applicable and

- in-situ regeneration (e.g., carbon depositions) of in-bed catalysts in the combustion reactor.

The bed material serves primarily as a heat carrier for the heat supply for the endothermic steam gasification. Furthermore, the bed material can fulfil the function of:

- in-bed catalyst to promote gas–gas reactions (e.g. tar reforming) in the gasification reactor,

- transport media (e.g., CO_2 in case of sorption enhanced reforming).

Based on investigations at the $100\,kW$ pilot plant (at the Vienna University of Technology), the feasibility of the DFB system for biomass gasification is demonstrated at an industrial scale of 8 MW fuel input at the combined heat and power plant (CHP) Güssing (Austria), [95, 96], see also Paper IV.

2.5 Review of DFB gasification units

During the past 20 years research and development on dual fluidised bed systems for the allothermal steam gasification of biomass has been promoted. Currently there are about 15 to 20 DFB research units and devices for biomass steam gasification. A considerable amount of literature has been published reporting the results of the research units and pilot plants. Comprehensive reviews of DFB gasifiers are given by Corella et al. [97] and Göransson et al. [98]. Table 2.7 shows a selection of some publications on DFB units at pilot plants or at the demonstration/industrial scale. However, so far there is no common agreement on the comprehensive reporting as the scope of the publications differs clearly. Thus, there is often a lack of data, which are important to describe the overall process (e.g., fluidised bed dynamics, residence times, conversion rates). In particular, data on tar content is a crucial issue, as this refers to different measurement methods.

Table 2.7: Overview of facilities for steam biomass gasification based on the dual fluidised bed concept

Parameter	Unit	CHP Güssing, Austria, [16]	Vienna University, [99], Paper V	MILENA gasifier ECN, [15]	Ferco/SilvaGas, USA, [100,101]	University of Canterbury, New Zealand, [10,102]	Chalmers University, Sweden, [9,103]	Mid Sweden University, [11]
scale	-	industrial	pilot plant	pilot plant	pilot plant	pilot plant	pilot plant	pilot plant
fuel power	[div.]	8 MW_{th}	100 kW_{th}	800 kW_{th}	n.a.	100 kW_{th}	2–4 MW_{th}	100 kW_{th}
fuel	-	wood	wood	wood	wood	wood	wood	wood
temperature	[°C]	850	850	850–900	n.a.	730–750	812	850
steam-to-fuel ratio	[-]	n.a.	0.8	n.a.	n.a.	0.8	n.a.	0.9
bed material	-	olivine	olivine	olivine	silica sand	greywacke sand	silica sand	silica sand
H_2	[vol%$_{db}$]	38–40	39–41	27.3	17.5	27–29	25.1	51.1
CO	[vol%$_{db}$]	24–26	25–26	27.5	50.0	32–34	33.1	36.9
CO_2	[vol%$_{db}$]	20–22	18–19	24.8	9.4	21–23	14.7	11.2
CH_4	[vol%$_{db}$]	10–11	9–10	9.5	15.5	12	11.8	11.0
C_2/C_3 HC	[vol%$_{db}$]	2.5–3.5	2.0–2.5	n.a.	7	5	4.5	6.5
N_2	[vol%$_{db}$]	<2	<1	<1	n.a.	n.a.	9.3	0.2
H_2O	[vol%$_{db}$]	30–45	40–55	n.a.	n.a.	n.a.	n.a.	n.a.
tar (in raw product)	[g/Nm^3_{db}]	2–5	5–8 (GCMS), 2–5 (grav.)	18 (GCMS)	16	27–31 (benzene)	7.5 (grav.)	10 (total tar)
LHV	[MJ/Nm^3_{db}]	12.9–13.6	12.5–13.5	n.a.	18.5 (HHV)	13	13.7	n.a.

2.6 Catalytic materials for in-bed tar reduction

A solid catalysed gas–gas reaction requires principally a surface. This enables the contact and interchange of the involved species. The catalytic activity of various materials can differ considerably. A general overview on the possible materials, which supports tar reduction is shown in Figure 2.20.
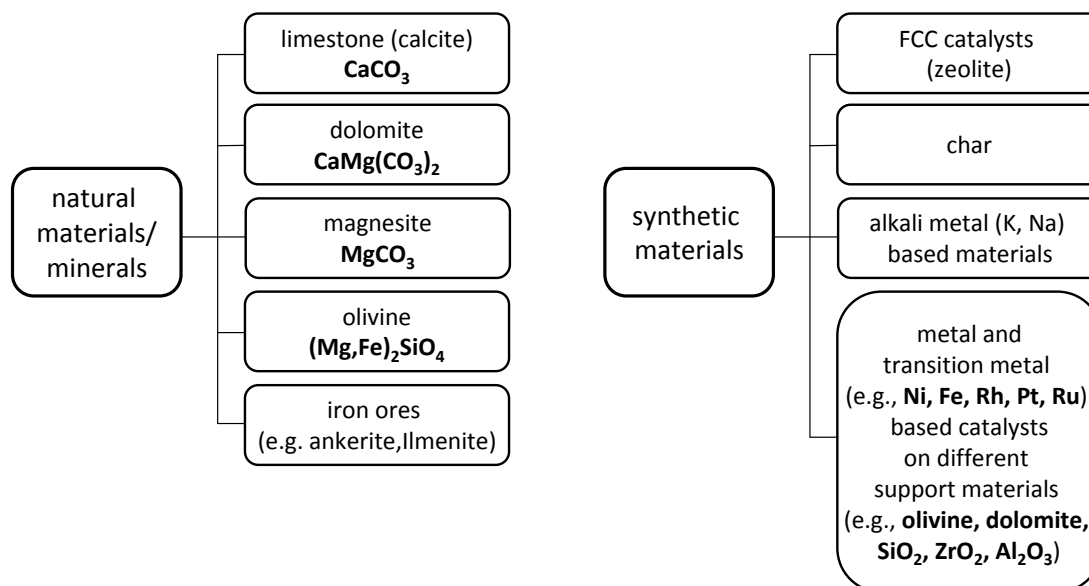
Figure 2.20: Possible materials for catalytic supported tar reduction in biomass gasification

Besides the catalytic activity of the material, further aspects with regard to the suitability of the materials have to be considered, which arise from the fluidised bed and the prevalent reaction atmosphere. Basically, in terms of the fluidised bed process, the catalyst, which is likewise the bed material[6] of the fluidised bed (in-bed catalyst) have to meet certain requirements. In particular, a high mechanical stability of the material is required, as rupture and abrasion causes particle entrainment and loss in material. Futher limitations to their activity and lifetime come from:

- coke formation or carbon deposition (on the catalyst surface),

- catalyst poisoning due to sulphur, chlorine or

- sintering, phase transformation, volatilisation (e.g. of Ni catalysts) due to high temperature processing, [104].

However, the impact of carbon deposition or poisoning can be neglected in the DFB system as the material passes through the zone of regeneration, which is the oxidising

---

[6]in parallel the term *solid inventory* is used

atmosphere in the combustion reactor. Further aspects for the evaluation of a material arise from econonic concerns:

- availability at low cost,

- disposal of the spent material,

- toxicity of the material (e.g., Ni containing materials), which can cause environmental hazards.

Very comprehensive reviews of the catalysts for catalytic supported biomass gasification are given by Sutton et al. [26], Dayton [104], Han and Kim [105], Abu El-Rub et al. [25], Huber et al. [106], Torres et al. [107], Wang et al. [108], Yung et al. [23] and Anis and Zainal [109].
Natural minerals (see Figure 2.20) have received much attention and were investigated in numerous studies for tar destruction. Above all, these materials are inexpensive, readily available, and exhibit from moderate up to good activities in tar reduction. Important studies on the application of natural materials were published by Delgado et al. [110,111], Corella et al. [112], and Simell et al. [113]. In general, the minerals dolomite and calcite show good activity in tar reforming. However, their mechanical stability is low and the application in the fluidised bed produces a high fraction of particulates due to attrition. The application of calcite (CaO) as the bed material in the DFB pilot plant and its effects on the tar content are shown in Paper I.
On the other hand, olivine is a fairly good material as the hardness of the mineral is high. The activity in tar reduction is found to be moderate in contrast to other natural minerals (limestone, dolomite). Olivine as an in-bed catalyst for biomass gasification has been the subject of various studies, e.g. Devi [21], Rapagna et al. [114]. A comprehenive review of the experimental studies on the behaviour of olivine in biomass gasification is given in Paper V. Furthermore, Paper V outlines the performance of olivine in contrast to silica sand, which is considered to be inert, in a DFB pilot plant and shows the tar reduction potential in real process conditions.
In the field of synthetic materials, Ni based catalysts, at different support materials, have gained much attention due to their very high activity in tar decomposition. However, the application in fluidised bed at the industrial scale is problematic as the disposal of Ni containing ash and entrained particulates are environmental hazards. Important studies which show their high potential for tar reduction in biomass gasification have been published by Courson et al. [115], Swierczynski et al. [30,116], Pfeifer et al. [28,117], and Zhang et al. [118].
Apart from the considerable amount of literature on Ni based catalysts and also the literature on other transition metal based materials, iron based catalysts have been the focus of numerous studies. Fe is well known as a catalyst and is employed as a catalyst in processes such as Fischer–Tropsch or ammonia synthesis.

The material considered and investigated in the thesis are as follows:

- **_silica sand_** as inactive bed material, reference case (see Paper V),

- **_natural olivine_** as in-bed catalyst, standard bed material, (Paper I, Paper II, Paper V),

- **_Fe-olivine_** as in-bed catalyst, O_2-carrier (Paper VII, III, VIII)

- **_limestone_** as in-bed catalyst, CO_2-carrier (Paper I, Paper IV).

The specific properties of the solid materials are given in the papers. Fe-olivine was developed at the University of Strasbourg (Laboratoire des Matériaux, Surfaces et Procédés pour la Catalyse). The material was prepared on a large scale by wet impregnation with an iron nitrate solution. Drying of the material was carried out at 100 °C. In addition the material was calcined at 1000 °C. The preparation and characterisation of the catalyst is described by Virginie et al. [119, 120]. Particle characteristics of the considered materials are summarised in Table 2.8.

Table 2.8: Particle characteristics of the considered solids

Parameter	Unit	silica sand	limestone	olivine	Fe-olivine
MgO	[wt%]	-	0.7	48.0–50.0	42.9
SiO_2	[wt%]	96.0–98.0	2.8	39.0–42.0	35.6
Fe_2O_3	[wt%]	< 0.25	0.6	8.0–10.5	20.7
$Al_2O_3 + Cr_2O_3 + Mg_3O_4$	[wt%]	< 2.0	1.4	0.8	0.2
CaO	[wt%]	-	-	< 0.4	< 0.2
NiO	[wt%]	-	-	< 0.1	< 0.1
$CaCO_3$	[wt%]	-	94.0	< 0.1	-
trace elements	[wt%]	n.a.	0.5	< 0.1	-
Hardness	Mohs scale	7[1]	2–4[2]	6–7[3]	6–7[4]
apparent particle density	[kg/m^3]	≈ 2650	≈ 2600	≈ 2850	≈ 2850

[1] [58, 121], [2] [58, 122], [3] [21, 58], [4] [21, 58]

2.7 Transfer processes by reactive bed materials

2.7.1 Oxygen transfer

Oxygen transfer is a side effect which arises from the presence of an oxidisable and reducable oxygen carrier material. In particular, the characteristic of the material comes into play as the material alternates between the reducing and oxidising atmosphere of the reactor parts in the dual fluidised bed system. Most notably, the oxygen transfer properties of certain materials are used for chemical looping combustion processes applied to dual fluidised bed systems. Interesting candidates for such processes are Ni, Cu, Co, Mn, and Fe. However in this thesis, contrary to chemical-looping combustion process, the oxygen transfer characteristics (of Fe-olivine) are not meant for the purpose of total fuel combustion. It is rather employed for:

- partial oxidation and internal heat supply as a substitute for solid heat carrier circulation,

- possible oxidation of hydrocarbons (tars) for in-bed tar reduction.

The mechanism of oxygen transfer arises from cyclic circulation in a reducing and oxidising reaction atmosphere. The chemistry of oxidation and reduction for a generally oxidisable material is simply expressed by Eq. 2.40:

$$MeO_{\alpha-1} \quad + \quad \frac{1}{2}O_2 \quad \longleftrightarrow \quad MeO_{\alpha} \tag{2.40}$$
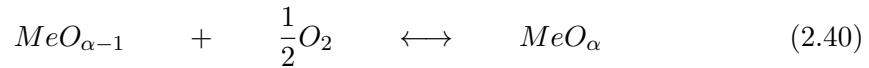
In terms of biomass gasification in the dual fluidised bed system, the material is oxidised in the combustion reactor and the reduction takes places in the gasification reactor. As an iron-based material is considered in this work, several states of oxidation exist based on the state of metalic iron Fe:

- FeO   (Fe_{II}, wustite)

- Fe_2O_3 (Fe_{III}, hematite)

- Fe_3O_4 ($Fe_{II}(Fe_{III})_2O_4$, magnetite)

For general considerations, the oxidation–reduction system of Fe is lumped into the formal expression of Eq. 2.41.

$$2FeO \quad + \quad \frac{1}{2}O_2 \quad \longrightarrow \quad Fe_2O_3 \quad \Delta H^0_{R,850} = -277\,\text{kJ/mol} \tag{2.41}$$
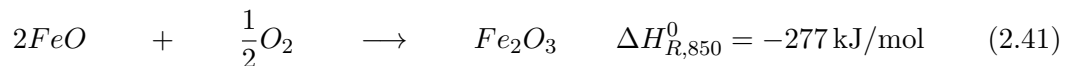
The possible oxidation interaction/reactions of the gas species (CO, H_2) with iron-oxide in the gasification reactor are given in Eq. 2.42 and 2.43.

$$H_2 + Fe_2O_3 \quad \longrightarrow \quad H_2O + 2FeO \quad \Delta H^0_{R,850} = 28.5\,\text{kJ/mol} \tag{2.42}$$

$$CO + Fe_2O_3 \quad \longrightarrow \quad CO_2 + 2FeO \quad \Delta H^0_{R,850} = -5.2\,\text{kJ/mol} \tag{2.43}$$

The oxygen transport capacity of an oxygen carrier material may be defined as shown in Eq. 2.44. This number is basically considered in chemical looping combustion, [36].

$$R_0 = \frac{m_{OC,ox} - m_{OC,red}}{m_{OC,ox}} \tag{2.44}$$

The theoretical oxygen transport capacity of Fe, which depends on the oxidation state, is shown in Figure 2.21.
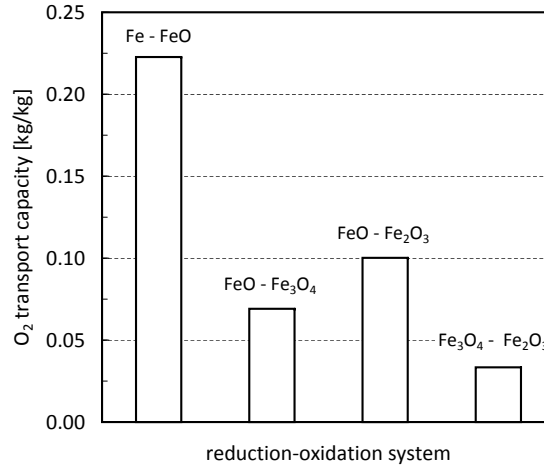
Figure 2.21: Theoretical O_2 transport capacity of different oxidation–reduction systems of iron

2.7.2 CO_2 transfer by calcium looping

The internal transport of CO_2 in the dual fluidised bed system via solid carriers is the subject of several process concepts. CO_2 transport is currently discussed as an option for post-combustion capture as a suitable CCS technology. However, with a view to the dual fluidised bed system, the combination of internal CO_2 sequestration and transport affects the mass and elementary balance for the gasifier, as the CO_2 is continuously separated from the gasification reactor. In the literature there are several notations used for calcium looping. In this thesis, the process is referred to as sorption enhanced reforming[7] (SER). The fundamentals of the process are given in Paper IV. Basically, calcite/limestone is used as the solid. The chemistry of CO_2 absorption (carbonation) and desorption (calcination) is shown in Eq. 2.45.

$$CaO \quad + \quad CO_2 \quad \longleftrightarrow \quad CaCO_3 \quad \Delta H_{R,850}^0 = -166.6\,\text{kJ/mol} \tag{2.45}$$
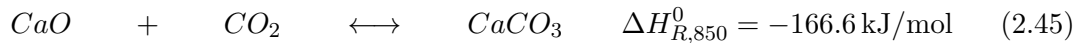
CO_2 is considered as an inert gaseous component in terms of the heating value. Notably, the CO-shift reaction (see Eq. 2.10) is favoured due to the partial sequestration of CO_2

---

[7]within the course of this work another term has also been used: absorption enhanced reforming, see Paper IV

from the reaction atmosphere as this lowers the CO_2 partial pressure and increases the driving force towards the products, such as H_2 (Chatelier's principle).

In general, the sorption enhanced reforming features:

- product gas with a high H_2 content,

- in-situ supply of process heat as the carbonation is an exothermic process and

- low tar content as the solid material is also a catalyst.

The thermodynamics of carbonation and calcination of limestone defines the temperature for the process operation, as the real CO_2 partial pressure has to be either above the CO_2 equilibrium partial pressure (for carbonation), or below the CO_2 equilibrium partial pressure (for calcination). Thus, the gasification process is operated in a temperature range of 650°C–700°C and the combustion reactor is operated at temperatures of 800°C–900°C.

Figure 2.22 shows the CO_2 equilibrium partial pressure for the system CaO-CaCO$_3$ versus temperature, which was calculated with HSC Chemistry [50]. Further, the appropriate areas for calcination and carbonation are labelled. A range of typical CO_2 partial pressures is shown for standard operation of the pilot plant between 800°C–850°C with wood pellets at a steam-to-fuel ratio of 0.8, taken from Paper V. The actual CO_2 partial
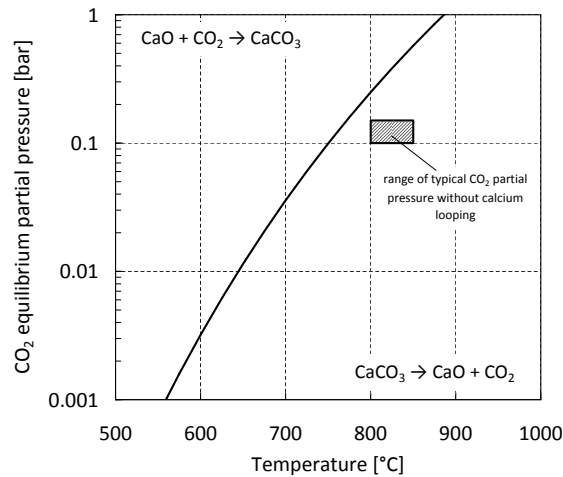
Figure 2.22: CO_2 equilibrium partial pressure versus temperature for the system CaO-CaCO$_3$ at 1 bar

pressure is below the equilibrium CO_2 partial pressure for the standard operation mode. Thus, carbonation does not occur. In this area, the material is present in the form of CaO, as the calcination is favoured. Decreasing the gasification temperature shifts the actual CO_2 partial pressure into the region where the CO_2 equilibrium partial pressure is lower. Hence, carbonation can occur. The mapping of the shift of the CO_2 partial pressure in the SER operation mode is presented in Paper IV.

3 Experimental devices

Different facilities were used for the experimental investigation. The 100 kW dual fluidised bed (DFB) pilot plant was used in the majority of the experimental test runs. The reactor system of this test facility is related to industrial application. The operation conditions are close to those of industrial application. The 120 kW dual circulating fluidised bed (DCFB) pilot rig was used for specific investigation of oxygen transfer and tar decomposition for olivine and Fe-olivine. This test facility is operated with gaseous fuels. The DCFB facility was fueled with a surrogate gas mixture and a model tar compound (1-methylnaphthalene) to represent product gas from steam gasification. Thus, the bed materials were investigated under conditions free of a solid fuel, which excludes possible side effects of ash components. Further, this arrangement enables the specific metering of the gasesous fuel input and the model tar compound.

3.1 Configuration of the DFB pilot plant

The concept of the pilot plant reactor is based on the DFB concept for steam gasification of biomass. Figure 3.1 highlights schematically the reactor part of the pilot plant. The geometry of the reactor is shown in Figure 3.2. A process diagram of the whole pilot plant setup is sketched in Figure 3.3. The reactor system is divided into a gasification reactor (bubbling fluidised bed) and a (fast fluidised) combustion reactor. Interconnection of the single reactors (fluidised beds) is realised by loop seal connections. Thus, continuous solid circulation between the fluidised beds is enabled.
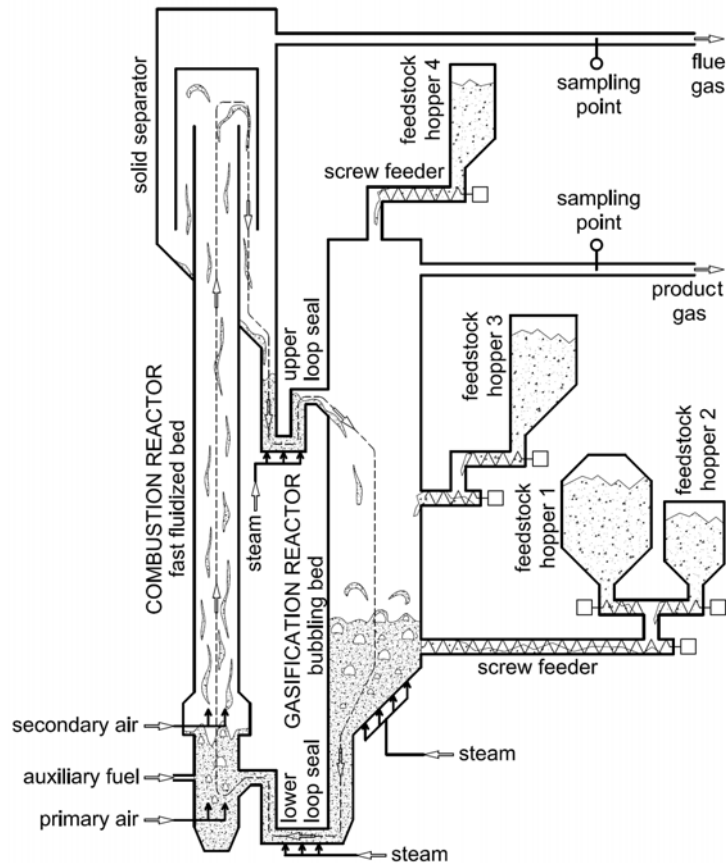
Figure 3.1: Scheme of the DFB reactor system of the pilot plant, see also Table 3.1

The heat supply for the endothermic steam gasification is provided by circulation of hot bed material. Bed material heat-up is obtained through combustion of residual fuel (char from the gasification part) or auxiliary fuel in the combustion reactor. The configuration of the fuel feeding system (which was adapted over the course of the work) enables fuel feed from different positions, which are:

- direct feed for feeding into the bubbling fluidised bed,

- top-down fuel feeding onto the bubbling bed.

Furthermore, superheated steam is used for fluidisation of the loop seals. Superheated steam for fluidisation of the gasifier is provided by an electrically heated steam generator. Combustion air is injected at two levels (primary and secondary air injection nozzles) into the combustion reactor. Light fuel oil is used as auxiliary fuel and is injected into the lower part of the combustor. Constant solid hold-up in the bottom part of the combustion reactor is enabled by primary air injection. The secondary air effects fast fluidisation of the solids resulting in solid transport to the top of the riser. A harsh turnaround of the gas–solid stream by means of a separator, which is arranged on the top of the riser, is used for solid separation of the solid-loaded flue gas stream. The product gas stream exits the gasifier and passes through a thermo-oil heat exchanger with a product gas outlet temperature of about 250°C–300°C. A sampling point for analysis of the product gas composition is installed after the heat exchanger. The product gas stream and flue gas stream are merged together and led into a post-combustion chamber for complete combustion of burnable species. Prior to the stack, a cyclone separates the particles from the exhaust gas. The nominal fuel power of the pilot plant is 100 kW. Due to the screw feeders of the feed-
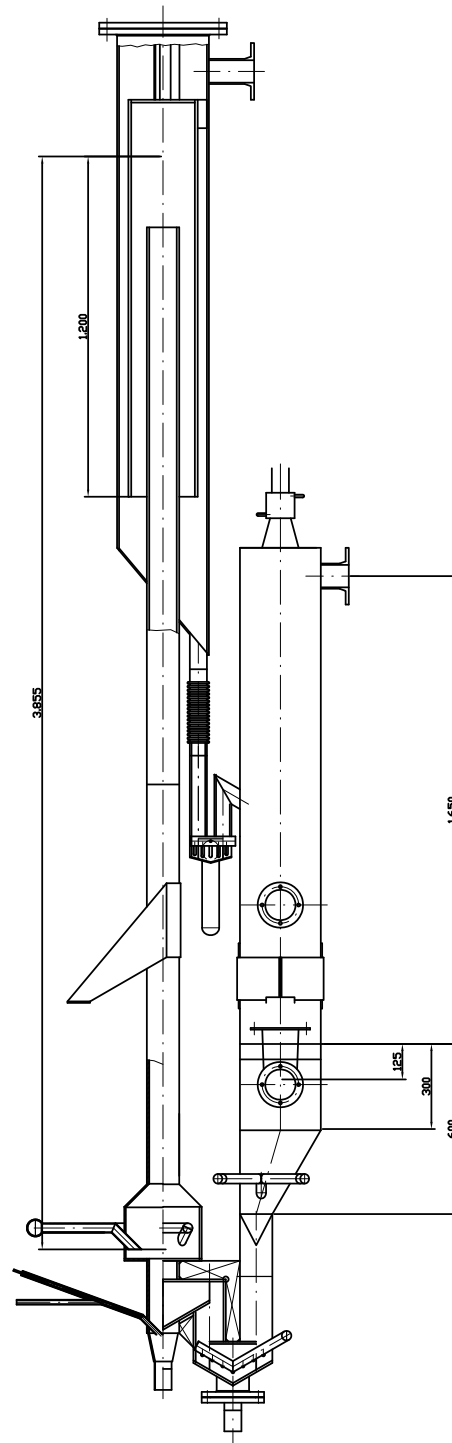
Figure 3.2: Geometry of the pilot plant, see also Table 3.1

ing system, the applicable fuel particle size is limited to below 40 mm. The applicable bed material particle size is in the range of 200 to 800 μm for an apparent particle density (ρ_p), which is sand-like in the range of 2600 to 2900 kg/m^3.

The geometry of the reactor is shown in Figure 3.2. Data for general operational ranges and geometry of the DFB pilot plant reactor are given in Table 3.1. The pilot plant is also described by Pfeifer [28].
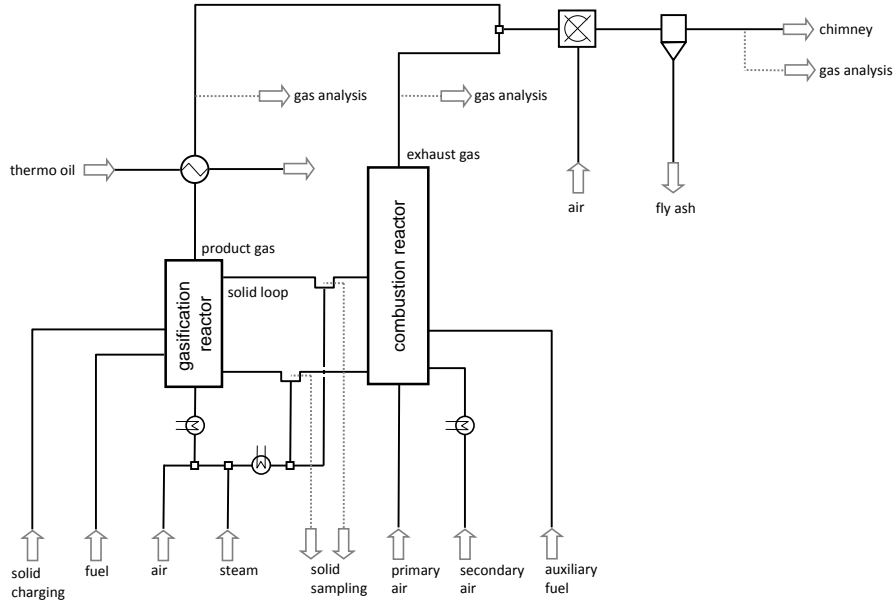
Figure 3.3: Arrangement of the reactor and auxiliary units of the pilot plant

Table 3.1: Operation and geometric data of the pilot plant

Parameter	Gasification reactor	Combustion reactor
operable temperature range	650°C–870°C	750°C–930°C
fluidisation regime	bubbling fluidised bed (steam blown)	fast fluidised bed air blown
cross section geometry	conical bottom section with square shaped upper freeboard section	circular
reactor free height	2.35 m	3.9 m (central tube section)
reactor inner diameter	304 mm (equivalent cylindrical diameter at square shaped freeboard section)	98 mm

Furthermore, Table 3.2 summarises the characteristic fluidised bed parameters of the DFB system related to a fuel input of 20 kg/h of wood pellets, which corresponds to a capacity of about 100 kW. The data are related to the following particle properties, which are typical for standard operation:

- particle size range (d_p): 400–600 μm

- apparent particle density of olivine (ρ_p): 2850 kg/m^3

The ratios U/U$_{mf}$ and U/U$_t$ are determined by the desired steam-to-fuel ratio in the gasifier (steam fluidisation) and the combustion behaviour in the riser (air fluidisation).

Table 3.2: Fluidised bed characteristics of the DFB system at 20 kg/h fuel feed with wood pellets

Parameter	Unit	Gasifier	Riser
temperature	[°C]	≈ 850	≈ 920
steam-to-fuel ratio, φ_{SF}	[kg/kg$_{daf}$]	0.8 ... 0.9	-
superficial gas velocity, U	[m/s]	0.51 ... 0.55	9 ... 10
minimum fluidisation velocity, U$_{mf}$	[m/s]	0.08 ... 0.18	0.07 ... 0.17
ratio U/U$_{mf}$	[-]	3.0 ... 7.0	60 ... 130
ratio U/U$_t$	[-]	U $<<$ U$_t$	1.8 ... 3.0

Further information on the hydrodynamics and specific values of the fluidised beds are given in Paper V and VI.

3.2 Diagnostic methods

The general process data (temperatures, pressures, volume-/mass flows) are recorded using LabVIEW. The pilot plant is equipped with:

- 27 thermocouples,

- 16 pressure inducers, and

- 8 flow meters with local indication and with online registration.

The measuring points for temperature and pressure are evenly positioned over the reactor height and entire pilot plant. The temperature sensing elements are Ni/CrNi thermocouples of Type K (range from 20°C to 1200°C). Pressure measurement is performed with Honeywell piezoresistive pressure sensors and Rosemount (Type 1151) pressure transmitters. The following measuring devices are used to determine the composition of the product gas, the flue gas, and the exhaust gas of the post-combustion chamber:

- product gas: Rosemount NGA 2000 (CO, CO$_2$, H$_2$, CH$_4$, O$_2$), and online gas chromatograph Syntech Spectras GC 955 (CO, CO$_2$ CH$_4$, O$_2$, N$_2$, C$_2$H$_4$, C$_2$H$_6$, C$_3$H$_8$) for cross-checking of carbon species and N$_2$ content and for determination of C$_2$/C$_3$ hydrocarbons

- flue gas: Rosemount NGA 2000 (CO, CO_2, O_2)

- exhaust gas (post-combustion chamber): Rosemount BINOS 1004 (CO, CO_2)

Calibration of the measuring devices is performed before each experimental run. Gas conditioning (separation of solid particles, water, and condensable hydrocarbons) of the product, flue, and post-combustion exhaust gas, is carried out before the gas analysis. The gas streams are taken by means of a diaphragm pump in each case. A dust filter for each gas stream is used to remove the fines. The flue gas and the exhaust gas from the post-combustion chamber are passed over a gas cooler and a collecting container to condense and separate the water from the gas streams. The product gas is passed through several impinger bottles filled with rapeseed methyl ester (as solvent) to condense the water fraction and to dissolve the condensable hydrocarbons (tar). The impinger bottels are arranged in a cooling bath, which is cooled down to 4°C by means of a cryostat. The sampling volume flows are kept at higher quantities than needed for the measuring device (the excess volume flow is discharged) to keep the delay in time of the measurement short.

3.3 Tar sampling

Determination of the tar content is carried out discontinuously. The wet chemical principle of the measurement applies impinger bottles to condense and dissolve the condensable hydrocarbons. Thus, the condensable tars are condensed and solved from the gas phase into the solvent. The tar measurement method is based on the tar protocol given by Neeft et al. [123] (CEN/TS 15439) focusing on tars originating from biomass gasification. However, the method is modified since toluene instead of isopropanol is used as the solvent for the high steam content product gas. The tar sampling setup is schematically presented in Figure 3.4. A slip stream is sampled isokinetically from the product gas
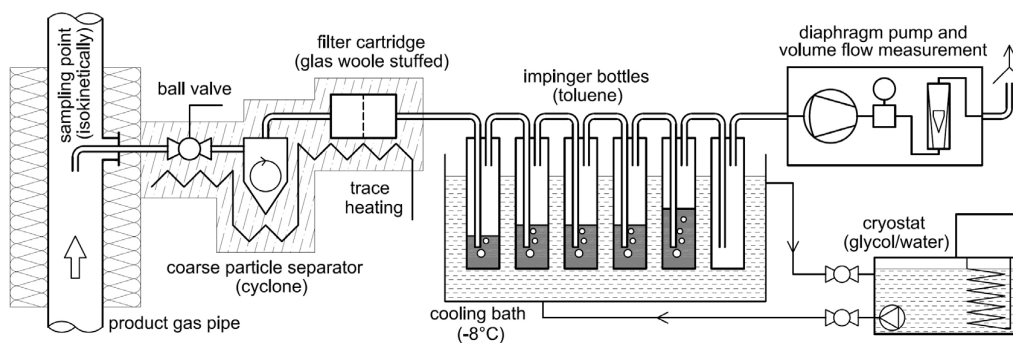
Figure 3.4: Scheme of the tar measurement

stream via a probe. Solid particles (dust and char) are separated in a cyclone and a filter cartridge stuffed with quartz wool. Trace heating of the sampling line avoids condensation and loss of analyte. The slip stream is led through six impinger bottles (five

are filled with toluene at different volumes, the last one in the line is empty), which are arranged in a cryostat and are kept at a temperature of -8°C. A volume meter is applied after the diaphragm pump to determine the volume flow as a reference basis. With regard to the analytic processing, the sampling method yields:

- particulate matter with condensed tars (from the cyclone and the filter cartridge)

- liquid phase (from the impinger bottles)

The condensed tars are extracted from the solid particles by soxhlet extraction with isopropanol. A sample of this phase is taken for GCMS analysis. The dust and char content are determined from the particulate matter by weighing, drying and incineration (at 550 °C). The liquid phases from the impinger bottles are merged together. The water phase is separated from the toluene phase (organic phase). A sample is taken from the toluene phase for GCMS analysis. The solvent (toluene) is removed from the organic phase by atmospheric evaporation in a rotary evaporator and dried at 105 °C in an oven. The residue is weighed and identified as gravimetric tar, since this part is non-detectable by the GCMS. The GCMS samples are analysed by a PerkinElmer Autosystem XL GC with PerkinElmer Turbomass mass spectrometer. Further details on the tar measurement are given in [67]. However, this method does not measure the BTX components (benzene, toluene and xylene) since toluene is used as a solvent.

3.4 Solid sampling

A solid sampling system has been installed at the pilot plant, which allows the sampling of solids during the hot operation of the unit. The upper and lower loop seal are equipped with one sampling point each, see Figure 3.3. The arrangement of the sampling system is illustrated in Figure 3.5. As the solid samples are taken directly (under inert argon
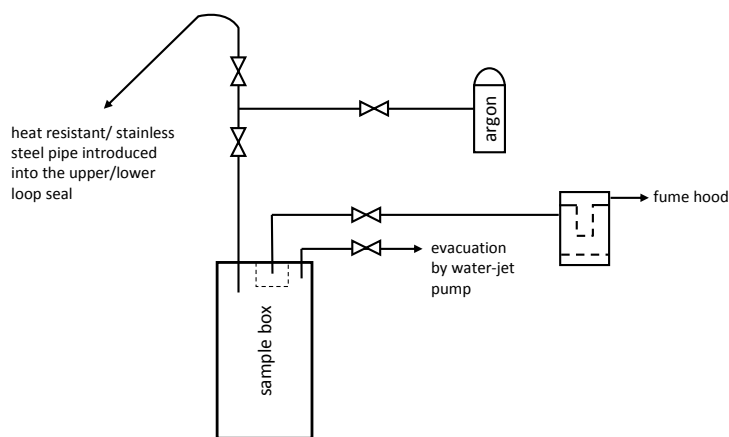
Figure 3.5: Arrangement of the solid sampling system

atmosphere) during the operation, the overall solid sample consists of bed material, which is the main fraction, and a certain quantity of residual fuel (char). The pure solid samples might be investigated with regard to the solid state (carbon depositions). Sampling from the lower loop seal yields a sample of particles coming from the gasification reactor. The sampling from the upper loop seals yields a sample of particles from the combustion reactor. As the sample box is flushed with argon before the sampling procedure, the samples are taken into the inert atmosphere in the sample box to avoid any side reactions (combustion of carbon depositions or char particles). The sample box is linked to a water-jet pump to partially evacuate them and develops a slight underpressure in the sample box. Hence, the solid flow into the sample box is supported, as overpressure in the loop seals might be insufficient for self-charging of the sample box.

3.5 Configuration of the DCFB pilot plant

The DCFB pilot rig consist of two interconnected circulating fluidised bed reactors, named as fuel reactor (FR) and air reactor (AR). The sketch of the pilot rig is presented in Figure 3.6. The coupling of the FR and AR enables continuously circulating of solid material between the reactors.
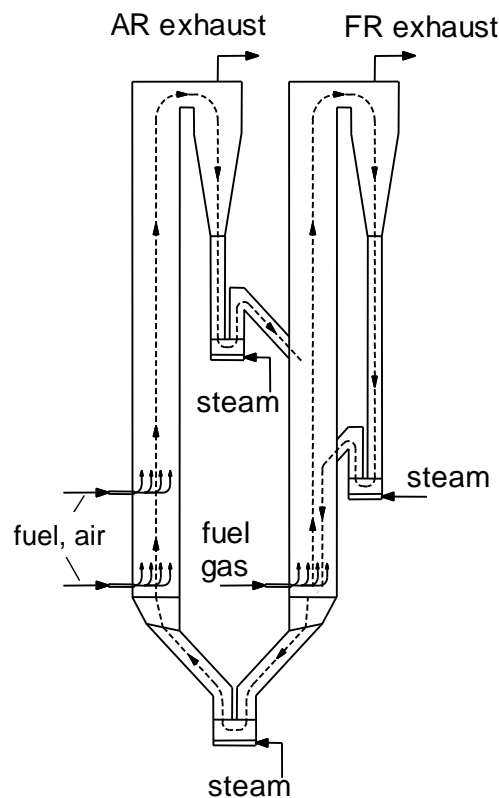
Figure 3.6: Sketch of the 120 kW DCFB pilot rig

The reactor system was developed for chemical looping combustion or chemical looping reforming processes for gaseous fuels. The circulating solids act as oxygen carrier from AR to FR or catalyst for reforming. Furthermore, heat transfer between the reactors is enabled by the circulation of the solids. The flow regime in AR is fast fluidisation and in the FR turbulent fluidisation. Mixing of gas phases is avoided by steam or nitrogen fluidised loop seals. Downstream of each reactor, gas and solids are separated in cyclone separators. After solid separation, the gas streams pass through a post combustion chamber, which is equipped with a support burner for complete combustion. The exhaust gas stream is cooled down, cleaned in a bag filter and sent to the chimney. The DCFB pilot rig and further auxiliary units are detailed by Pröll et al. [37,124] and Kolbitsch et al. [36]. A solid sampling system is installed at the pilot rig and allows solid sampling from the lower and upper loop seal. The solid sampling system is similar to that of the DFB pilot plant, see Section 3.4. The measurement of the gas composition of the FR and AR exhaust gas is done with the diagnostic infrastructure as described in Section 3.2. A Rosemount NGA 2000 (CO, CO_2, H_2, CH_4, O_2) is used for determination of the FR exhaust gas composition. Additionally, the online gas chromatograph Syntech Spectras GC 955 is used for cross-checking of carbon species and determination of the N_2 content for evaluation of possible gas leakages from the air reactor to the fuel reactor. The AR exhaust stream is analysed using the Rosemount NGA 2000 (CO, O_2, CO_2). The tar sampling method as described in Section 3.3 is applied.

4 Process modeling and simulation

4.1 Process simulation and the software IPSEpro

The basic principle of process simulation is to represent the real process by a mathematical model based on physical regularities. The model describes the real process with a certain accuracy. Process models may be differentiated by whether the model is time-independent (static) or time-dependent (dynamic). Dynamic process modeling is more complex than static process modeling. Numerical methods are used to solve the mathematical system of equations. The strategy of solution of the overall system is either sequential/modular or equation oriented.

The software package IPSEpro$^{\text{TM}}$ is used in this work for modeling and simulation of the process. The software originates from the power plant sector and is a static process simulation software based on flow sheet handling. The modular structure of the software package includes the user interface (process simulation environment), the model library, and the equation solver. In the course of solving the mathematical system of equations, the equation solver accesses external function (e.g. properties of substances), which are part of the dynamic link libraries. A more detailed description of the software package IPSEpro can be found n [125]. Process simulation serves the (in relation to the real process):

- determination of the mass and energy balance,

- determination of states or conditions (e.g. pressure, chemical composition),

- evaluation of process properties (e.g. efficiencies),

- predictive statements on process behaviour and

- process control

4.2 Validation of process data

The measured operational process data are subjected to measurement errors. In the validation mode these process data are integrated as additional data to the existing data set, which already represent a determined system of equations. Thus, a redundance of the system is obtained, which allows of drawing a conclusion on the quality of a single measurement. The software package involves the calculation mode of measurement validation. This validation mode, which integrates the measured process data, is used for:

- checking the mass and energy balance for the experimental test run/operation based

- validation of single measurement (e.g., volume flow) data with regard to its accuracy/consistency.

A standard procedure, the method of least squares, is used to solve the over-determined equation system due to inclusion of measured data. Within the procedure the deviation between the measured value and the equilibrated solution is minimized. The dimensionless procedure of minimization is given in Eq. 4.1, wherein x_i is the value of the measurement and $\bar{x}_i$ is the mean value of the measurement.

$$\sum_i \left(\frac{x_i - \bar{x}_i}{tol_{x_i}} \right)^2 \to min \tag{4.1}$$

As the measured values of different dimensions are combined, a tolerance value (tol_{x_i}) is required. The tolerance value corresponds to a confidence interval for the measurement value in which the value might change. In case of availability of an acceptable data set for the measured value, the standard deviation (4.2) of the measured value may be used as the tolerance value.

$$s_{x_i} = \sqrt{\frac{1}{N-1} \sum_{i=1}^{N} (x_i - \bar{x}_i)^2} \tag{4.2}$$

The solution of the over-determined equation system in accordance with the given tolerances describes the most likely state of the process, and therefore the most likely values of the process variables.

4.3 The model library biomass gasification

The biomass gasification library (BG-Lib) allows the presentation of the biomass gasification process as a flow sheet for the process simulation. The BG-Lib involves the process relevant devices as model components (e.g. gasification reactor, combustion reactor, heat exchanger, cyclone, mixer for solid, liquid or gasesous streams). The description of the composition and thermodynamic state of the process streams is accomplished by different substance classes, which are:

- pure water/steam,

- mixture of ideal gases,

- solid or liquid organic substances and

- inorganic solids (bed material components, ash components).

The formulation of the thermodynamic data is based on:

- the IAPWS-IF97 for the properties of water and steam, [126];

- the formulation accoring to Burcat and McBride for formulation of the ideal gas data, [127] and

- polynomials reported by Barin [128] for formulation of inorganic solids.

A profound description of the BG-Lib (process components, process stream and thermodynamic data) is given by Pröll and Hofbauer, [129].

4.4 Flow sheet of the DFB gasification process

Figure 4.1 shows the flow sheet model of the pilot plant arrangement. The model is used for determination of the mass and energy balance and data validation of a desired process state. The process data recorded during the experimental runs (steady state) are used as input data.
The input data for the flow sheet are either the data of the process feed streams (e.g. fuel feed, composition of fuel, volume flows of fluidisation agent) or the data of the process output streams (e.g., product/flue gas composition, tar content).

Figure 4.1: Example for process flow sheet of the DFB gasification in IPSEpro, PG = product gas, FG = flue gas
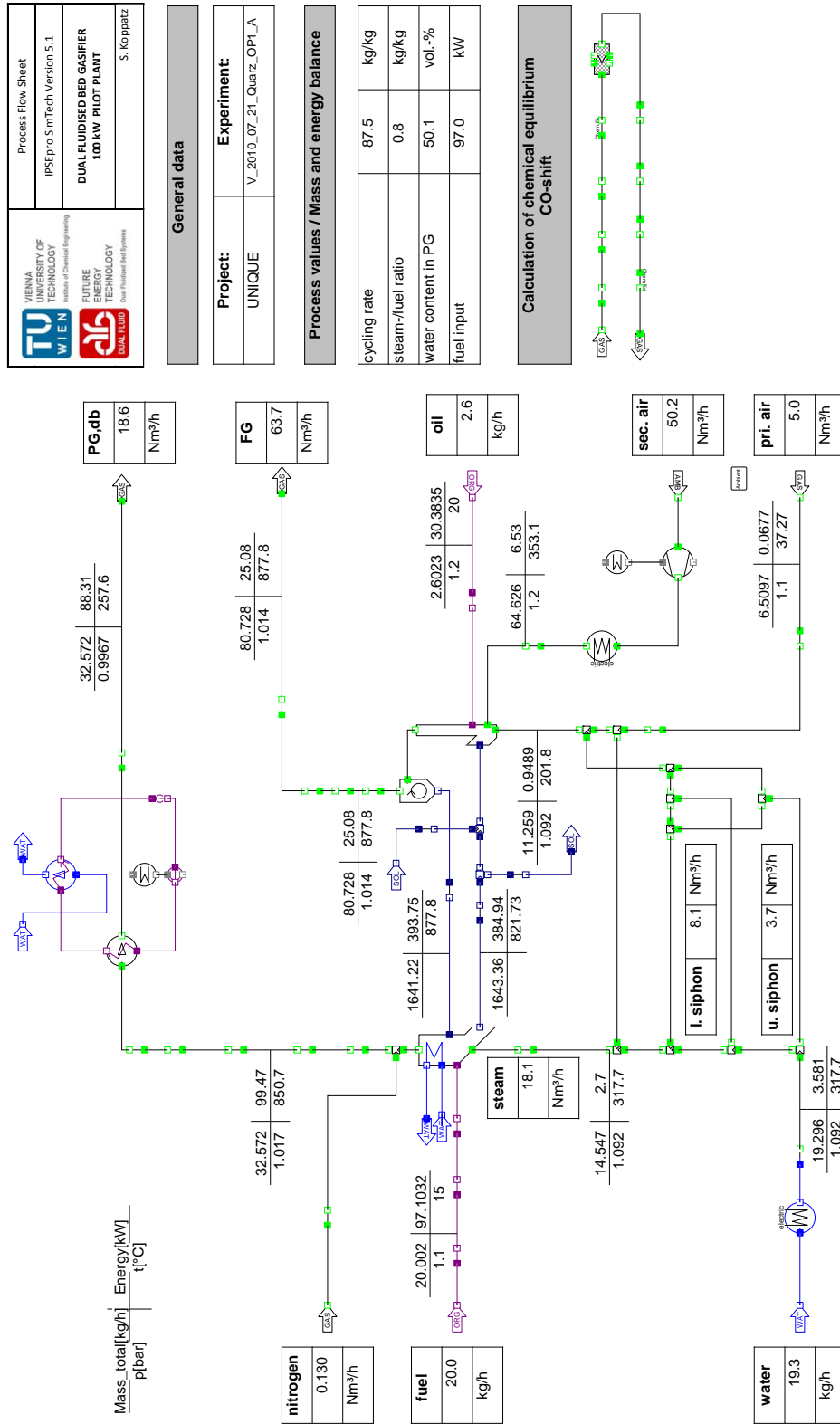
5 Experimental results and discussion

The presentation of the experimental results is organised according to the following aspects:

- brief summary of main findings of the papers,

- outline of: general performance and catalytic activity for tar reduction of the solid materials considered in the thesis,

- considerations on fluidised bed and tar,

- O_2 and CO_2 transfer characteristics, investigation of solid samples.

Table 5.1 provides a rough overview of the experimental content of the papers grouped according to the different solid materials considered in this thesis.

Table 5.1: Overview of the experimental focus of the papers

Solid material	Experimental focus	Paper
silica sand	general performance behaviour in the DFB pilot plant and comparison to olivine	V
limestone	general performance behaviour in the DFB pilot plant and comparison to olivine	I
olivine	general performance behaviour in the DFB pilot plant	I, V, VI, VII
Fe-olivine	general performance behaviour in the DFB pilot plant and comparison to olivine	VII
olivine	study of oxygen transfer and reforming behaviour in the DCFB pilot rig	II
Fe-olivine	study of oxygen transfer and reforming behaviour in the DCFB pilot rig	III
limestone	calcium looping for CO_2 transport in the industrial CHP Güssing	IV

5.1 Summary of the papers

- **Paper I**

The paper presents an experimental study with limestone and olivine as the bed materials in the DFB pilot plant. The gasification test runs with wood pellets were carried out at about $850\,°C$. The relative H_2 content of the product gas was found to be significantly higher for limestone ($\approx 50 \text{vol}\%_{db}$) compared to that of olivine ($\approx 38\,\text{vol}\%_{db}$), see Figure 5.1. GCMS and gravimetric tar content in the product gas was found to be lower for

- limestone (GCMS: 0.9-2.7g/Nm^3_{db} ; grav.: 0.3-1.0$\,g/Nm^3_{db}$) compared to that of

- olivine (GCMS: 8.0-12.0$\,g/Nm^3_{db}$; grav.: 1.6-5.4$\,g/Nm^3_{db}$).

GCMS analysis is presented in the paper and show that the relative content of naphthalene is higher for limestone.
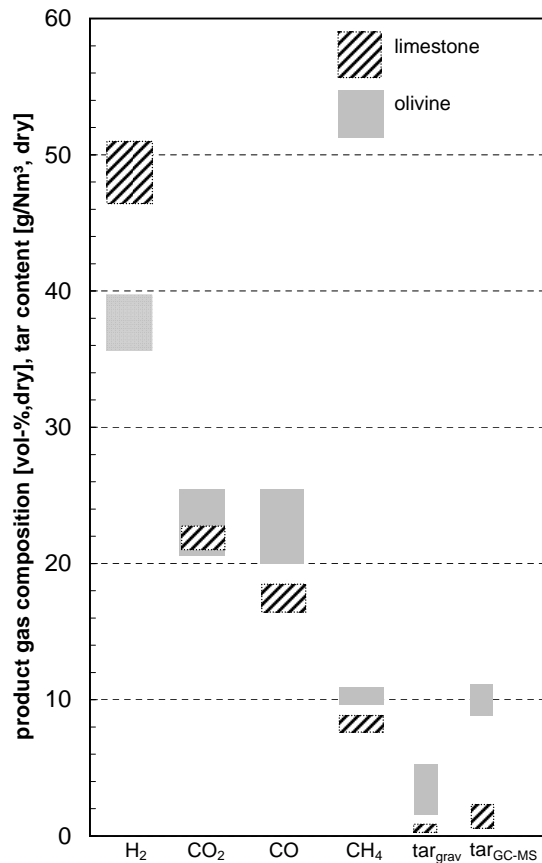
Figure 5.1: Typical range of product gas composition and tar content for limestone and olivine, [Paper I]

- **Paper II**

Natural olivine is investigated in the DCFB pilot rig as the bed material with regard to its behaviour in oxygen transfer (from the AR to the FR) and reforming capability. The solids are exposed in the FR to a surrogate gas mixture including 1-methylnaphthalene as model tar compound. The temperature in the FR were kept between 845 and 858 °C. The results show that a low content of oxygen was transported by the olivine due to the redox-cycling in the reactor system. The oxygen transport has no significant impact on the tar conversion and gas composition. The tar conversion was found to be between 67.0 and 73.0 % for different tar loads. GCMS analysis show that 95 % of the residual tar in the exhaust gas is naphthalene besides indene or acenapthylene.

- **Paper III**

The synthetic bed material Fe-olivine is investigated in the DCFB pilot rig. The focus of the study is oxygen transfer and reforming behaviour. Similar to the experimental study in Paper II, the solid particles are exposed in the FR to a surrogate gas mixture including 1-methylnaphthalene as model tar compound. The FR exhaust gas composition for each operation point is shown in Figure 5.2. Different operation points were
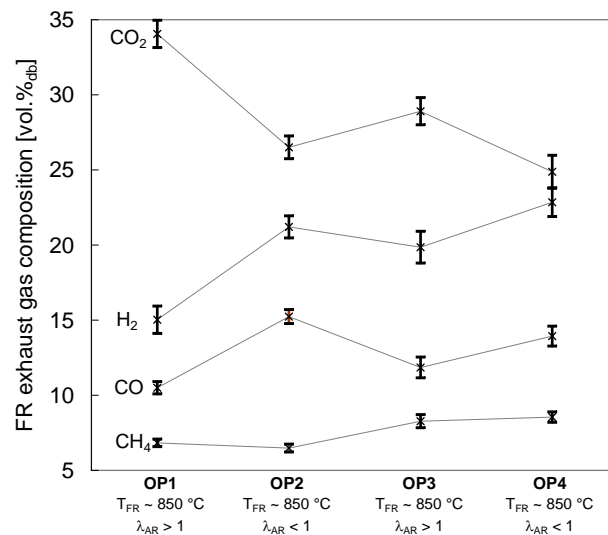
Figure 5.2: FR exhaust gas composition for the operation points, mean values and standard deviation of measurement, [Paper III], operation points with oxygen excess in the AR are denoted as $\lambda_{AR} > 1$, substoichimetric conditions are denoted as $\lambda_{AR} < 1$, OP3 and OP4 were performed with tar feed

carried out, whereas the excess of air in the AR was varied and the tar feed. High oxygen transport is developed by the redox-cycling between AR and FR. However, the tar decomposition was marginally affected by oxygen transport and oxidation. It was found that the oxygen transport from the AR to the FR results in partial oxidation of

the gas species CO and H_2. The model tar compound 1-methylnaphthalene was decomposed to about 99 %. However, a certain fraction of gravimetric tars was formed due to re-combination. Naphthalene was found as the main component (with $\approx$ 94 wt%) in the GCMS analysis. Other components which were found in the GCMS analysis are: 1H-indene, 1-benzothiophene or acenaphthylene. The tar conversion based on the GCMS measurement was approximately 73 %.

• **Paper IV**

The paper presents results from an experimental campaign at the CHP Güssing. Limestone was applied as the bed material for biomass gasification with sorption enhanced reforming (also referred to as AER). The gasification temperature was kept at $\approx$675 °C to enable the transport of CO_2 from the gasification reactor to the combustion reactor. Thus, the reaction progress of CO-shift is favoured due to the partial sequestration of CO_2. The H_2 content in the product gas was significantly increased due to the sorption enhanced reforming. A comparison of the product gas composition between the standard operation mode (with olivine as the bed material) and the sorption enhanced reforming operation mode is shown in Figure 5.3. Further considerations and specification of the CO_2 transport is given in Section 5.5.2.
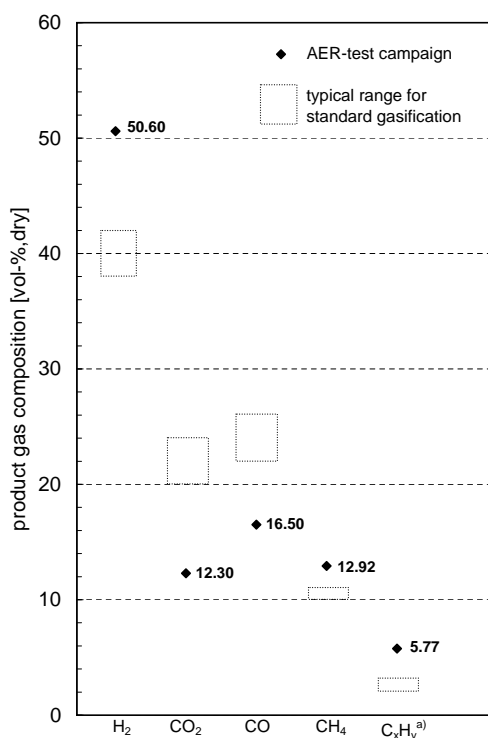
Figure 5.3: Product gas composition: standard gasification and AER test campaign; [a]sum of C_2H_4, C_2H_6 and C_3H_8, [Paper IV]

- **Paper V**

The paper presents a comparative experimental study on the effect of silica sand and olivine on the gas production in the DFB pilot plant. Silica sand is considered as the reference bed material. The application of olivine as the bed exhibit changes in gas composition and tar content, which is due to the catalytic activity of the olivine. The general reactor performance is shown by means of the pressure and temperature profile. The shift in product gas composition is discussed. Figure 5.4 shows the product gas composition for silica sand, olivine and a mixture of silica sand and olivine. It was found
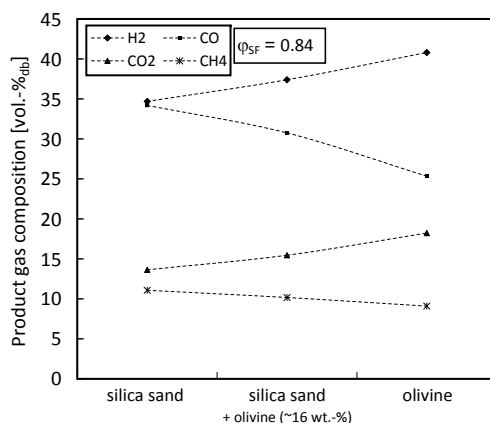
Figure 5.4: Gas composition (main components) versus different solid inventories, [Paper V]

that the product gas composition is shifted in presence of olivine. The relative content of H_2 in the product gas is increased by 5 percentage points in volume. The relative contents of CO and CO_2 are shifted up to 10 percentage points in volume. Olivine is identified as increasing:

- the specific product gas yield
  (silica sand: $0.99 \, \mathrm{Nm^3_{db}/kg_{fuel,daf}}$, olivine: $1.13 \, \mathrm{Nm^3_{db}/kg_{fuel,daf}}$) and

- the relative water conversion
  (silica sand: $0.04 \, \mathrm{kg_{H_2O}/kg_{fuel,daf}}$, olivine: $0.12 \, \mathrm{kg_{H_2O}/kg_{fuel,daf}}$).

In turn, olivine acts as a promoter for CO-shift as the logarithmic deviation from CO-shift equilibrium is decreased (silica sand: -0.83, olivine: -0.38) in presence of olivine. Further, it was found that olivine reduces the GCMS detectable tar content in the product gas by approximately 35 %. The content of gravimetrically detectable tars in product gas was reduces by approximately 60 %. The paper presents a discussion of tar species, which were detected with the GCMS tar measurement. Napthalene was found to contribute to the GCMS tar complex at quantities of 40-45 wt% for olivine and 31-33 wt% for silica sand. Further, a tar classification from literature is used to lump the detected tar species into appropriate groups. The change of the tar groups is presented and discussed in the paper.

- **Paper VI**

The paper presents an experimental study on the effect of bed particle inventories with different particle sizes in the DFB pilot plant. Bed particle inventories of olivine with different mean particle sizes are applied. The mean particle sizes are 520 μm and 260 μm, and therefore differ in coarse and fine solid particle inventories. Several experimental test runs were carried with the both coarse and fine solid particle inventory, whereas temperature, fuel input and/or steam-to-fuel ratio was varied. Thus, hydrodynamic behaviour and gas residence times were influenced. Hydrodynamic considerations, gas composition, tar content, tar composition and specific data are discussed in the work. It is found that the main gas composition is similar for different solid inventory but is influenced by temperature and steam-to-fuel ratio. The experimental runs with fine particle inventory exhibit an enhanced gas-solid interaction, higher gas residence times in the bubbling bed, and higher specific surface area of the solids. Figure 5.5 shows the GCMS and gravimentric tar content in the product gas for different experimental runs with coarse and fine particle inventory. A significant effect is found for the tar reduction.
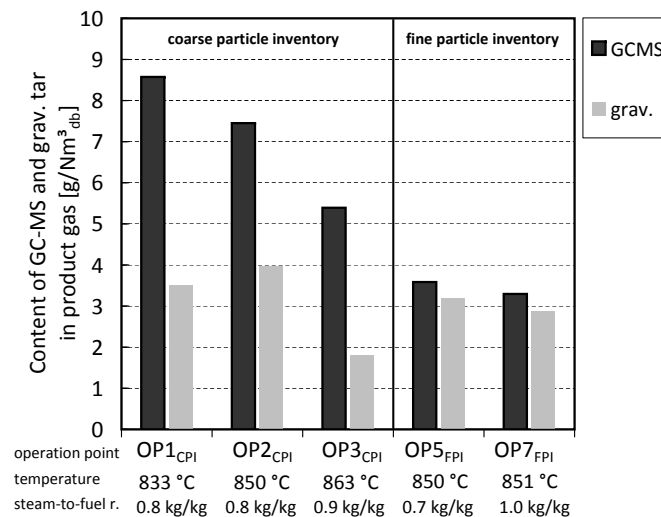
Figure 5.5: Mapping of tar measurement (mean values): GCMS and gravimetric tar content in product gas versus operation points, [Paper VI]

The content of GCMS detectable tars in the product gas is reduced by about 50 % for the fine particle inventory. Further, the global nature of the GCMS tar composition is found to be independent of the solid particle inventory. By contrast, higher gasification and freeboard temperature shift the GCMS tar composition towards a higher fraction of tertiary tar compounds.

- **Paper VII**

This paper presents experimental results with different bed materials. The considered catalytically active materials are grouped into non-metallic oxides (limestone) and metallic oxides (olivine, Fe-olivine and Ni-olivine). The presentation of the results also covers the inert bed material silica sand. Figure 5.6 displays the product gas composition for different metallic oxide bed materials including silica sand. The comparison shows that Ni-olivine exhibit a high catalytic activity. The product gas is characterised by a high content in H_2 ($\approx 44 \, vol\%_{db}$) for Ni-olivine. In turn the CO-shift reaction is highly favoured in presence of Ni-olivine. Likewise the GCMS and gravimentric tar content is found to be very low for Ni-olivine (GCMS: $1.2 \, g/Nm^3_{db}$, gravimetric: $0.4 \, g/Nm^3_{db}$).
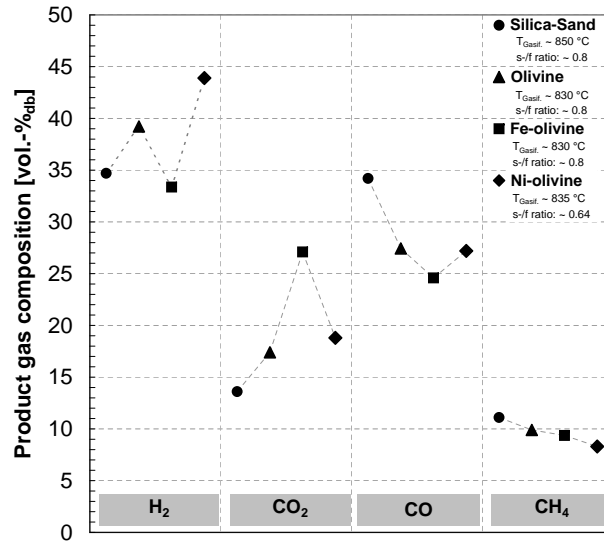
Figure 5.6: Product gas composition for different solid bed materials, [Paper VII]

- **Paper VIII**

This paper presents the experimental series with Fe-olivine as the bed material in the DFB pilot plant. The experimental series involve the variation of gasification temperature and steam-to-fuel ratio. Besides, a mixture of natural olivine and Fe-olivine (50/50 wt%) was applied as the bed inventory. It was found that the product gas composition is highly influenced by the oxygen transport from the combustion reactor to the gasification reactor. In consequence the gas species CO and H_2 are partially oxidised. The mapping of the GCMS tar content in the product gas is shown in Figure 5.7.
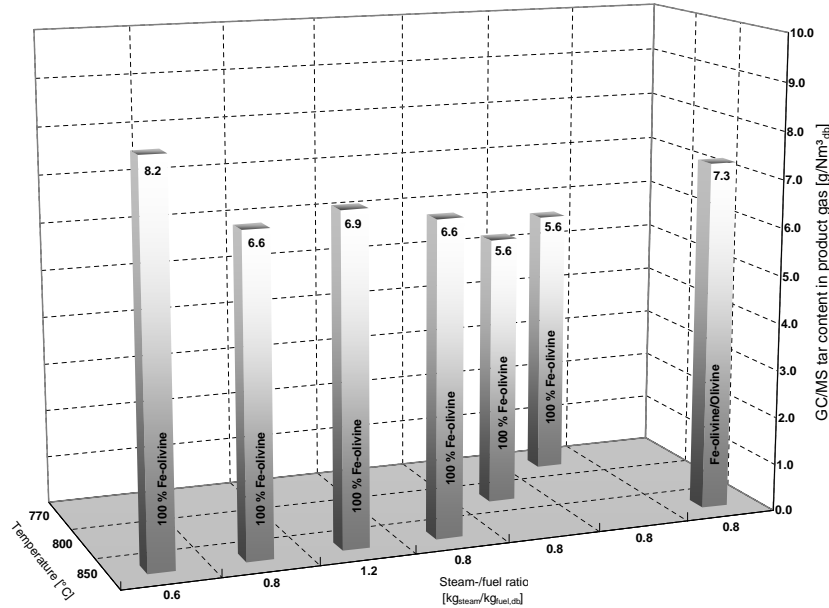
Figure 5.7: Mapping of the GCMS tar measurement of the experimental runs, [Paper VIII]

- **Paper IX**

In this paper, the iron supported material Fe-olivine is compared to natural olivine with regard to the amount and distribution of GCMS detectable tar compounds. The experimental results show that the tar content in product gas is significantly lower at gasification temperatures between 770-830 °C for Fe-olivine. However, at gasification temperatures of approximately 850 °C the tar content for Fe-olivine is similar to that of olivine. It was found that the distribution of the substance groups is similar between Fe-olivine and olivine.

The following section provides additional data, which are not included in the papers.

5.2 Outline of the solid materials

Paper I provides a comparison of experimental results with limestone and olivine in the DFB pilot plant. The comparison of the performance of silica sand and olivine is given in Paper V. Furthermore, the behaviour of Fe-olivine is discussed in the Papers VII and VIII. The general reactor performance (e.g., temperature and pressure profile) is shown in Paper V. A comparison of olivine and Fe-olivine with regard to tar decomposition and the character of the tar is given in Paper IX. Paper VI shows the fluidised bed performance and hydrodynamic considerations for a typical operation point and variations.

A brief presentation of experimental results derived from different materials can be found in Paper VII. In this section a summary and outline as well as further experimental data and results are presented. The results are presented in Tables 5.3, 5.4 and in Figures 5.8a-d, 5.9a-d. The Tables contain process data, which were recorded during the experimental run by the measurement devices. Further data are included, which are derived by calculation of the mass and energy balances.

The experimental test run with limestone exhibits the highest content and specific yield in hydrogen.

- The following order of hydrogen content and yield was found (see also Table 5.3, 5.4 and Figure 5.8a):

$$\textit{limestone} > \textit{olivine} > \textit{Fe-olivine} > \textit{silica sand}.$$

Due to the higher fuel input (fuel power load) and the slightly higher steam-to-fuel ratio, the gas residence times for limestone are lower than for the other operation points. It is supposed that the initial chemical composition (see Paper I) of the limestone is modified during the course of the experimental run as the real CO_2 partial pressure in the reaction atmosphere (in the gasifier and the riser) is below the CO_2 equilibrium partial pressure (see Section 2.7.2 and Figure 2.22). Thus, the initial material ($CaCO_3$) is modified towards CaO during the course of the experiment. The fairly good activity in CO-shift is generally associated to CaO. This is confirmed by the H_2 content and the logarithmic deviation from CO-shift equilibrium.

The activity of CaO as a catalyst for CO-shift and tar reforming is confirmed by several authors, e.g., Delgado et al. [111], Simell [130], and Dayton [104]. The performance with Fe-olivine is highly influenced by the oxygen transfer, which is shown in Paper VIII. It was found that H_2 and CO are partially oxidised to H_2O and CO_2, due to the oxygen transfer into the gasification reactor. As a result, the contents of H_2 and CO are reduced in the product gas. The materials can be assessed with regard to their capacities for water conversion. Principally, high water conversion is desired as this indicates an efficient use of the water input.

In contrast, a process operation with low water conversion reveals that a considerable amount of water remains unused without contributing to the H_2 yield.

- The water conversion rates are found to be of the order (see Table 5.4 and Figure 5.8c):

$$limestone/olivine \gg Fe\text{-}olivine/silica\ sand$$

As the water is mainly converted and consumed by the CO-shift reaction (see Eq. 2.10), the logarithimic deviation of the actual gas composition ($p\delta_{eq,CO-shift}$) from the CO-shift equilibrium is used to assess the extent of the CO-shift reaction.

- The order of best approaching the CO-shift equilibrium is found to be (see Table 5.4 and Figure 5.8d):

$$limestone > Fe\text{-}olivine > olivine > silica\ sand$$

The tar content for the different solids is shown and discussed in the Papers I,V,VII,VIII and IX.

- The following order of tar reduction potential was found (see also Table 5.3 and Figure 5.8b):

$$limestone > Fe\text{-}olivine > olivine > silica\ sand^{1}.$$

A final summary of the materials is shown in Table 5.2. Figures 5.9a-d show a comparison of the measured gas composition (see also Table 5.3) to the gas composition involving that the CO-shift reaction has reached thermodynamic equilibrium. In each Figure, it appears that reaction progress towards higher hydrogen yield and content is possible, which is also illustrated by the logarithmic deviation from CO-shift equilibrium in Figure 5.8d.

Table 5.2: Outline of the materials

	silica sand	limestone	olivine	Fe-olivine
hydrogen yield	low	high	moderate	low
water conversion	low	high	high	low
log. dev. from CO-shift eq.	high	low	moderate	moderate
tar content in product gas	high	low	moderate	moderate

---

[1]although silica sand is listed in this order, this material is not considered as being active, but has been added as a reference

Table 5.3: Experimental operation data, part I

Parameter	Solid material / Unit	Notation	silica sand OP_{silica}	limestone $OP_{limestone}$	olivine $OP_{olivine}$	Fe-olivine $OP_{Fe\text{-}olivine}$
data from Paper			V	I	V	VII, VIII
fuel input (wood pellets)	[kg/h]		20	24	20	20
fuel power load	[kW]		97	116	97	97
fuel			wood pellets	wood pellets	wood pellets	wood pellets
mean particle diameter of solid	[µm]		450	850	430	500
steam fluidisation gasifier	[kg/h]		9.8	13.1	9.8	9.8
steam fluidisation ULS and LLS	[kg/h]		9.5	11.6	9.5	9.5
fluidisation secondary air	[Nm^3/h]		50	50	50	50
ratio primary to secondary air	[-]		1/10	1/10	1/10	1/10
initial solid inventory	[kg]		100	100	100	100
steam-to-fuel ratio, $\varphi_{SF,wt}$	[kg$_{H_2O}$/kg$_{fuel,daf}$]		0.8	0.9	0.8	0.8
steam-to-carbon ratio, $\varphi_{SC,mol}$	[mol$_{H_2O}$/mol$_C$]		1.1	1.2	1.1	1.1
steam-to-carbon ratio, $\varphi_{SC,wt}$	[kg$_{H_2O}$/kg$_C$]		1.6	1.8	1.6	1.6
H_2	[vol.%$_{db}$]		34.7	50.8	40.8	35.2
CO	[vol.%$_{db}$]		34.2	18.9	25.9	22.8
CO_2	[vol.%$_{db}$]		13.6	20.1	18.7	26.9
CH_4	[vol.%$_{db}$]		11.1	7.8	9.4	8.7
C_2H_4	[vol.%$_{db}$]		3.0	1.5	2.0	2.1
C_2H_6	[vol.%$_{db}$]		0.2	0.5	0.1	0.1
C_3H_8	[vol.%$_{db}$]		0.3	0.2	0.3	0.2
tar content in product gas, GCMS	[g/Nm$^3_{db}$]		10.8	2.6	7.4	6.3
tar content in product gas, grav.	[g/Nm$^3_{db}$]		8.2	0.3	4.0	6.2
specific tar content, GCMS	[g/kg$_{fuel,daf}$]		10.8	2.7	8.7	7.0
specific tar content, grav.	[g/kg$_{fuel,daf}$]		8.1	0.3	4.6	6.9

The product gas contains also some low amounts of N_2 and C_4/C_5 hydrocarbons, which complete the composition to 100vol%$_{db}$, see also Papers V and VI

OP = operation point

Table 5.4: Experimental operation data, part II

Parameter	Unit	OP_{silica}	$OP_{limestone}$	$OP_{olivine}$	$OP_{Fe\text{-}olivine}$
gasification temperature	[°C]	851	849	850	847
combustion temperature, riser	[°C]	878	893	904	893
total product gas yield	[Nm^3/h]	37.3	45.4	38.2	39.6
H_2O content in product gas	[vol%]	50.1	47.7	43.1	47.1
product gas yield	[Nm^3_{db}/h]	18.6	23.8	21.7	20.9
specific product gas yield	[$Nm^3_{db}/kg_{fuel,daf}$]	0.99	1.06	1.16	1.12
lower heating value	[MJ/Nm^3_{db}]	14.4	11.6	12.8	11.5
mean gas residence time in BB, $\overline{\tau}_{BB}$	[s]	0.26	0.22	0.26	0.25
mean gas residence time in FB, $\overline{\tau}_{FB}$	[s]	2.9	2.4	2.8	2.7
mean gas residence time in riser, $\overline{\tau}_R$	[s]	0.8	0.7	0.8	0.8
specific H_2 yield	[$Nm^3_{H_2}/kg_{fuel,daf}$]	0.350	0.501	0.489	0.412
specific CO yield	[$Nm^3_{CO}/kg_{fuel,daf}$]	0.353	0.200	0.308	0.312
specific CO_2 yield	[$Nm^3_{CO_2}/kg_{fuel,daf}$]	0.138	0.188	0.221	0.263
specific CH_4 yield	[$Nm^3_{CH_4}/kg_{fuel,daf}$]	0.110	0.077	0.110	0.098
specific C_2H_4 yield	[$Nm^3_{C_2H_4}/kg_{fuel,daf}$]	0.030	0.010	0.023	0.023
sum of specific C_2H_6 and C_3H_8 yield	[$Nm^3_{C_2H_6+C_3H_8}/kg_{fuel,daf}$]	0.005	0.005	0.005	0.003
log. deviation from CO-shift eq., $p\delta_{eq,CO-shift}$	[-]	-0.83	-0.19	-0.36	-0.27
abs. water conversion, $X_{H_2O,abs}$	[kg_{H_2O}/kg_{H_2O}]	0.05	0.15	0.16	0.05
rel. water conversion, $X_{H_2O,rel}$	[$kg_{H_2O}/kg_{fuel,daf}$]	0.04	0.13	0.14	0.04

(a) Product gas composition, main components

(b) Tar content in product gas, GCMS and gravimetric

(c) Water conversion and water content in product gas

(d) Logarithmic deviation from CO-shift equilibrium
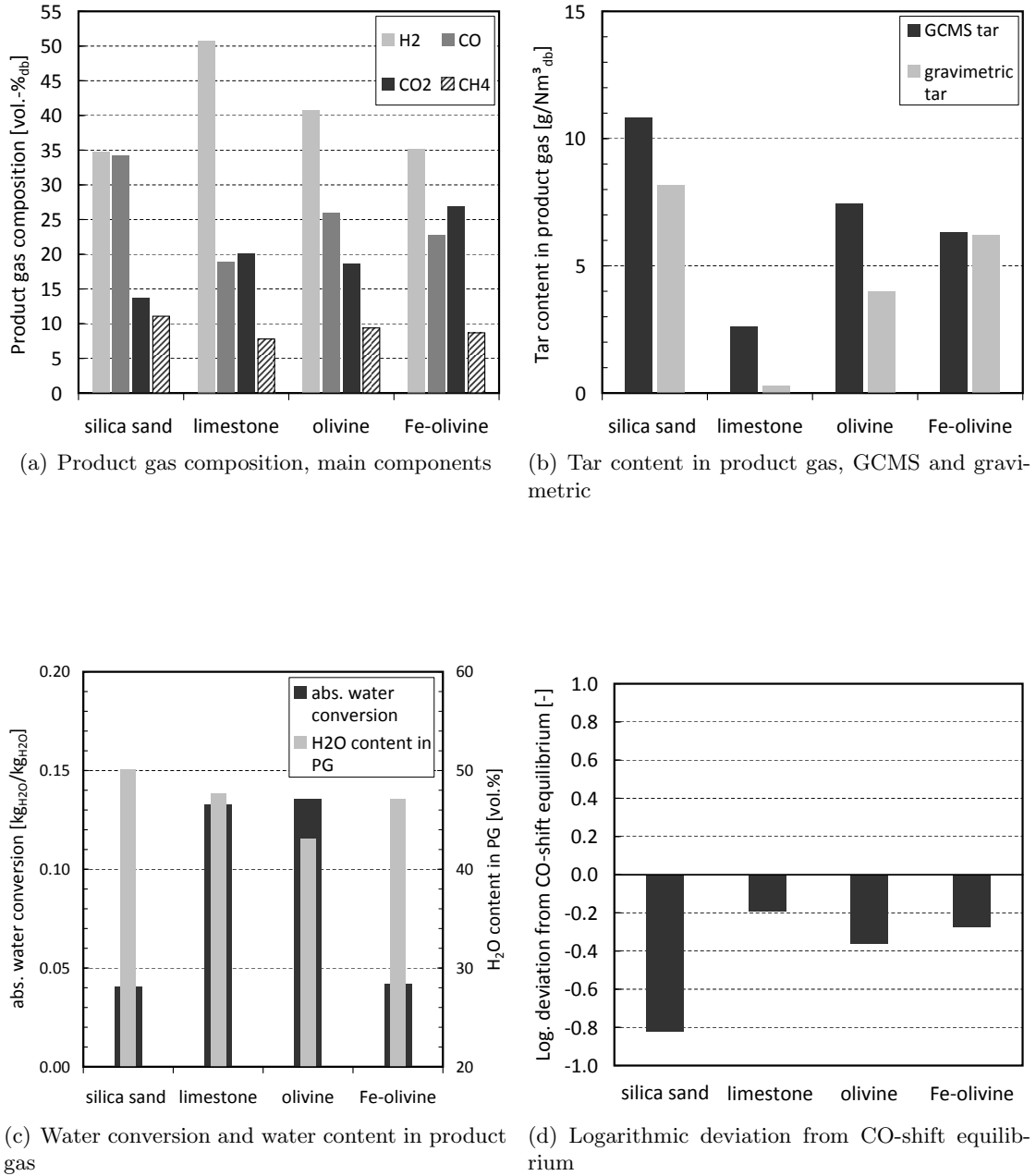
Figure 5.8: Mapping and outline of experimental results, according to Table 5.3 and 5.4

(a) silica sand

(b) limestone

(c) olivine

(d) Fe-olivine
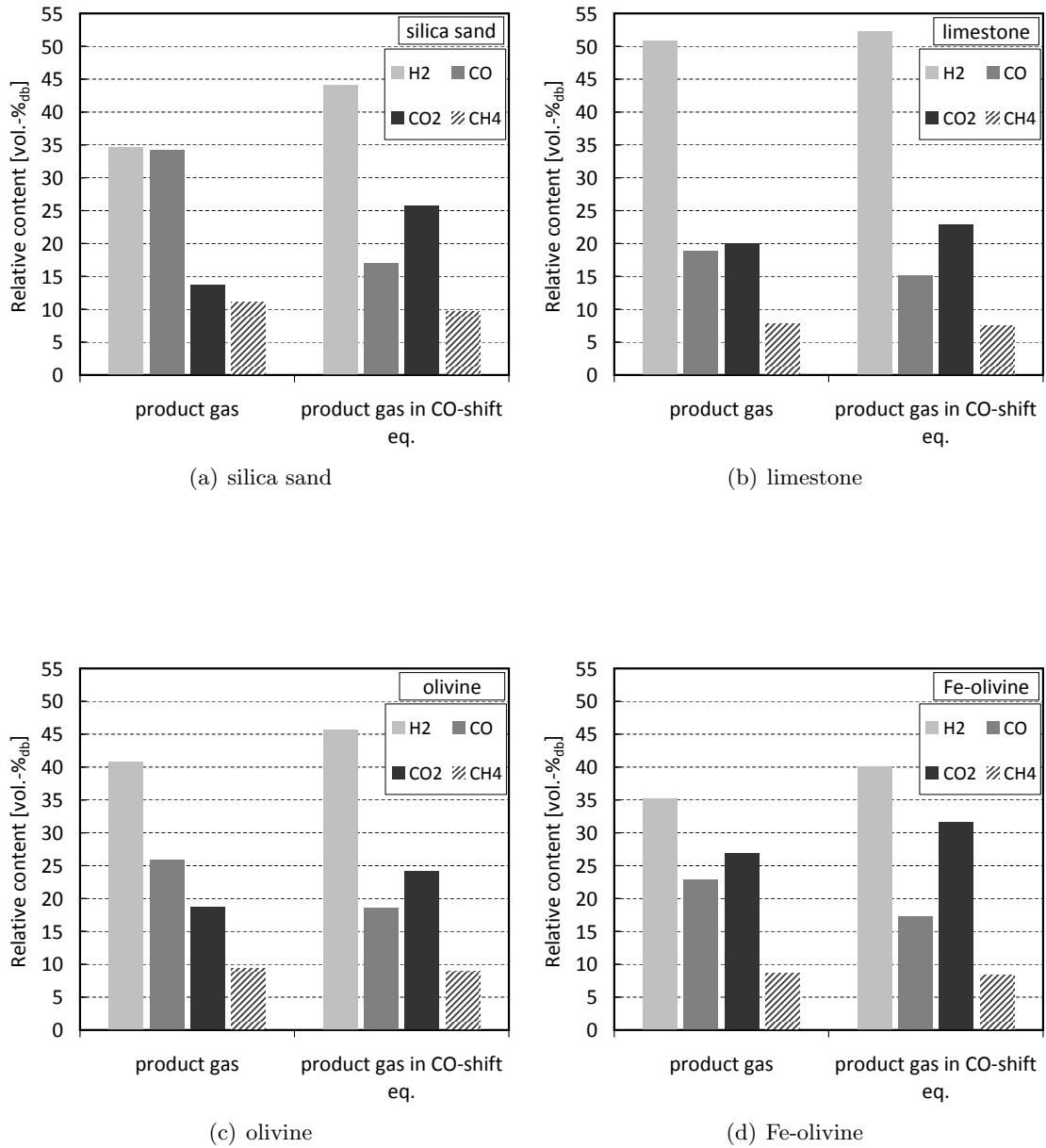
Figure 5.9: Comparison of real product gas composition to theoretical product gas composition with equilibrium of the CO-shift reaction, calculation with IPSEpro

5.3 Fluidised bed considerations

This section is related to the experimental results and findings presented in Paper VI. The last section has shown the general capability of the different solids. However, the principal catalytic activity of the material might be influenced by the fluidised bed characteristics. This addresses the interaction of the solids with the gaseous species in the bubbling bed. The following aspects are of importance:

- intensity of gas–solid contact in the fluidised bed,

- gas residence time in the fluidised bed.

A comprehensive experimental study was carried out to examine fluidised bed effects. This study considers solid inventories with different mean particle sizes. The experimental approach and the results, in particular the effect on tar content and component distribution, are described in Paper VI. Figure 5.10 shows a simplified illustration to comment on the findings of Paper VI. The sketch in Figure 5.10 illustrates the pathway of the gaseous species (permanent gases and tar) through the gasification reactor by passing the bubbling bed and the freeboard zone. Further, the predominant character of the reaction atmosphere is indicated.
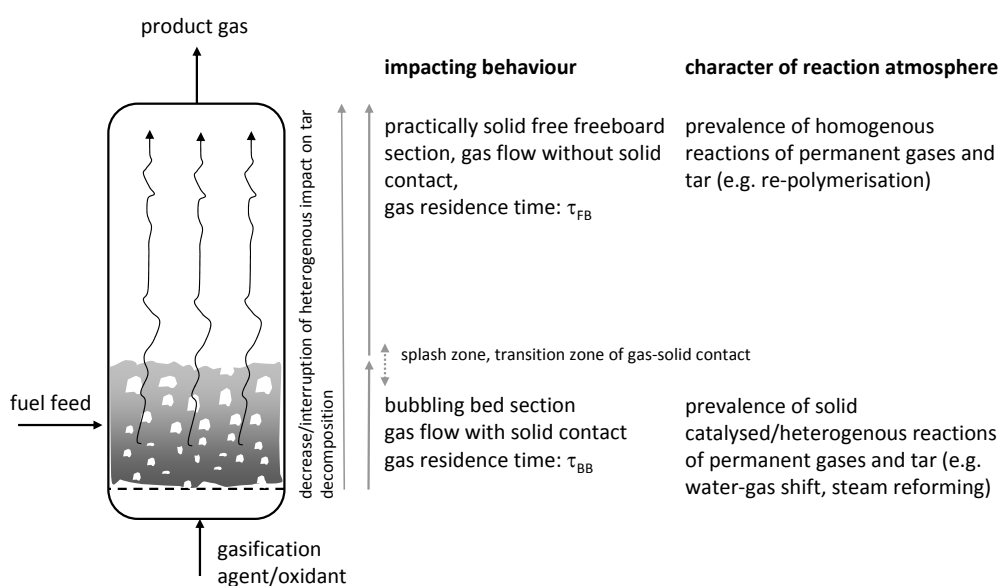
Figure 5.10: Simplified sketch of gas–solid contacting and non gas–solid contacting zones in the gasifier and their relevance for the evolution of tar

The experimental study shows that higher turbulence in the bubbling bed (which is the case for small particles) favours tar conversion in combination with higher mean gas residence times in the bubbling fluidised bed ($\overline{\tau}_{BB}$).

A simplified approach is used to calculate the mean gas residence time ($\overline{\tau}_{BB}$) in the bubbling bed. The calculation considers:

- an ideal stirred vessel for all solids (fuel and bed material particles),

- a plug flow of the gaseous phase,

- a typical bubbling fluidized bed porosity (ε_{BB}),

- and a linear release of volatiles of the fuel particles over the bubbling bed height.

Thus, the mean gas residence time is defined according to Eq. 5.1, wherein A is the cross-sectional area, H the mean bed height and $\dot{V}_{PG}$ the product gas volume flow.

$$\overline{\tau}_{BB} = \frac{A \cdot H \cdot \varepsilon_{BB}}{\dot{V}_{PG}} \qquad (5.1)$$

Besides, the findings show that significant decomposition is effected even at comparatively low gas residence times in the bubbling bed of $\overline{\tau}_{BB} < 0.5$ sec. This tendency is supported by the findings of Kirnbauer et al. [131], who reported a significant decrease of tar content with a CaO-based catalyst (CaO coating on olivine) contrasted to fresh olivine at comparable mean gas residence times[2] in the pilot plant. Finally, the impact of gas–solid contact and gas residence time is emphasised by these studies and findings. The splash zone is not further discussed as this region can not be exactly defined. This zone might be rather matched to the bubbling bed in terms of the gas–solid contact.

---

[2]The gas residence times are not explicitly given in that paper, but the operation point is fairly similar to those reported in this context

5.4 Considerations on the tar decomposition and formation

5.4.1 Bubbling bed section

The **bubbling bed section** is apparently the part with the predominance of heterogenous reaction at the surface of particles of the solid inventory. For simplicity, the bubbling bed section is considered to be ideally stirred and mixed of gas and solids. However, the the upwards rising gas bubbles are free of solid particles in their interior.

The detailed substeps of heterogenous catalysed tar decomposition are not yet clarified in the literature. However, some authors have proposed model or reaction schemes for the decomposition of certain components (e.g. naphthalene). Devi [21] proposes a model scheme for the decomposition of naphthalene; Corella et al. [132] proposed a mechanisms for the catalytic decomposition of phenanthrene on CaO surfaces.

The bulk overall process of heterogeneous catalysis is assumed to proceed as follows [133]:

- adsorption[3] of the reactants at the solid surface,

- reaction between the reactants, and

- desorption of the products from the solid surface.

The mechanisms which are relevant for the kinetics can be distinguished by, [133]:

- the adsorption of both reactants to subsequently form the product (*Langmuir-Hinshelwood* mechanism);

- or the adorption of one reactant to subsequently react with another molecule from the gas phase without adsorbing (*Eley-Rideal* mechanism).

With regard to non-substituted aromatic tar compounds (PAH), the C–C or C–H bond scission is apparently the first step in decomposition of the species. The cleavage of the bond effects the ring opening of the aromatic compound. Consecutive reactions can proceed, which yield a gradually decomposition of the hydrocarbon. The further progress can be characterised by radical reactions. Besides, a dimerisation of intermediate products can also occur, which in turn yields an aromatic compound, (see the reaction scheme proposed by Devi [21]). It is further reported in the literature that certain gaseous species may influence the decomposition behaviour. In particular H_2O, CO_2 and H_2 have been revealed as influencing species. H_2O and CO_2 were found to enhance the decomposition reactions whereas H_2 can have an inhibiting effect, Devi [21], Vreugdenhil and Zwart [134], Garcia and Hüttinger [135], Jess [136,137]. However, this subject of heterogenous catalysis and decomposition pathways of hydrocarbons is not futher detailed, as this is not included in the focus of this work.

---

[3]Which is a chemisorption in terms of heterogeneous catalysis. However, both terms are used in parallel in this section

The solid materials in this thesis may be detailed with regard to the active parts for the heterogeneous catalysis.

- CaO is the active part of limestone. At gasification temperatures of about 850 °C, as considered in the latter section, limestone is constantly kept at calcination conditions, see Figure 2.22.

  A possible mechanism is that the CaO supplies OH radicals from H_2O, [73, 132]. Consequently, the radicals effect the ring opening of aromatic structures. Besides, the formation of radicals is also affiliated to the reaction of CaO and CO_2.

  Another mechanism is possible, which is based on the fact that CaO acts as a Lewis acid, [138]. Thus, the CaO features the character of an electron pair acceptor. The chemisorption of species and consecutive reactions are enabled.

  Further it is assumed that the polar (phenols, oxygenated compounds, methoxy-type compounds) tar compounds are preferably decomposed in the presence of CaO due to the character of electron pair acceptor. Alden et al. [139] reported that almost all tar components after a catalytic cracking with dolomite (which also contains CaO) were non-polar components (which are the PAH). Furthermore, this fact is supported by the findings presented in Paper I as phenol was not detected during the test run with limestone. A similar finding is reported by Kirnbauer et al. [131].

- In the case of iron, the catalytic activity might be attributed to the state of the iron, which is either metallic iron or iron oxide (see Section 2.7.1). Metallic iron is considered to be responsible for C–C and C–H bond scission, [140]. Nordgreen et al. [141, 142] have stated that metallic iron is active in tar decomposition, which was based on experimental studies in air gasification. With regard to the oxides of iron, various statements can be found in the literature. However, there is no general agreement on iron oxides as to their activity in tar decomposition. Rhodes et al. [143] found that iron oxide is an important catalyst for the water gas shift reaction. Experimental studies with air gasification by Nordgreen et al. [141, 142, 144] revealed that iron oxide is almost not active in tar decomposition. On the contrary, Polychronopoulou et al. [145] showed the activity of an Fe-based catalyst in steam reforming of phenol. A catalytic activity in tar decomposition of an Fe-based catalyst is also reported by Uddin et al. [146] and Noichi et al. [147].

  The modification of the Fe phase in terms of the oxidation state is hard to estimate. Due to the solid circulation in the DFB system, the particles are affected by a strongly oxidising atmosphere (combustion reactor) and a prevalent reducing atmosphere (gasification reactor) with different solid residence times. Besides, the reaction atmospheres in the gasification reactor exhibits also the presence of oxidising gaseous components (H_2O and CO_2).

5.4.2 Freeboard section

The aspect of the possible interactions of the tar during its pass through the **freeboard section** could not be clarified within the scope of this work. The freeboard is practical free of solid particle except the very fine particles. The mean gas residence time in the freeboard (τ_{BB}) is calculated as plug flow. It was found that the freeboard is characterised by relatively high gas residence times of about 2.5 to 4.5 seconds, which strongly depends on the steam-to-fuel ratio and the fuel feed, see Paper VI and Tables 5.3 and 5.4. The study shows that the gravimetric tar content is marginally reduced whereas the GCMS tar is noticeably reduced. Thus, it is supposed that reactions occur which produce high molecular tar components (Class 5 and/or gravimetric tar). The impact of the freeboard, in particular the residence time, on the character (ECN classification) of the tar was investigated by Paasen and Kiel [65], and Vreugdenhil and Zwart [134]. They noticed a production of Class 4 and Class 5 tars in the freeboard. They stated that Class 4 and Class 5 (which might overlap with the gravimetric tar/Class 1) components are:

- either produced by decomposition of even higher PAH or by

- growth of lower PAH, due to dimerisation, cyclisation or polymerisation.
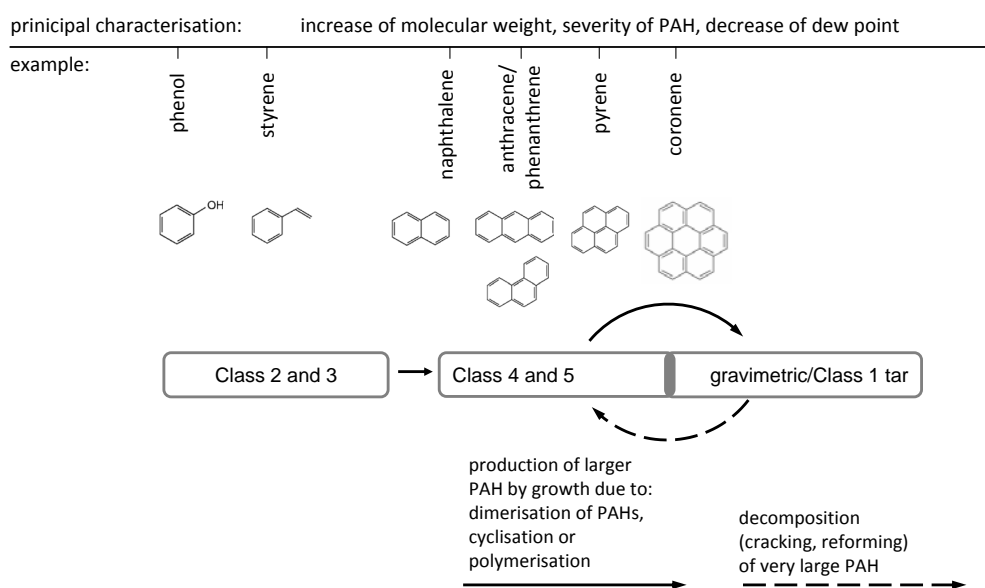
Figure 5.11: Possible interactions of PAH (represented in terms of the ECN classification) due to decomposition and growth; Class 5 and Class 1 (which are the gravimetric tars) overlap

Figure 5.11 presents a possible scheme of PAH interaction, which might occur in the freeboard. In this scheme it is assumend that the very heavy PAH (Class 5 and gravimentric tar) are formed by the growth of smaller PAH. The thermal decomposition of

higher PAH to smaller PAH might also take place. Thus, finally, it is supposed that the reaction atmosphere in the freebard might be characterised by a simultaneous interaction of both decomposition and production of PAH. It is therefore likely that the growth of large PAH components is predominant, as the temperature in the freeboard (800°C–850°C) is relativley low compared to the temperatures which are needed for an uncatalysed thermal decomposition ($>1000\,°C$). These assumptions are supported by the findings of several authors. Thermal transformation of light PAH to larger PAH is reported by Egsgaard and Larsen [72]. Paasen and Kiel [65] reported that large PAH are apparently produced by a PAH growth reaction mechanism above $850\,°C$.

5.4.3 Final considerations

The last sections have shown that the zones of the gasifier (bubbling bed and freeboard) have to be considered separately from each other. Figure 5.12 presents a simple assumption of the influences on the final character of the tar in the product gas. It can therefore be assumed that it is likely that such connections exist between the bubbling bed section and the freeboard section as the character of tar exiting the bubbling bed is further exposed to the action of the freeboard section. Apart from gas residence times,
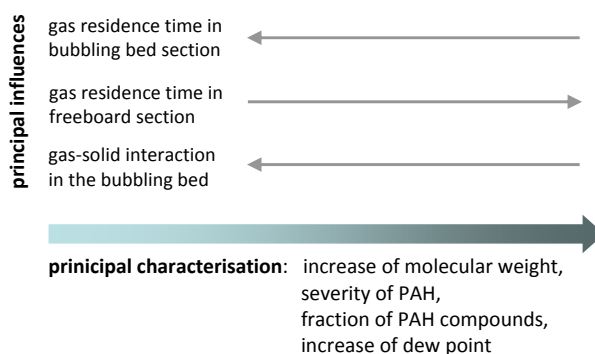
Figure 5.12: Principal influences on the character of the tar

lower gasification temperatures (700°C–800°C) would yield secondary tar components instead of tertiary tar components, see Figure 2.12. The tertiary tar components are PAH with increasing size, which are hard to decompose. But the secondary tar components are smaller molecules, which are more reactive (polar components, e.g. phenol) and decompose more readily. Furthermore, the prevalence of secondary tar components would lower the tar dew point.

5.5 O$_2$ and CO$_2$ transport

5.5.1 Considerations for Fe-olivine

Results from DCFB pilot rig

Oxygen transport from combustion to gasification reactor and its effects on the tar decomposition is presented in Paper III and is also illustrated in Paper IX. Natural olivine was further investigated in terms of its ability to transfer oxygen and decompose tar, see Paper II. The experimental studies of Papers II and III were carried out in the DCFB pilot rig. This reactor system is similar to that of the DFB pilot plant, as the circulating solids are exposed to a reducing reaction atmosphere and an oxidising reaction atmosphere.

The materials were investigated in a surrogate gas mixture which represents the reaction atmosphere in the gasification reactor and also contains 1-methylnaphthalene as model tar compound. Details on the experimental procedure and the results are given in Papers II and III, which have shown that O$_2$ is marginally transported in the case of natural olivine whereas Fe-olivine exhibits a well marked capacity for O$_2$ transfer.

However, no clear effect on the tar decomposition was found. Furthermore, the solid samples taken during the experimental test runs with Fe-olivine were investigated by X-ray diffraction (XRD) to detect the iron phases present at the particle surface. The characterisation of the solid samples was carried out at the University of Strasbourg (Laboratoire des Matériaux, Surfaces et Procédés pour la Catalyse).

The results of the characterisation of the solid samples are summarised in a deliverable [148] from the UNIQUE project. Solid samples were taken from the upper and lower loop seal from the DCFB pilot rig. Thus, the samples were affected by:

- an oxidising reaction atmosphere (upper loop seal, ULS) in the air reactor (which is comparable to the combustion reactor in the DFB pilot plant) and

- a reducing reaction atmosphere (lower loop seal, LLS) in the fuel reactor (which is comparable to the gasification reactor in the DFB pilot plant).

Table 5.5 presents the pattern of the experimental operation points that were carried out.

Table 5.5: Overview of the experimental focus of the papers

experimental conditions /operation point[1]		OP1	OP3	OP4
λ in air reactor	[-]	>1	>1	<1
temperature in fuel reactor	[°C]	≈ 850	≈ 850	≈ 850
tar feed[2]	[-]	no	yes	yes
sample from ULS	Figure	5.13	5.14	5.14
sample from LLS	Figure	5.13	-	-

[1] same labels as used in Paper III to refer to the operation point

[2] 1-methylnaphthalene was used as the model tar compound

[2] dependent on the operation point tar was fed to the reactor or not

Figure 5.13 presents the XRD diffractogram for the solid sample of OP1 from the ULS and LLS, [148]. The solid sample of the ULS (reducing conditions) show that the wustite phase FeO (at $2\theta = 36.32°$ and $42.19°$) appears and the iron oxide phase (α-Fe$_2$O$_3$) dissappears compared to the solids samples (from OP1) of the LLS (oxidising conditions). Thus, the XRD diffractogram indicate that the iron phase (iron oxide state) differs for the materials. Thus, the findings suggest that oxygen was selectively transported. The results are in good agreement with the results shown in Paper III as the O$_2$ transport is also evaluated in this work.
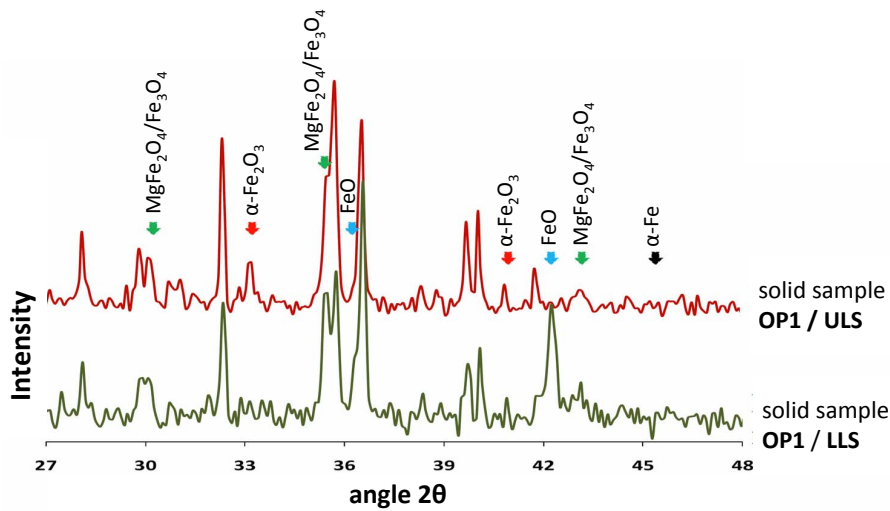
Figure 5.13: XRD diffractogram of the solid samples from ULS and LLS for OP1, [148]

Figure 5.14 shows the XRD for the solid samples of OP3 and OP4 from the ULS. OP3 and OP4 differ from each other as the λ in the air reactor was varied. For OP4 ($\lambda < 1$), the solids were affected by a reducing reaction atmosphere in the air reactor and in the fuel reactor. However, a fully reducing reaction atmosphere is probably not generated in the
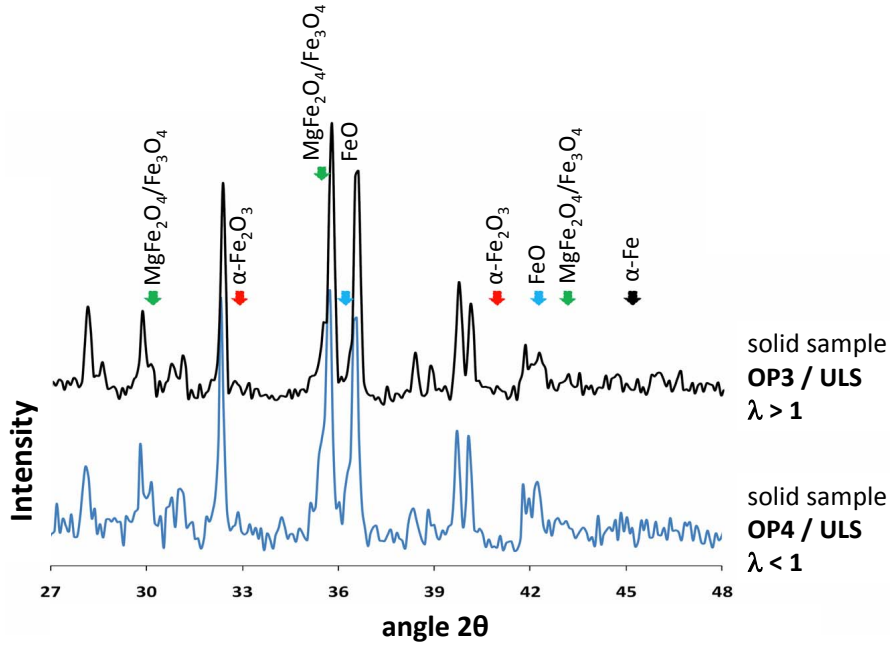
Figure 5.14: XRD diffractogram of the solid samples from ULS for OP3 and OP4, [148]

air reactor, which is consecutively exposed to the particle inventory. Thus, the particles are partially contacted with oxygen in the air reactor, which might again develop iron oxide. However, these latter facts are supported by the XRD diffractogram as the peaks of the reduced iron phases (FeO, Fe_3O_4) are more intense for OP4. Basically, it is found that the Fe-olivine particles (represented by the solid samples) are:

- neither fully reduced (in terms of the prevalence of FeO) nor

- fully oxidised (in terms of the prevalence of Fe_2O_3).

Thus, it can be assumend that the character of the Fe-olivine particles is rather characterised by a certain equilibrium of FeO, Fe_2O_3 and Fe_3O_4. It is supposed that the fractions of the iron phases depend on the particle residence time in the fuel reactor and air reactor.

Results from DFB pilot plant

The following section presents a sample of the experimental results with Fe-olivine in the DFB pilot plant. Within this part, the aim is to illustrate the oxygen transfer within the biomass gasification at the DFB pilot plant. Refer to Paper VIII, which contains a comprehensive and general overview of experimental results. Two experimental operation points were chosen for this section. The experimental operation point (referred to as $OP_{\lambda > 1}$) at standard operation (i.e., $850\,°C$) is contrasted to the experimental operation point that involves a mode of operation (referred to as $OP_{\lambda < 1}$) with CO excess in the combustion reactor (substoichimetric conditions). This approach best promotes the possible capacity of oxygen transfer as the substoichiometric conditions in the combustion reactor mostly inhibites the oxidation of the iron. Figure 5.15 shows the transition from the experimental operation with oxygen transfer towards the operation with inhibition of oxygen transfer. It is apparent that the substoichiometric character of the combustion
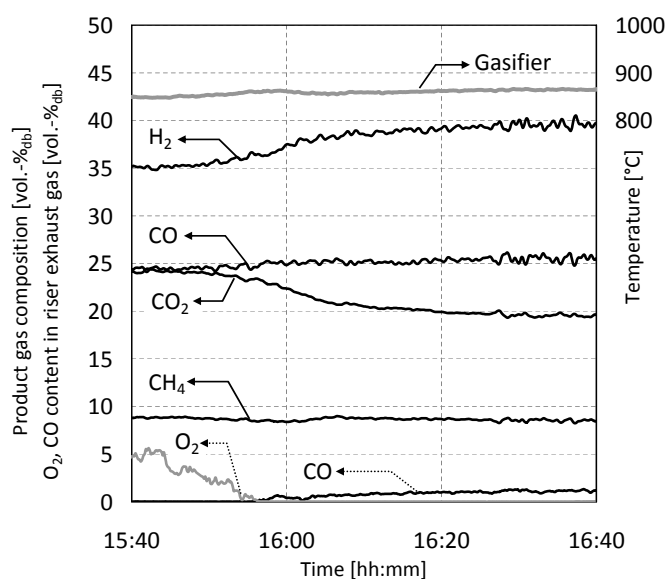
Figure 5.15: Product gas composition (arrows with bold line), CO and O_2 content in the riser exhaust gas (arrows with dashed line) in transition from the oxygen transfer operation to the inhibition of the oxygen transfer (excess of CO in riser)

(undersupply in O_2) generates an excess of CO in the riser. Hence, the H_2 content is increased as less H_2 is oxidised into H_2O by O_2. The CO_2 content decreases as less CO is oxidised. The general operation characteristics and the results of the experimental points are listed in Table 5.6. Wood pellets were used as fuel, whose properties are detailed in Papers VIII or V.

The data in Table 5.6 show that oxygen input strongly influences the product gas composition and the balance of the water regime in the gasifier. Apparently, H_2 is more affected by partial oxidation than CO, as the differences between the H_2 content are

85

higher than the differences between the CO content. Water conversions are shifted to low ratios as the partial oxidation of hydrogen yields additional H_2O in the gasifier. The logarithmic deviation from the CO-shift equilibrium is seen to differ between $OP_{\lambda > 1}$ and $OP_{\lambda < 1}$. The difference between the water content is in line with the latter facts, as the water content is much lower for $OP_{\lambda < 1}$. Despite the global substoichiometric operation in the riser, the oxidation of the iron is not completely inhibited as the particles are still in contact with the oxygen in the riser. However, the results in Table 5.6 show that a considerable quantity of O_2 is transported to the gasifier. The equivalence ratio amounts to 0.12. It is assumed that the heat demand for the endothermic gasification might be partially met by the oxidation.

Figure 5.16 shows the GCMS content and gas composition versus the experimental progress for both $OP_{\lambda > 1}$ and $OP_{\lambda < 1}$. Thus, it is specified that the GCMS tar content remains at a stable level between 6 to $7\,g/Nm_{db}^3$ for $OP_{\lambda > 1}$. But for $OP_{\lambda < 1}$, the content of GCMS tar decreases over time. Ultimately, the GCMS content is lowered to about $3\,g/Nm_{db}^3$. This finding suggest a relation between the capacity for tar decomposition and the iron phase present at the particle. Due to the substoichiometric conditions, it is assumend that the iron is increasingly reduced during the progress of the operation. The increasing reduction of the particle might be confirmed by the slight rise in H_2 during the progress of the operation. Thus, the iron is probably transformed to a higher fraction of FeO or Fe_3O_4. This assumption might be confirmed also by the experimental results of Rapagna et al. [149] who investigated Fe-olivine as the bed material in an externally heated device for biomass steam gasification. They reported a good tar reduction capactiy of the Fe-olivine within this configuration. However, their study was carried out in a single reactor, which was externally (electrical) heated. Thus, Fe-olivine was permanently impacted by a reducing atmosphere and was not in contact with O_2.
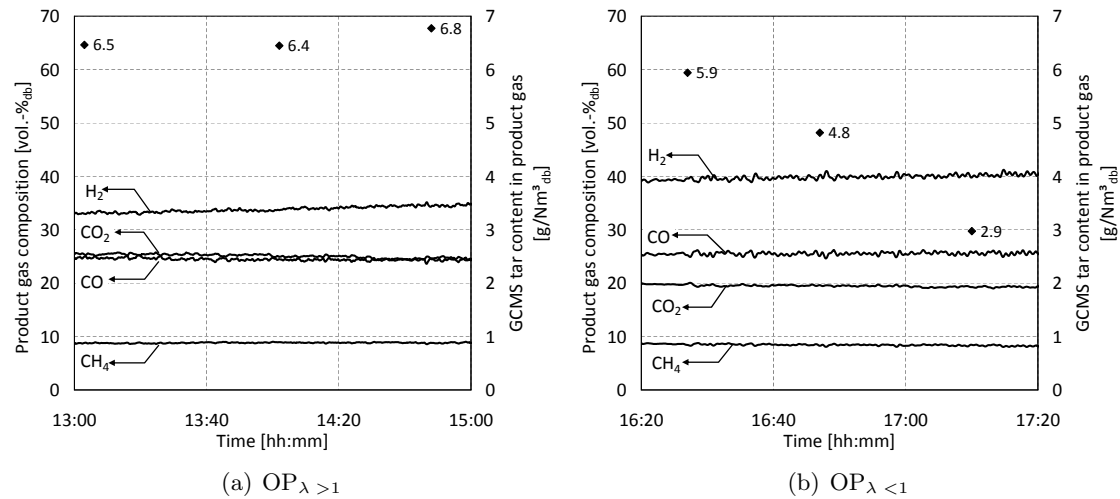

(a) $OP_{\lambda > 1}$ (b) $OP_{\lambda < 1}$

Figure 5.16: Sample of experimal run for $OP_{\lambda > 1}$(a) and $OP_{\lambda < 1}$(b), product gas composition and GCMS tar content over experimental progress

Table 5.6: Experimental operation data

Parameter	Unit/notation	$OP_{\lambda > 1}$	$OP_{\lambda < 1}$
fuel input (wood pellets)	[kg/h]	20	20
fuel power load	[kW]	97	97
mean particle diameter of solid	[μm]	500	500
steam fluidisation gasifier	[kg/h]	9.8	9.8
steam fluidisation ULS and LLS	[kg/h]	9.5	9.5
fluidisation secondary air	[Nm^3/h]	50	50
ratio primary to secondary air	[-]	1/10	1/10
initial solid inventory	[kg]	100	100
steam-to-fuel ratio, $\varphi_{SF,wt}$	[kg$_{H_2O}$/kg$_{\text{fuel,daf}}$]	0.8	0.8
steam-to-carbon ratio, $\varphi_{SC,mol}$	[mol$_{H_2O}$/mol$_C$]	1.1	1.1
steam-to-carbon ratio, $\varphi_{SC,wt}$	[kg$_{H_2O}$/kg$_C$]	1.6	1.6
H_2	[vol%$_{db}$]	33.8	39.9
CO	[vol%$_{db}$]	24.5	25.5
CO_2	[vol%$_{db}$]	25.1	19.5
CH_4	[vol%$_{db}$]	8.8	8.4
C_2H_4	[vol%$_{db}$]	2.2	1.7
C_2H_6	[vol%$_{db}$]	0.1	0.1
C_3H_8	[vol%$_{db}$]	0.2	0.3
gasification temperature	[°C]	850	866
combustion temperature, riser	[°C]	920	968
total product gas yield	[Nm^3/h]	39.4	38.8
H_2O content in product gas	[vol%]	48.1	36.9
product gas yield	[Nm$^3_{db}$/h]	20.4	24.5
specific product gas yield	[Nm$^3_{db}$/kg$_{\text{fuel,daf}}$]	1.09	1.36
lower heating value	[MJ/Nm$^3_{db}$]	11.9	12.2
mean gas residence time in BB, $\overline{\tau}_{BB}$	[s]	0.25	0.25
mean gas residence time in FB, $\overline{\tau}_{FB}$	[s]	2.7	2.7
mean gas residence time in riser, $\overline{\tau}_R$	[s]	0.8	0.8
specific H_2 yield	[Nm$^3_{H_2}$/kg$_{\text{fuel,daf}}$]	0.366	0.533
specific CO yield	[Nm$^3_{CO}$/kg$_{\text{fuel,daf}}$]	0.261	0.334
specific CO_2 yield	[Nm$^3_{CO_2}$/kg$_{\text{fuel,daf}}$]	0.267	0.255
specific CH_4 yield	[Nm$^3_{CH_4}$/kg$_{\text{fuel,daf}}$]	0.092	0.109
specific C_2H_4 yield	[Nm$^3_{C_2H_4}$/kg$_{\text{fuel,daf}}$]	0.023	0.022
sum of specific C_2H_6 and C_3H_8 yield	[Nm$^3_{C_2H_6+C_3H_8}$/kg$_{\text{fuel,daf}}$]	0.003	0.004
log. dev. from CO-shift eq., $p\delta_{eq,CO-shift}$	[-]	-0.36	-0.20
rel. water conversion, $X_{H_2O,rel}$	[kg$_{H_2O}$/kg$_{\text{fuel,daf}}$]	0.03	0.19
abs. water conversion, $X_{H_2O,abs}$	[kg$_{H_2O}$/kg$_{H_2O}$]	0.035	0.226
O_2 transfer from riser to gasifier[1)]	[Nm^3/h]	2.3	0.7
specific O_2 input into gasifier	[Nm^3/kg$_{\text{fuel,daf}}$]	0.12	0.04
O_2 demand for full combustion of the fuel	[Nm^3/kg$_{\text{fuel,daf}}$]	0.95	0.95
ER (ratio of O_2 input to stoich. O_2 demand)	[-]	0.12	0.04

[1)] the O_2 transfer is calculated with IPSEpro by closing the mass balance

The product gas contains a low amount of N_2 and C_4/C_5 species, which completes to 100 vol%$_{db}$

5.5.2 Considerations for limestone

The selective transport of CO_2 in the DFB system is enabled by cyclic carbonation and calcination of CaO and $CaCO_3$, respectively. The fundamental considerations are given in Section 2.7.2. The fundamentals are also given in Paper IV, which presents the application of limestone as the bed material in the CHP Güssing, Austria. Within this study, the principal feasibility of this material in combination with selective CO_2 transfer was demonstrated. In particular, the product gas composition was shifted towards higher yields of hydrogen. Alltogether, the results bring up new aspects to be considered. In terms of the overall process concept, there might be considered:

- maximum CO_2 transport (uptake) capacity,

- loss in transport capacity due to material modifications (sintering) or attrition,

- shifting of the heat balance (in-situ supply of heat in the gasifier) due to the exothermic carbonation reaction.

The maximum CO_2 capacity amounts to $0.785\,\mathrm{kg_{CO_2}/kg_{CaO}}$, which is derived by the equimolar ratio of CO_2 to CaO. However, in practical application this maximum capacity is not achieved. Basically, this is due to the limited particle residence time in the reactor. Further considerations in terms of the transport capacity are detailed in Paper IV. Table 5.7 reports CO_2 transport capacities, which are derived by experimental runs at the DFB pilot plant. These experimental runs are described in [150]. Furthermore, the CO_2 capacity arising from the operation at large scale (see Paper IV) is listed in Table 5.7.

Table 5.7: CO_2 transport capacity determined from the experimental runs

Reference	CO_2 capacity $[\mathrm{kg_{CO_2}/kg_{CaO}}]$	fraction acc. to max. capacity
experiments at the DFB pilot plant, [150]	0.001–0.0378	0.13%–4.8%
operation at CHP Güssing, Paper IV	0.0642	8.2%

Based on the experimental data presented in Table 5.7, it is assumend that the maximum CO_2 capacity in real process conditions may not exceed 10%. With a view to the real process conditions, it is assumed that only the outer layer of the particle surface contributes to carbonation/calcination. Thus, the core of the particle is not influenced by cyclic carbonation/calcination as this would require high reaction times. Futher aspects are detailed in Paper IV.

6 Conclusions and outlook

The dual fluidised bed system (DFB) presented in this thesis is a reliable process concept for the thermo-chemical biomass conversion into a valuable product gas. The system involves the combination of two fluidised bed reactors, which are operated in different fluidisation regimes. The fluidised bed configuration involves a steam blown bubbling bed in the gasification reactor and an air blown fast fluidised bed in the combustion reactor. Loop seals are used as the hydraulic interconnections. The endothermic steam gasification proceeds in the gasification reactor. The combustion reactor provides the heat required in the gasification reactor for the conversion of the solid fuel. The DFB technology has been put into practice and is already being applied at an industrial scale. This thesis addresses the research topic of active bed materials. Several materials were considered:

- silica sand (as reference material),

- natural olivine (as standard material),

- Fe-olivine (synthetic material), and

- limestone

The foci of the investigation were:

- general product gas composition,

- capability of tar decomposition,

- capability of water conversion,

- extent of CO-shift, and

- selective transport of O_2, CO_2.

In terms of the operation of the DFB pilot plant, these aspects serve to indicate the activity of the material. Furthermore, the consideration on the reactor system are elucidated with regard to the maturation of the tar. The DFB pilot plant was used for the greater part of the experimental studies. The pilot plant configuration and the conditions of experimental operation are close to those of a industrial process conditions. Thus, the results are qualified to be assumptions for the behaviour of the process at a large scale.

The following order for the content of H_2 and yield was found:

$$limestone > olivine > Fe\text{-}olivine > silica\ sand$$

The following order of decreasing capability in tar decomposition and CO-shift was found:

$$limestone > Fe\text{-}olivine > olivine > silica\ sand$$

Water conversion was found to decrease in the following order:

$$limestone/olivine \gg Fe\text{-}olivine/silica\ sand$$

The low water conversion, in the case of Fe-olivine, is due to the selective oxidation of hydrogen in the gasification reactor. Limestone has been identified within the experiments at the DFB pilot plant as the in-bed catalyst with the highest capacity for tar decomposition and CO-shift promotion. However, the low attrition resistance of limestone is unfavourable and is the principal drawback for its application in fluidised bed systems. Natural olivine and the synthetic material such as Fe-olivine were identified as in-bed catalysts with medium capacity for tar decomposition. Their hardness and high attrition resistance is a clear benefit for their use as the bed material in a fluidised bed system.

Besides, the oxygen transfer capacity of the Fe-olivine has been shown in the experiments. Oxygen transfer is achieved by cyclic oxidation and reduction of the iron fraction of the particle. This transfer affects input of oxygen into the gasification reactor. Consequently the oxidation of certain gas species, which are predominately CO and H_2, occurs. Due to the oxidation, additional heat is released, which contributes to the endothermic steam gasification. Further, it was found that the oxygen transfer exhibit no clear effect on the tar decompositon. This principal effect of selective oxygen transfer might contribute to a reactor concept that considers the gasification of solid fuel with oxygen as the gasification agent.

Limestone can be used as a carrier material for selective transport of CO_2. The selective CO_2 transport by cyclic carbonation and calcination of limestone has been shown. This selective sequestration yield a product gas which is CO_2 depleted and is characterised by a high fraction of H_2.

The central importance of intense gas–solid contact and gas residence time in the gasification reactor has been shown. In particular the impact on tar decomposition was illustrated. A scheme is proposed which relates the experimental results with the considerations on the composition of the tar. The scheme include possible interactions of tar compounds in the gasification reactor.

The interactions are distinguished between the bubbling bed zone and the freeboard zone. Thus, it is supposed that:

- decomposition of tar in the bubbling bed is highly affected by heterogenous catalysis,

- a high gas residence time in the bubbling bed is favourable for tar decomposition[1],

- in the freeboard section, the tar species tend to undergo secondary reactions, which mainly involve the growth of polyaromatic hydrocarbons (PAH),

- these recombination effects of condensable hydrocarbons are clearly promoted through high gas residence time[2],

- the gas residence time might be kept short in the freeboard to counteract any recombination reactions of PAH compounds.

The scheme shows that the bubbling bed is the active zone for effective conversion, as the catalyst is present. Expanding this particle dense zone will enhance tar decomposition, water conversion, and CO-shift. Hence, a turbulent or fast fluidised regime will lead to:

- higher gas–solid interaction,

- presence of solids over the entire reactor height to promote the heterogenous catalysed reactions.

In addition, the operation of the gasification reactor as a turbulent or fast fluidised bed without a freeboard section might prevent the growth of heavy PAH (components with high boiling points), as their formation occurs at high temperatures in the absence of a catalyst.

The experimental results underline the potential of active bed materials in the DFB system and the importance of gas-solid interaction. Effective use of the catalyst in the gasifier reduces the efforts of downstream gas cleaning, which is a crucial aspect for industrial application.

Various aspects of the material performance have been drawn together for this investigation. The reactor system and the range of other possible active bed materials in general is an area which contains much scope for further development and elaboration. A number of directions for further work are suggested by the work in this thesis.

- experimental investigation of *other active bed materials*: The following criteria can be applied to assess the capability: tar content and composition, hydrogen content and yield, water conversion, deviation from CO-shift equilibrium. Further important aspect to be investigated, which decide on the material appropriateness for their application, are: attrition resistance, deactivation and poisoning (i.e., due to sulphur, chlorine), lifetime, cost or toxicity. Beside these issues, specific

---

[1] the mean gas residence time in the bubbling bed was at about 0.2–0.5 s for the experimental operations

[2] the mean gas residence time in the freeboard was at about 2.4–4.5 s for the experimental operations

aspects arise which addresses consideration of: long term behaviour, changes of the material or of the material surface, interactions with fuel ash or formation of a layer on the particle. These considerations may be supported by particle examinations with X-ray diffraction, X-ray fluorescence or scanning electron microscopy.

- experimental investigation of pathways of *formation and decomposition of tar*: This aspect addresses the changes of tar content and composition along the height of the solid particle free freeboard section of the gasification reactor. Measurements of the tar content and its composition at several reactor heights could give important information on the decomposition or recombination of the overall tar or certain tar species.

- considerations *(O_2, CO_2) transfer processes and capabilities*: These transport processes are interesting options for process modifications. The partial sequestration of CO_2 may be used for adjusting of the H_2 to CO ratio. The O_2 transfer character may be used in future for gasification with O_2. However, in the first instance a theoretical study on thermodynamic and mass and energy balances could be realised to indicate thermodynamic limits and general process boundaries.

7 Notation

7.1 Abbreviations

atm	atmospheric pressure (1.0133 bar)
AR	air reactor
BG-Lib	biomass gasification library, IPSEpro
BTX	benzene, toluene, xylenes
cat.	catalyst, catalysed reaction
CCS	carbon capture and storage
CHP	Combined heat and power plant
CLC	chemical looping combustion
CLR	chemical looping reforming
div.	diverse
DCFB	dual circulating fluidized bed
DFB	dual fluidised bed
DTGA	Differential thermogravimetric analysis
ECN	Energy Research Centre of the Netherlands
ER	equivalence ratio
FCC	Fluid catalytic cracking
FICFB	Fast internally circulating bed
FR	fuel reactor
HC	hydrocarbons
HHV	higher heating value
LHV	lower heating value
LLS	lower loop seal
Mtoe	million tons of oil equivalent
OC	oxygen carrier
OECD	Organization for Economic Co-operation and Development
OP	operation point
PAH	polyaromatic hydrocarbons
PNA	polynuclear aromatic hydrocarbons,
IEA	International Energy Agency
IAPWS-IF97	International Association for the Properties of Water and Steam - Industrial Formulation 1997
WEO	World Energy Outlook, 2008 by IEA
SER	sorption enhanced reforming
TGA	thermo-gravimetric analysis
ULS	upper loop seal
XRD	X-ray diffraction

7.2 Symbols

A,B,C,D	general chemical component	$(-)$
A	cross section	m^2
Ar	Archimedes number	$(-)$
C_W	drag coefficient	$(-)$
d_p	general particle diameter	m, m
d_p^*	dimensionless particle diameter	$-$
g	standard gravity (9.80665)	$\mathrm{m/s}^2$
H	height	m
H_u	lower heating value	$\mathrm{MJ/Nm}^3$
K_p	equilibrium constant	$(-)$
L	length	m
MeO	metal oxide	
N	number of values	$(-)$
m_i	mass of substance i	kg
$\dot{m}_{steam}$	mass flow of steam	$\mathrm{kg/h}$
$\dot{m}_{fuel}$	mass flow of fuel	$\mathrm{kg/h}$
$\dot{m}_i$	mass flow of substance i	$\mathrm{kg/h}$
p_i	actual partial pressure of species i	(bar)
p_i^*	equilibrium partial pressure of species i	$(div.)$
R_0	oxygen transport capacity	$\mathrm{kg/kg}$
Re	Reynolds number	$(-)$
s_{x_i}	standard deviation to measured value	$(-)$
T	thermodynamic temperature	K
U	superficial gas velocity	$\mathrm{m/s}$
U^*	dimensionless gas velocity	$-$
U_c	transition velocity from bubbling to turbulent fluidisation	$\mathrm{m/s}$
U_{mf}	minimum fluidisation velocity	$\mathrm{m/s}$
U_{se}	velocity where solids begin to be entrained significantly	$\mathrm{m/s}$
U_t	terminal velocity	$\mathrm{m/s}$
tol_{x_i}	tolerance of the measurement value	$(-)$
x_i	value of the measurement	$(div.)$
$\bar{x}_i$	mean value of the measurment	$(div.)$
x	molality of carbon in the fuel at dry, ash, N, Cl and S free basis	$\mathrm{mol/kg_{C,H,O}}$
y	molality of hydrogen in the fuel at dry, ash, N, Cl and S free basis	$\mathrm{mol/kg_{C,H,O}}$
z	molality of oxygen in the fuel at dry, ash, N, Cl and S free basis	$\mathrm{mol/kg_{C,H,O}}$
$\dot{V}$	volume flow	m^3/h
$X_{H_2O,abs}$	absolut water conversion	$\mathrm{kg_{H2O}/kg_{H2O}}$
$X_{H_2O,rel}$	relative water conversion	$\mathrm{kg_{H2O}/kg_{fuel,daf}}$
$p\delta_{eq,CO-shift}$	logarithmic deviation from CO-shift equilibirium	$-$
Δ_p	pressure drop	$\mathrm{bar}, \mathrm{mbar}$
ε	void fraction	$(-)$

ε_{BB}	porosity of bubbling bed	$(-)$
λ	air/fuel ratio	$(-)$
λ_{H_2O}	stoichiometric H_2O ratio	$(-)$
ρ	density	kgm^{-3}
ρ_g	gas density	kgm^{-3}
ρ_p	particle density	kgm^{-3}
$\overline{\tau}_{BB}$	mean gas residence time in the bubbling bed	s
$\overline{\tau}_{FB}$	mean gas residence time in the freeboard	s
$\overline{\tau}_R$	mean gas residence time in the riser	s
Φ_{H_2O}	stoichiometric H_2O demand	$mol_{H_2O}/kg_{daf,N,S,Cl\ free}$
ν	kinematic viscosity	m^2/s
μ_i	mass fraction of the component i	kg/kg
μ_{H_2O}	mass fraction of H_2O	kg/kg
ν_{ash}	mass fraction of ash	kg/kg
ν	kinematic gas viscosity	m^2/s
ν_i	stoichiometric factor of species i	bar
$\varphi_{SF,wt}$	steam-to-fuel ratio, weight	$kg_{H_2O}/kg_{fuel,db}$
$\varphi_{SC,wt}$	steam-to-carbon ratio, weight	kg_{H_2O}/kg_C
$\varphi_{SC,mol}$	steam-to-carbon ratio, molar	mol_{H_2O}/kg_C

7.3 Sub and superscripts

abs.	absolute
CO-shift	CO-shift reaction
conv.	converted/consumed
daf	dry and ash free basis
db	dry basis
eq.	equilibrium
f	fluid
fuel	fuel
g	gas
grav.	gravimetric
mf	minimum fluidisation
ox	oxidized form
OC	oxygen carrier
p	particle
PG	product gas
red	reduced form
rel.	relative
s	solid
steam	steam
stoich.	stoichiometric
SF	steam-fuel
wt	weight
*	dimensionless parameter

8 References

[1] Birol F. World Energy Outlook 2008. Technical report, International Energy Agency (IEA), 2008.

[2] Yoichi Kaya and Keiichi Yokobori, editors. *Environment, energy, and economy: Strategies for sustainability.* United Nations University Press, Tokyo, New York, Paris, 1997.

[3] Directive 2009/28/EC of the European Parliament and of the Council of 23 April 2009 on the promotion of the use of energy from renewable sources. 23th 2009.

[4] Ökostromgesetz (Green Electricity Act), enected in 2003, 2002.

[5] Erneuerbare-Energien-Gesetz (German Renewable Energy Act), commencement on April, 1st, 2000., 2000.

[6] Decision No 406/2009/EC of the European Parliament and of the Council of 23 April 2009 on the effort of Member States to reduce their greenhouse gas emissions to meet the Communitys greenhouse gas emission reduction commitments up to 2020.

[7] Markus Kleinhappl. Festbett-Vergasung - Stand der Technik. In *Biomasse-Vergasung - Der Königsweg für eine effiziente Strom- und Kraftstoffbereitstellung?*, volume 24 of *Schriftenreihe Nachwachsende Rohstoffe*, pages 45–70. Landwirtschaftsverlag, Münster, 2004.

[8] H. Hofbauer, S. Koppatz, J.C. Schmid, T. Pröll, C. Pfeifer, J. Kotik, R. Rauch, A. Reichhold, and M. Fuchs. Dual Fluidized Beds at Vienna University of Technology. *manuscript in preparation*, 2011.

[9] Henrik Thunman and Martin Seemann. First experiences with the new Chalmers gasifier. In *proceeding of the 20th International Conference on Fluidized Bed Combustion, Xi'an, China*, volume 2, pages 659–663, 2009.

[10] D. Bull, I. Gilmor, C. Williamson, and S. Pang. The development and operation of a 100 kW dual fluidised bed biomass gasifier for production of high quality producer gas. In *proceedings of the ICPS 2009, International Conference on Polygeneration Strategies, Vienna, Austria*, 2009.

[11] K. Göransson, U. Söderlind, and W. Zhang. Experimental test on a novel dual fluidised bed biomass gasifier for synthetic fuel production. *Fuel*, 90(4):1340 – 1349, 2011.

[12] Ligang Wei, Shaoping Xu, Jingang Liu, Chunlan Lu, Shuqin Liu, and Changhou Liu. A Novel Process of Biomass Gasification for Hydrogen-Rich Gas with Solid Heat Carrier: Preliminary Experimental Results. *Energy & Fuels*, 20(5):2266–2273, 2006.

[13] Koichi Matsuoka, Koji Kuramoto, Takahiro Murakami, and Yoshizo Suzuki. Steam Gasification of Woody Biomass in a Circulating Dual Bubbling Fluidized Bed System. *Energy & Fuels*, 22(3):1980–1985, 2008.

[14] Li Dong, Guangwen Xu, Toshiyuki Suda, and Takahiro Murakami. Potential approaches to improve gasification of high water content biomass rich in cellulose in dual fluidized bed. *Fuel Processing Technology*, 91(8):882 – 888, 2010. Gasification: Fundamentals and application.

[15] C.M. van der Meijden, H.J. Veringa, A. van der Drift, and B. J. Vreugdenhil. The 800 kW$_{th}$ Allothermal Biomass Gasifier Milena. In *Proceedings of the 16th European Biomass Conference & Exhibition, 2008, Valencia, Spain*, 2008.

[16] Tobias Pröll, Ingmar G. Siefert, Anton Friedl, and Hermann Hofbauer. Removal of nh3 from biomass gasification producer gas by water condensing in an organic solvent scrubber. *Industrial & Engineering Chemistry Research*, 44(5):1576–1584, 2005.

[17] R.W.R. Zwart, A. Van der Drift, A. Bos, H.J.M. Visser, M.K. Cieplik, and H.W.J. Könemann. Oil-based gas washing - Flexible tar removal for high-efficient production of clean heat and power as well as sustainable fuels and chemicals. *Environmental Progress & Sustainable Energy*, 28(3):324–335, 2009.

[18] A.V. Bridgwater. Catalysis in thermal biomass conversion. *Applied Catalysis A: General*, 116(1-2):5 – 47, 1994.

[19] Christoph Pfeifer and Hermann Hofbauer. Development of catalytic tar decomposition downstream from a dual fluidized bed biomass steam gasifier. *Powder Technology*, 180(1-2):9 – 16, 2008.

[20] Pekka Simell, Esa Kurkela, Pekka Stahlberg, and Jouko Hepola. Catalytic hot gas cleaning of gasification gas. *Catalysis Today*, 27(1-2):55 – 62, 1996.

[21] Lopamudra Devi. *Catalytic removal of biomass tars; Olivine as prospective in-bed catalyst for fluidized-bed biomass gasifiers*. PhD thesis, University Eindhoven, 2005.

[22] Jos Corella, Jos M. Toledo, and Rita Padilla. Catalytic Hot Gas Cleaning with Monoliths in Biomass Gasification in Fluidized Beds. 1. Their Effectiveness for Tar Elimination. *Industrial & Engineering Chemistry Research*, 43(10):2433–2445, 2004.

[23] Matthew M. Yung, Whitney S. Jablonski, and Kimberly A Magrini-Bair. Review of Catalytic Conditioning of Biomass-Derived Syngas. *Energy & Fuels*, 23(4):1874–1887, April 2009.

[24] Chunbao Xu, Jaclyn Donald, Enkhsaruul Byambajav, and Yasuo Ohtsuka. Recent advances in catalysts for hot-gas removal of tar and NH3 from biomass gasification. *Fuel*, 89(8):1784 – 1795, 2010.

[25] Z. Abu El-Rub, E. A. Bramer, and G. Brem. Review of Catalysts for Tar Elimination in Biomass Gasification Processes. *Industrial & Engineering Chemistry Research*, 43(22):6911–6919, 2004.

[26] D. Sutton, B. Kelleher, and J. R. H. Ross. Review of literature on catalysts for biomass gasification. *Fuel Processing Technology*, 73(3):155–173, 2001.

[27] F. Miccio, B. Piriou, G. Ruoppolo, and R. Chirone. Biomass gasification in a catalytic fluidized reactor with beds of different materials. *Chemical Engineering Journal*, 154(1-3):369 – 374, 2009.

[28] Christoph Pfeifer, Reinhard Rauch, and Hermann Hofbauer. In-Bed Catalytic Tar Reduction in a Dual Fluidized Bed Biomass Steam Gasifier. *Industrial & Engineering Chemistry Research*, 43(7):1634–1640, 2004.

[29] Bruno Piriou. *Catalytic Biomass Gasification Process in Fluidized bed Reactor*. PhD thesis, University of Naples, 2009.

[30] D. Swierczynski, C. Courson, L. Bedel, A. Kiennemann, and J. Guille. Characterization of Ni-Fe/MgO/Olivine Catalyst for Fluidized Bed Steam Gasification of Biomass. *Chemistry of Materials*, 18(17):4025–4032, 2006.

[31] C. Varga, S. Koppatz, C. Pfeifer, and H. Hofbauer. Hot Gas Cleaning of Biomass Derived Syngas by Catalytic Filter Candles. In *Proceedings of the 18th European Biomass Conference & Exhibition, Lyon, France*, 2010.

[32] Sergio Rapagna, Katia Gallucci, Manuela Di Marcello, Pier Ugo Foscolo, Manfred Nacken, and Steffen Heidenreich. In Situ Catalytic Ceramic Candle Filtration for Tar Reforming and Particulate Abatement in a Fluidized-Bed Biomass Gasifier. *Energy & Fuels*, 23(7):3804–3809, 2009.

[33] Manfred Nacken, Lina Ma, Steffen Heidenreich, and Gino V. Baron. Performance of a catalytically activated ceramic hot gas filter for catalytic tar removal from biomass gasification gas. *Applied Catalysis B: Environmental*, 88(3-4):292 – 298, 2009.

[34] E. Simeone, M. Siedlecki, M. Nacken, S. Heidenreich, and W. de Jong. High temperature gas filtration with ceramic candles and ashes characterisation during steam-oxygen blown gasification of biomass. *Fuel*, (0), 2011.

[35] Nicolas Berguerand, Fredrik Lind, Martin Seemann, and Henrik Thunman. Producer Gas Cleaning in a Dual Fluidized Bed Reformer using Two Catalysts. In *proceedings of the International Conference on Polygeneration Strategies 2011, Vienna, Austria*, pages 147–155, 2011.

[36] P. Kolbitsch, T. Pröll, J. Bolhar-Nordenkampf, and H. Hofbauer. Design of a Chemical Looping Combustor using a Dual Circulating Fluidized Bed (DCFB) Reactor System. *Chemical Engineering & Technology*, 32(3):398–403, 2009.

[37] Tobias Pröll, Philipp Kolbitsch, Johannes Bolhàr-Nordenkampf, and Hermann Hofbauer. A novel dual circulating fluidized bed system for chemical looping processes. *AIChE Journal*, 55(12):3255–3266, 2009.

[38] Martin Kaltschmitt, Hans Hartmann, and Hermann Hofbauer, editors. *Energie aus Biomasse*, volume 2. Springer–Verlag Berlin Heidelberg New York, 2000.

[39] John Finn Siau. *Transport Prosses in Wood*. Springer-Verlag, 1983.

[40] H. Wenzl, editor. *Mitteilungen zur Chemie, Physik und Technologie des Holzes und der pflanzlichen Faserrohstoffe*. Techn. Verlag Herbert Cram, 1970.

[41] B. Elvers et. al, editor. *Ullmann's Encyclopedia of Industrial Chemistry*. WILEY-VCH, Verlagsgesellschaft, Weinheim, Germany, 6 edition, 2002.

[42] M.A. Serio, M.A. Wjtowicz, and S. Charpenay. Pyrolysis. In *Encyclopedia of Energy Technology and the Environment*, volume 3, pages pp.2281–2308. John Wiley & Sons, New York, 1999.

[43] F. Shafizadeh and G.D. McGinnis. Chemical composition and thermal analysis of cottonwood. *Carbohydrate Research*, 16(2):273 – 277, 1971.

[44] Morten Gunnar Grønli. *A theoretical and experimental study of the thermal degradation of biomass*. PhD thesis, Norwegian University of Science and Technology, Norwegian University of Science and Technology, 1996.

[45] K. Raveendran, Anuradda Ganesh, and Kartic C. Khilar. Pyrolysis characteristics of biomass and biomass components. *Fuel*, 75(8):987 – 998, 1996.

[46] Haiping Yang, Rong Yan, Hanping Chen, Chuguang Zheng, Dong Ho Lee, and David Tee Liang. In-Depth Investigation of Biomass Pyrolysis Based on Three Major Components: Hemicellulose, Cellulose and Lignin. *Energy & Fuels*, 20(1):388–393, 2006.

[47] Matheus Poletto, Juliane Dettenborn, Vinacios Pistor, Mara Zeni, and Ademir Jose Zattera. Materials produced from plant biomass: Part I: evaluation of thermal stability and pyrolysis of wood. *Materials Research*, 13:375 – 379, 09 2010.

[48] Lukas Gasparovi, Zuzana Koreova, and Ludovit Jelemensky. Kinetic study of wood chips decomposition by TGA. *Chemical Papers*, 64:174–181, 2010.

[49] Tantely Randriamanantena, Fils Lahatra Razafindramisa, Georgette Ramanantsizehena, Alain Bernes, and Colette Lacabane. Thermal behaviour of three woods of Madagascar by thermogravimetric analysis in inert atmosphere. In Stephan Narison, editor, *Proceedings of the Fourth High-Energy Physics International Conference HEP-MAD 09, Antananarivo, Madagascar, August 21-28, 2009.*

[50] *HSC. (2002). HSC Chemistry 5.1, Outokumpu Research Oy, Pori, Finland*, 2002.

[51] Philipp Oliver Morf. *Secondary reactions of tar during thermochemical biomass conversion.* PhD thesis, ETH Zrich, 2001.

[52] Dominic Trommer. *Thermodynamic and kinetic analyses of the solar thermal gasification of petroleum coke.* PhD thesis, Swiss Federal Insitut of Technology Zuerich, 2006.

[53] Mark Jan Prins. *Thermodynamic analysis ofbiomass gasification and torrefaction.* Phdthesis, University Eindhoven, 2005.

[54] L. Damiani and A. Trucco. An Experimental Data Based Correction Method of Biomass Gasification Equilibrium Modeling. *Journal of Solar Energy Engineering*, 132(3):031011, 2010.

[55] Enrique Salaices. *Catalytic Steam Gasification of Biomass Surrogates: A Thermodynamic and Kinetic Approach.* PhD thesis, The University of Western Ontario, Canada, 2010.

[56] M. Detournay, M. Hemati, and R. Andreux. Biomass steam gasification in fluidized bed of inert or catalytic particles: Comparison between experimental results and thermodynamic equilibrium predictions. *Powder Technology*, In Press, Corrected Proof, 2010.

[57] J.P.A. Neeft, H.A.M. Knoef, U. Zielke, K. Sjstrm, P. Hasler, P.A. Simell, M.A. Dorrington, N. Abatzoglou L. Thomas, S. Deutch, C.Greil, G.J. Buffinga, C. Brage, and M. Suomalainen. Guideline for Sampling and Analysis of Tar and Particles in Biomass Producer Gases. Technical report, 1999.

[58] Thieme Chemistry, editor. *Römpp Lexikon Chemie (Online Version 3.18)*. Georg Thieme Verlag, Stuttgart 2011, 2007.

[59] J. Dykyj, J. Svoboda, R. C. Wilhoit, M. Frenkel, and K. R. Hall. *SpringerMaterials - The Landolt-Börnstein Database - Group IV Physical Chemistry, Numerical Data and Functional Relationships in Science and Technology.* Springer.

[60] T. A. Milne, N. Abatzoglou, and R. J. Evans. *Biomass Gasifier 'Tars': Their Nature, Formation, and Conversion.* National Renewable Energy Lab, Golden, CO, Golden, Colorado, 1998.

[61] Robert J. Evans and Thomas A. Milne. Molecular characterization of the pyrolysis of biomass. 1. Fundamentals. *Energy & Fuels*, 1(2):123–137, 1987.

[62] Robert J. Evans and Thomas A. Milne. Molecular characterization of the pyrolysis of biomass. 2. Applications. *Energy & Fuels*, 1(4):311–319, 1987.

[63] R.J. Evans and T.A. Milne. Chemistry of Tar Formation and Maturation in the Thermochemical Conversion of Biomass. In A.V. Bridgwater and D.G.B. Boocock, editors, *Developments in Thermochemical Biomass Conversion*, volume 2., pages pp. 803–816. London: Blackie Academic & Professional, 1997.

[64] ECN. Tar Classification System, http://www.thersites.nl, 2009.

[65] S. van Paasen and J. Kiel. Tar formation in a fluidised-bed gasifier - Impact of fuel properties and operating conditions. Technical report, ECN Biomass, 2004.

[66] J. Corella, M.A. Caballero, and M.P. Aznar. A 6-lump model for the kinetics of the catalytic tar removal in biomass gasification. In *Proceedings of the 1st World Conference on Biomass for Energy and Industry*, volume 2, pages pp.1472–1475, 2000.

[67] Ute Wolfesberger, Isabella Aigner, and Hermann Hofbauer. Tar content and composition in producer gas of fluidized bed gasification of wood: Influence of temperature and pressure. *Environmental Progress & Sustainable Energy*, 28(3):372–379, 2009.

[68] P. Perez, P. M. Aznar, M. A. Caballero, J. Gil, J. A. Martin, and J. Corella. Hot Gas Cleaning and Upgrading with a Calcined Dolomite Located Downstream a Biomass Fluidized Bed Gasifier Operating with Steam-Oxygen Mixtures. *Energy Fuels*, 11(6):1194–1203, 1997.

[69] Jose Corella, Jose M. Toledo, and Maria-Pilar Aznar. Improving the Modeling of the Kinetics of the Catalytic Tar Elimination in Biomass Gasification. *Industrial & Engineering Chemistry Research*, 41(14):3351–3356, 2002.

[70] Philipp Morf, Philipp Hasler, and Thomas Nussbaumer. Mechanisms and kinetics of homogeneous secondary reactions of tar from continuous pyrolysis of wood chips. *Fuel*, 81(7):843 – 853, 2002.

[71] C. D. Elliott. *Relation of Reaction Time and Temperature to Chemical Composition of Pyrolysis Oils*, volume 376, chapter 7, pages 55–65. 1988.

[72] H. Egsgaard and E. Larsen. Thermal Transformation of light tar - specific routes to aromatic aldehydes and PAH. In *Proceedings of the 1st World Conference on Biomass for Energy and Industry*, volume 2, pages pp.1472–1475, 2000.

[73] Michael Kübel. *Teerbildung und Teerkonversion bei der Biomassevergasung - Anwendung der nasschemischen Teerbestimmung nach CEN Standard*. PhD thesis, Universität Stuttgart, 2007.

[74] Christoph Unger and Markus Ising. Mechanismen und Bedeutung der Teerbildung und Teerbeseitigung bei der thermochemischen Umwandlung fester Kohlenstoffträger. Technical report, Fraunhofer Institut für Umwelt-, Sicherheits-, Energietechnik; UMSICHT, 2002.

[75] Markus Ising. *Zur katalytischen Spaltung teerartiger Kohlenwasserstoffe bei der Wirbelschichtvergasung von Biomasse*. PhD thesis, Universität Dortmund, 2002.

[76] Chunshan Li and Kenzi Suzuki. Tar property, analysis, reforming mechanism and model for biomass gasification–an overview. *Renewable and Sustainable Energy Reviews*, In Press, Corrected Proof, 2008.

[77] Pekka A. Simell, Jouko O. Hepola, and A. Outi I. Krause. Effects of gasification gas components on tar and ammonia decomposition over hot gas cleanup catalysts. *Fuel*, 76(12):1117 – 1127, 1997.

[78] Lopamudra Devi, Krzysztof J. Ptasinski, and Frans J.J.G. Janssen. Pretreated olivine as tar removal catalyst for biomass gasifiers: investigation using naphthalene as model biomass tar. *Fuel Processing Technology*, 86(6):707 – 730, 2005.

[79] W.C. Yang. *Handbook of Fluidization and Fluid-Particle Systems*. Chemical Industries Series. Marcel Dekker, 2003.

[80] Daizo Kunii and Octave Levenspiel. *Fluidization Engineering*. Series in Chemical Engineering. Butterworth-Heinemann, second edition edition, 1991.

[81] L.S. Fan and C. Zhu. *Principles of Gas-Solid Flows*. Cambridge Series in Chemical Engineering. Cambridge University Press, 2005.

[82] J.R. Grace, A.A. Avidan, and T.M. Knowlton. *Circulating fluidized beds*. Blackie Academic & Professional, 1997.

[83] J.R. Grace, J.M. Matsen, and Engineering Foundation (U.S.). *Fluidization*. Plenum Press, 1980.

[84] John R. Grace. Contacting modes and behavior classification of gas-solid and other two-phase suspensions. *Canadian Journal of Chemical Engineering*, 64:353–363, 1986.

[85] D. Geldart. Types of gas fluidization. *Powder Technology*, 7(5):285 – 292, 1973.

[86] Wen-Ching Yang. Modification and re-interpretation of Geldart's classification of powders. *Powder Technology*, 171(2):69 – 74, 2007.

[87] J.G. Yates. Effects of temperature and pressure on gas-solid fluidization. *Chemical Engineering Science*, 51(2):167 – 205, 1996.

[88] J. R. Grace. *Fluidized-Bed Hydrodynamics*, chapter 8.1, pages 5–64. Hemisphere, Washington, 1982, 1982.

[89] C. Y. Wen and Y. H. Yu. A generalized method for predicting the minimum fluidization velocity. *AIChE Journal*, 12(3):610–612, 1966.

[90] K.S Lim, J.X Zhu, and J.R Grace. Hydrodynamics of gas-solid fluidization. *International Journal of Multiphase Flow*, 21:141 – 193, 1995.

[91] J.R. Grace. High-velocity fluidized bed reactors. *Chemical Engineering Science*, 45(8):1953 – 1966, 1990.

[92] H. Bi and J. Grace. Flow regime diagrams for gas-solid fluidization and upward transport. *International Journal of Multiphase Flow*, 21(6):1229–1236, 1995.

[93] A. Haider and O. Levenspiel. Drag coefficient and terminal velocity of spherical and nonspherical particles. *Powder Technology*, 58(1):63 – 70, 1989.

[94] I. A. Abba, J. R. Grace, H. T. Bi, and M. L. Thompson. Spanning the flow regimes: Generic fluidized-bed reactor model. *AIChE Journal*, 49(7):1838–1848, 2003.

[95] H. Hofbauer, R. Rauch, and K. Bosch. Biomass CHP Plant Güssing - A Success Story. In A. V. Bridgwater, editor, *Expert Meeting on Pyrolysis and Gasification of Biomass and Waste, Strasbourg, France*, pages 527 – 536, Newbury, UK, 30 Sept. - 1 Oct 2002. CPL Press.

[96] Markus Bolhàr-Nordenkampf, Hermann Hofbauer, Klaus Bosch, Reinhard Rauch, and Sebastian Kaiser. Scale-up of a 100kWth pilot FICFB-gasifier to a 8 MWth FICFB-gasifier demonstration plant in Güssing (Austria). In *1st International Ukrainian Conference on Biomass for Energy, 2002*, pages 167 – 172, Kiev, 23.-26. September 2002.

[97] Jose Corella, Jose M. Toledo, and Gregorio Molina. A Review on Dual Fluidized-Bed Biomass Gasifiers. *Industrial & Engineering Chemistry Research*, 46(21):6831–6839, 2007.

[98] Kristina Göransson, Ulf Söderlind, Jie He, and Wennan Zhang. Review of syngas production via biomass DFBGs. *Renewable and Sustainable Energy Reviews*, 15(1):482 – 492, 2011.

[99] Stefan Koppatz, Christoph Pfeifer, and Hermann Hofbauer. Comparison of the performance behaviour of silica sand and olivine in a dual fluidised bed reactor system for steam gasification of biomass at pilot plant scale. *Chemical Engineering Journal*, 175(0):468 – 483, 2011.

[100] M. A. Paisley, J. M. Irving, and R. P. Overend. A Promising Power Option – The FERCO SILVAGAS Biomass Gasification Process Operationg Experience at the Burlington Gasifier. In *Proceedings of ASME Turbo Expo 2001*, 2001.

[101] M. A. Paisley, M. C. Farris, J. W. Black, J. M. Irving, and R. P. Overend. Preliminary Operating Results from the Battelle/Ferco Gasification Demonstration Plant in Burlington, Vermont, U.S.A. In S. Kyritsis, A. Beenackers, P. Helm, A. Grassi, and D. Chiaramonti, editors, *1st World Conference on Biomass for Energy and Industry*, volume 2, pages 1494–1497, Sevillia, Spain, 5.-9. June 2000.

[102] W. L. Saw, I. A. Gilmor, , and S. S. Pang. The influence of contact time on the performance of a 100 kW dual fluidised bed gasifier in steam gasification of woody biomass. In *proceedings of the ICPS 2011, International Conference on Polygeneration Strategies, Vienna, Austria*, 2011.

[103] M. C. Seemann and H. Thunman. The new Chalmers research-gasifier. In *proceedings of the ICPS 2009, International Conference on Polygeneration Strategies, Vienna, Austria*, 2009.

[104] D. Dayton. A Review of the Literature on Catalytic Biomass Tar Destruction; NREL milestone report (NREL/TP-510-32815). Technical report, National Renewable Energy Lab: Golden, CO, USA, 2002.

[105] Jun Han and Heejoon Kim. The reduction and control technology of tar during biomass gasification/pyrolysis: An overview. *Renewable and Sustainable Energy Reviews*, 12(2):397 – 416, 2008.

[106] George W. Huber, Sara Iborra, and Avelino Corma. Synthesis of Transportation Fuels from Biomass: Chemistry, Catalysts, and Engineering. *Chemical Reviews*, 106(9):4044–4098, 2006.

[107] Walter Torres, Sourabh S. Pansare, and James G. Goodwin. Hot Gas Removal of Tars, Ammonia, and Hydrogen Sulfide from Biomass Gasification Gas. *Catalysis Reviews*, 49(4):407–456, 2007.

[108] Lijun Wang, Curtis L. Weller, David D. Jones, and Milford A. Hanna. Contemporary issues in thermal gasification of biomass and its application to electricity and fuel production. *Biomass and Bioenergy*, 32(7):573 – 581, 2008.

[109] Samsudin Anis and Z.A. Zainal. Tar reduction in biomass producer gas via mechanical, catalytic and thermal methods: A review. *Renewable and Sustainable Energy Reviews*, 15(5):2355 – 2377, 2011.

[110] Jesus Delgado, Maria P. Aznar, and Jose Corella. Calcined Dolomite, Magnesite, and Calcite for Cleaning Hot Gas from a Fluidized Bed Biomass Gasifier with Steam: Life and Usefulness. *Industrial & Engineering Chemistry Research*, 35(10):3637–3643, 1996.

[111] Jesus Delgado, Maria P. Aznar, and Jose. Corella. Biomass Gasification with Steam in Fluidized Bed: Effectiveness of CaO, MgO, and CaO-MgO for Hot Raw Gas Cleaning. *Ind. Eng. Chem. Res.*, 36(5):1535–1543, 1997.

[112] Jose Corella, Jose M. Toledo, and Rita Padilla. Olivine or Dolomite as In-Bed Additive in Biomass Gasification with Air in a Fluidized Bed: Which is Better? *Energy & Fuels*, 18(3):713–720, 2004.

[113] Pekka A. Simell, Jukka K. Leppalahti, and Esa A. Kurkela. Tar-decomposing activity of carbonate rocks under high CO2 partial pressure. *Fuel*, 74(6):938 – 945, 1995.

[114] S. Rapagna, N. Jand, A. Kiennemann, and P. U. Foscolo. Steam-gasification of biomass in a fluidised-bed of olivine particles. *Biomass and Bioenergy*, 19(3):187–197, 2000.

[115] C. Courson, E. Makaga, C. Petit, and A. Kiennemann. Development of Ni catalysts for gas production from biomass gasification. Reactivity in steam- and dry-reforming. *Catalysis Today*, 63(2-4):427 – 437, 2000.

[116] D. Swierczynski, S. Libs, C. Courson, and A. Kiennemann. Steam reforming of tar from a biomass gasification process over Ni/olivine catalyst using toluene as a model compound. *Applied Catalysis B: Environmental*, 74(3-4):211 – 222, 2007.

[117] C. Pfeifer, R.Rauch, H.Hofbauer, D.Swierczynski, C.Courson, and A.Kiennemann. Hydrogen-rich gas production with a ni-catalyst in a dual fluidized bed biomass gasifier. In *proceeding of the Conference for Science in Thermal and Chemical Biomass Conversion, Vancouver, Canada*, 2004.

[118] Ruiqin Zhang, Yanchang Wang, and Robert C. Brown. Steam reforming of tar compounds over Ni/olivine catalysts doped with CeO2. *Energy Conversion and Management*, 48(1):68 – 77, 2007.

[119] Mirella Virginie, Claire Courson, and Alain Kiennemann. Toluene steam reforming as tar model molecule produced during biomass gasification with an iron/olivine catalyst. *Comptes Rendus Chimie*, 13(10):1319 – 1325, 2010.

[120] Mirella Virginie, Claire Courson, Daniel Niznansky, Nouari Chaoui, and Alain Kiennemann. Characterization and reactivity in toluene reforming of a Fe/olivine catalyst designed for gas cleanup in biomass gasification. *Applied Catalysis B: Environmental*, 101(1-2):90 – 100, 2010.

[121] Otto W. Flörke, Heribert A. Graetsch, Fred Brunk, Leopold Benda, Siegfried Paschen, Horacio E. Bergna, William O. Roberts, William A. Welsh, Cristian Libanati, Manfred Ettlinger, Dieter Kerner, Monika Maier, Walter Meon, Ralf Schmoll, Hermann Gies, and Dietmar Schiffmann. *Silica. Ullmann's Encyclopedia of Industrial Chemistry*. Wiley-VCH Verlag GmbH & Co. KGaA, 2000.

[122] Martyn Kenny and Tony Oates. *Lime and Limestone. Ullmann's Encyclopedia of Industrial Chemistry*. Wiley-VCH Verlag GmbH & Co. KGaA, 2000.

[123] J. P. A. Neeft, H. A. M. Knoef, U. Zielke, K. Sjöström, P. Hasler, P. A. Simell, and et al. Guideline for Sampling and Analysis of Tar and Particles in Biomass Producer Gases (Tar Protocol). ERK6-CT1999-20002 Version 3.1, ECN, 1999.

[124] Tobias Pröll, Johannes Bolhàr-Nordenkampf, Philipp Kolbitsch, and Hermann Hofbauer. Syngas and a separate nitrogen/argon stream via chemical looping reforming - a 140 kw pilot plant study. *Fuel*, 89(6):1249 – 1256, 2010.

[125] E. Perz. A computer method for thermal power cycle calculation. *Journal of Engineering for Gas Turbines and Power*, 113(2):184–189, 1991.

[126] Wolfgang Wagner. *Properties of water and steam : the industrial standard IAPWS-IF97 for the thermodynamic properties and supplementary equations for other properties : tables based on these equations.* Springer-Verlag, Berlin, New York, 1998.

[127] Alexander Burcat and Bonnie McBride. *1997 ideal gas thermodynamic data for combustion and air-pollution use.* Technion Israel Institute of Technology, Haifa, 1997.

[128] Ihsan Barin. *Thermochemical Data of Pure Substances.* Wiley-VCH, 2004.

[129] Tobias Pröll and Hermann Hofbauer. Development and application of a simulation tool for biomass gasification based processes. *International Journal of Chemical Reactor Engineering*, 6, 2008.

[130] Pekka Simell. *Catalytic hot gas cleaning of gasification gas.* PhD thesis, Helsinki University of Technology, 1997.

[131] Friedrich Kirnbauer, Veronika Wilk, Hannes Kitzler, Stefan Kern, and Hermann Hofbauer. The positive effects of bed material coating on tar reduction in a dual fluidized bed gasifier. *Fuel*, page Article in press, 2011.

[132] Jose Corella, Miguel A. Caballero, Maria-Pilar Aznar, and Claes Brage. Two Advanced Models for the Kinetics of the Variation of the Tar Composition in Its Catalytic Elimination in Biomass Gasification. *Industrial & Engineering Chemistry Research*, 42(13):3001–3011, 2003.

[133] W.J. Moore. *Grundlagen der physikalischen Chemie.* de Gruyter, 1990.

[134] B.J. Vreugdenhil and R.W.R. Zwart. Tar formation in pyrolysis and gasification. Technical report, ECN, 2009. Report ECN-E-08-087.

[135] Ximena A. Garcia and Klaus J. Hüttinger. Steam gasification of naphthalene as a model reaction of homogeneous gas/gas reactions during coal gasification. *Fuel*, 68(10):1300 – 1310, 1989.

[136] A. Jess. Catalytic upgrading of tarry fuel gases: A kinetic study with model components. *Chemical Engineering and Processing*, 35(6):487 – 494, 1996.

[137] Andreas Jess. Mechanisms and kinetics of thermal reactions of aromatic hydrocarbons from pyrolysis of solid fuels. *Fuel*, 75(12):1441 – 1448, 1996.

[138] Cliff Chen-Shiou Chang. *Thermal reactions of freshly generated coal tar over calcium oxide.* PhD thesis, Massachusetts Institute of Technology, 1986.

[139] H. Alden, B. G. Espenas, and E. Rensfelt. *Conversion of Tar in Pyrolysis Gas from Wood Using a Fixed Dolomite Bed in: Research in thermochemical biomass conversion.* Elsevier Applied Science, 1988.

[140] Satish S. Tamhankar, Katsumi Tsuchiya, and James B. Riggs. Catalytic cracking of benzene on iron oxide-silica: catalyst activity and reaction mechanism. *Applied Catalysis*, 16(1):103 – 121, 1985.

[141] Thomas Nordgreen, Truls Liliedahl, and Krister Sjöström. Metallic iron as a tar breakdown catalyst related to atmospheric, fluidised bed gasification of biomass. *Fuel*, 85(5-6):689 – 694, 2006.

[142] Thomas Nordgreen, Vera Nemanova, Klas Engvall, and Krister Sjöström. Iron-based materials as tar depletion catalysts in biomass gasification: Dependency on oxygen potential. *Fuel*, (0), 2011.

[143] C. Rhodes, G. J. Hutchings, and A. M. Ward. Water-gas shift reaction: finding the mechanistic boundary. *Catalysis Today*, 23(1):43 – 58, 1995. Recent Advances in C1 Chemistry.

[144] Vera Nemanova, Thomas Nordgreen, Klas Engvall, and Krister Sjöström. Biomass gasification in an atmospheric fluidised bed: Tar reduction with experimental iron-based granules from Höganäs AB, Sweden. *Catalysis Today*, 176(1):253 – 257, 2011.

[145] K. Polychronopoulou, A. Bakandritsos, V. Tzitzios, J.L.G. Fierro, and A.M. Efstathiou. Absorption-enhanced reforming of phenol by steam over supported Fe catalysts. *Journal of Catalysis*, 241(1):132 – 148, 2006.

[146] Md. Azhar Uddin, Hiroshi Tsuda, Shengji Wu, and Eiji Sasaoka. Catalytic decomposition of biomass tars with iron oxide catalysts. *Fuel*, 87(4-5):451 – 459, 2008. The 9th China-Japan Symposium on Coal and C1 Chemistry.

[147] Hiroyuki Noichi, Azhar Uddin, and Eiji Sasaoka. Steam reforming of naphthalene as model biomass tar over iron-aluminum and iron-zirconium oxide catalyst catalysts. *Fuel Processing Technology*, 91(11):1609 – 1616, 2010.

[148] M. Virginie, C. Courson, and A. Kiennemann. Characterizations of Fe/olivine catalyst after biomass gasification in pilot plant. Deliverable of EU-project: UNIQUE, www.uniqueproject.eu, University Louis Pasteur (ULP), Strasbourg, France, 2010.

[149] Sergio Rapagna, Mirella Virginie, Katia Gallucci, Claire Courson, Manuela Di Marcello, Alain Kiennemann, and Pier Ugo Foscolo. Fe/olivine catalyst for biomass steam gasification: Preparation, characterization and testing at real process conditions. *Catalysis Today*, 176(1):163 – 168, 2011.

[150] Gerald Soukup. *Der AER-Prozess, Weiterentwicklung in einer Technikumsanlage und Demonstration an einer Grossanlage*. PhD thesis, Vienna University of Technology, 2009.

Paper I

Koppatz, S., Pfeifer, C., Kreuzeder, A., Soukup, G., Hofbauer, H.,

"Application of CaO-based bed material for dual fluidized bed steam biomass gasification",

Paper II

Koppatz, S., Pröll, T., Pfeifer, C., Hofbauer, H.,

"Investigation of reforming activity and oxygen transfer of olivine in a dual circulating fluidised bed system with regard to biomass gasification",

Paper III

Koppatz, S., Pfeifer, C., Pröll, T., Hofbauer, H.,

"Experimental Study on Reforming Activity and Oxygen Transfer of Fe-Olivine in a Dual Circulating Fluidized Bed System",

Paper IV

Koppatz, S., Pfeifer, C., Rauch, R., Hofbauer, H., Marquard-Moellenstedt, T., Specht, M.,

"H$_2$ rich product gas by steam gasification of biomass with in situ CO$_2$ absorption in a dual fluidized bed system of 8 MW fuel input",

Paper V

Koppatz, S., Pfeifer, C., Hofbauer, H.,

"Comparison of the performance behaviour of silica sand and olivine in a dual fluidised bed reactor system for steam gasification of biomass at pilot plant scale",

Paper VI

Koppatz, S., Schmid, J. C., Pfeifer, C., Hofbauer, H.,

"The effect of bed particle inventories with different particle sizes in a dual fluidised bed pilot plant for biomass steam gasification",

Paper VII

Pfeifer, C., Koppatz, S., Hofbauer, H.,

"Catalysts for dual fluidised bed biomass gasification—an experimental study at the pilot plant scale",

Paper VIII

Koppatz, S., Pfeifer, C., Hofbauer, H.,

"Application of Fe-olivine as catalytic active bed material in biomass gasification",

Paper IX

Wolfesberger, U., Koppatz, S., Pfeifer, C., Hofbauer, H.,

"Effect of iron supported olivine on the distribution of tar compounds derived by steam gasification of biomass",

in: *Proceedings of the International Conference on Polygeneration Strategies (ICPS11)*, 30 August–1 September, **2011**, Vienna, Austria.